8-2013

DESCRIBING PLUTONIUM CONTAMINATION ISSUES IN HANFORD SOILS: DEVELOPMENT OF A THERMODYNAMIC SURFACE COMPLEXATION MODEL

Sarah Herr
Clemson University, srudy@clemson.edu

DESCRIBING PLUTONIUM CONTAMINATION ISSUES IN HANFORD SOILS: DEVELOPMENT OF A THERMODYNAMIC SURFACE COMPLEXATION MODEL

A Thesis
Presented to
the Graduate School of
Clemson University

In Partial Fulfillment
of the Requirements for the Degree
Master of Science
Environmental Engineering and Science

---

by
Sarah Marie Herr
August 2013

Accepted by:
Dr. Brian Powell, Committee Chair
Dr. Fred Molz
Dr. Lindsay Shuller-Nickles

ABSTRACT

The development of remediation strategies for long-term site management requires knowledge of an actinide's geochemical behavior. Understanding this behavior can lead to the formation of a subsurface transport model. For example, plutonium mobility in the subsurface environment is significantly influenced by oxidation-reduction and complexation reactions. This work considered the surface-mediated reduction of plutonium, as well as the hydrolysis and carbonate complexation of the actinide.

Evaluating the significance of these reactions required several variable pH batch sorption studies. Experiments incorporated plutonium and neptunium sorption to sediments from the Hanford Nuclear Reservation in Washington State. Two different sediments were examined: coarse-grained and fine-grained. Batch sorption experiments utilized either the pristine or acid-leached forms of these soils. Suspensions contained actinide concentrations of either 1×10^{-9} M or 1×10^{-8} M and sediment concentrations of either 25 g/L or 100 g/L. Sorption profiles were developed for these initially Pu(V) and Np(V) systems. Typically, the fraction sorbed increased with pH. The stronger sorption of plutonium relative to the Np(V) systems suggested the surface-mediated reduction of Pu(V) to Pu(IV).

A component additivity model was developed using mineralogical characterization results and a FITEQL-based modeling program. The FIT4FD model used during this project predicted sorption onto a mineral assemblage by the summation of sorption to each specific sorbent. The target solid phases included gibbsite (AlOOH), silica (SiO_2), and goethite (FeOOH). Surface complexation constants for these phases

were calculated or taken from available literature. Surface site concentrations were varied in order to fit the batch sorption data.

In the best fit models, speciation was generally controlled by the strongly hydrolyzed $Pu(OH)_x^{4-x}$ species, not the weakly complexing PuO_2^+ ion. The models attempted to predict plutonium oxidation speciation. As expected, Pu(IV) dominated the solid phase, while Pu(V) dominated the aqueous phase. Silica and gibbsite reactive fractions remained at 0.1%, and goethite reactive fractions ranged from 0.02% to 2.0% for the coarse-grained sediment models. Alternatively, silica and gibbsite reactive fractions ranged from 0.26%% to 2.6%, and goethite reactive fractions ranged from 0.0032% to 3.2% for the fine-grained sediment models.

ACKNOWLEDGEMENTS

I would like to thank Dr. Brian Powell for all of his assistance, feedback, and patience over the last three years. Also, I would like to thank Daniel Kaplan and Kimberly Roberts for performing the mineralogical assessments of the soils.

This work was supported by the Subsurface Biogeochemical Research Program of the U.S. Department of Energy's Office of Biological and Environmental Research.

TABLE OF CONTENTS

Page

Table of Contents (Continued)

Page

LIST OF TABLES

List of Tables (Continued)

Table Page

List of Tables (Continued)

Table Page

List of Tables (Continued)

Table Page

LIST OF FIGURES

List of Figures (Continued)

Figure Page

List of Figures (Continued)

Figure Page

List of Figures (Continued)

Figure Page

List of Figures (Continued)

Figure Page

List of Figures (Continued)

Figure Page

List of Figures (Continued)

Figure Page

List of Figures (Continued)

Figure Page

List of Figures (Continued)

Figure Page

CHAPTER ONE – INTRODUCTION

Beginning in 1945, weapons production activities at the Hanford Nuclear Reservation located in Washington State resulted in the discharge of transuranics to the subsurface. Approximately 12,000 curies of ^{239}Pu were released across the site at eighty different locations (Felmy *et al.*, 2010). The vast majority of plutonium was placed within seven closure zones in the central plateau, and the largest discharge occurred near the Z-Plant (Plutonium Finishing Plant, PFP) complex (Felmy *et al.*, 2010). More than 10,000 curies of ^{239}Pu, 33,000 curies of ^{241}Pu, 27,000 curies of ^{241}Am, and 40 curies of ^{237}Np were discharged between 1945 and 1990 near the Z-Plant complex (Felmy *et al.*, 2010).

Minimum plutonium mobility was expected under typical Hanford site subsurface conditions due to its insolubility and strong sorptive behavior toward the sediment (Cantrell and Riley, 2008). However, remedial investigations conducted within the site operable units revealed significant plutonium and americium movement to depths up to 150 feet below ground surface (Cantrell and Riley, 2008). Investigators noted that the contaminant plume was associated with a low pH, high ionic strength influent solution containing organic complexants (e.g. CCl_4, MBP, DBP, and TBP) (Cantrell and Riley, 2008). A profile of the contaminant plume is shown in **Figure 1.1**.

During the operational period, significant quantities of particulate plutonium were filtered out of the acidic waste and remained near the disposal point below the trench (Cantrell and Riley, 2008). The majority of the plutonium and americium dissolved in the liquid wastes migrated to the two silt layers beneath the trench. In addition,

plutonium, americium, and co-contaminants spread laterally along these silt layers. Essentially all of the transported plutonium accumulated in the silt layer located at a depth of 65 feet within the Hanford formation; the americium, however, migrated in significant concentration beyond the bottom of the silt layer and also accumulated in the fine-grained layer.

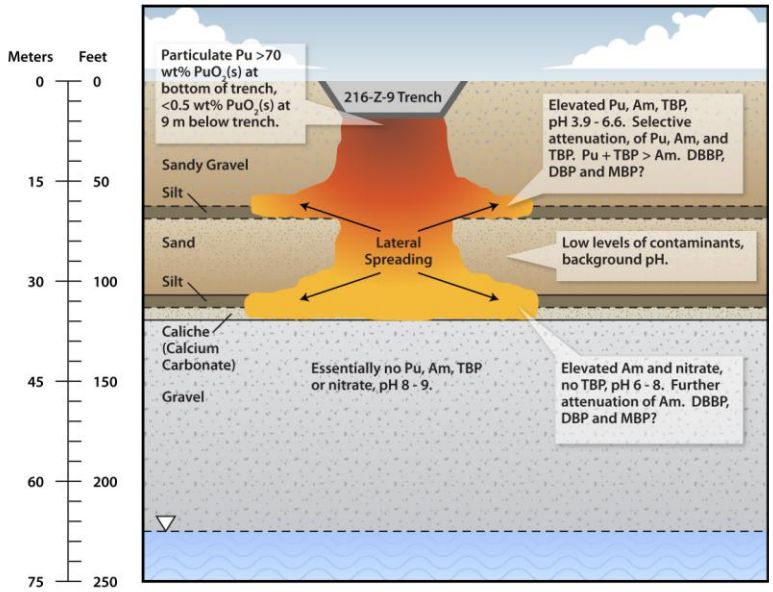

Figure 1.1. Model of past plutonium and americium migration beneath the 216-Z-9 trench (Cantrell and Riley, 2008).

The pH of the Hanford formation silt layer ranged from 4 to 7, likely due to the loss of buffering capacity during the operational period (Cantrell and Riley, 2008). This limited buffering capacity allowed the highly acidic waste to pass through the silt layer and continue downward until it reached the silt layer of the unit. The pH of the unit appeared to be somewhat below to slightly above neutral (Cantrell and Riley, 2008). Any acidic waste that reached the caliche layer appeared to have been neutralized by the carbonate (Cantrell and Riley, 2008). No significant amounts of waste were detected

below the unit. Only trace levels of plutonium and americium were found in the sediment directly below the unit in the Ringold Formation; these trace levels were likely a result of contaminant spreading during drilling operations (Cantrell and Riley, 2008). The pH below the unit ranged from 8 to 9.5.

This work primarily examined plutonium and neptunium sorption to Hanford subsurface sediments with the goal of developing a quantitative model describing the observed sorption behavior. The research sought to improve the ability to predict the transport of these actinides by developing a redox-coupled model of plutonium speciation in subsurface environments. Batch sorption experiments and detailed sediment characterization supported the development of a thermochemically-based surface complexation model. Laboratory experiments focused on plutonium and neptunium sorption to two types of Hanford soil. These data, along with mineralogical characterization, resulted in the development of a component additivity model describing plutonium and neptunium sorption to the sediments and their components.

CHAPTER TWO - BACKGROUND

Plutonium Geochemistry

The unique behavior of the actinide elements produces several challenges when predicting their subsurface fate and transport. In the natural environment, plutonium can exist in four possible oxidation states—(III), (IV), (V), and (VI) (Silva and Nitasche, 1995). Each oxidation state possesses a different chemical behavior and, thereby, complicates fate and transport predictions (Choppin, 2007). The coexistence of plutonium in several oxidation states is due to the proximity of electrochemical potentials of each redox couple, shown in **Table 2.1** (Clark *et al*., 2006).

Table 2.1. Formal electrochemical potentials for plutonium redox couples (Clark *et al.*, 2006).

Couple	Electrochemical Potentials		
	Acidic[a]	*Neutral*[b]	*Basic*[c]
Pu(IV)/Pu(III)	0.982	-0.39	-0.96
Pu(V)/Pu(IV)	1.17	0.7	-0.67, 0.52[d]
Pu(VI)/Pu(V)	0.913	0.6	0.12
Pu(VI)/Pu(IV)	1.043	0.65	0.34

[a]In 1M $HClO_4$
[b]pH 8
[c]In 1M NaOH
[d]Formal oxidation potential

The predominant oxidation states in neutral oxic solutions include Pu(IV), Pu(V), and Pu(VI). Plutonium(III) can be oxidized by water at neutral pH values due to the negative formal potential of the Pu(IV)/Pu(III) couple. Therefore, the primary oxidation states of relevance in natural environments are (IV), (V), and (VI).

Inspection of the Eh-pH diagram in **Figure 2.1** shows that Pu(IV) and Pu(V) will dominate under natural system conditions like the ones expected for this work. These oxidation states represent the plutonium species with the lowest and highest subsurface mobilities. Plutonium(III) and Pu(VI) dominate only under extreme E_H or pH conditions.

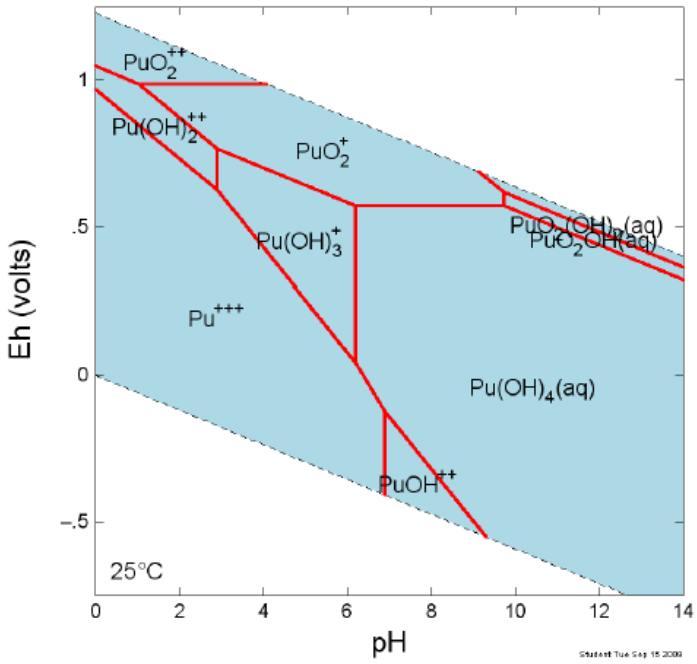

Figure 2.1. E_H-pH diagram of plutonium in an aqueous system. Total plutonium concentration set at 1 x 10^{-9} M with an ionic strength of 0.1M NaCl. Modeled using Geochemists Workbench.

In some cases, several species exist simultaneously in the aqueous mixtures at fixed E_H and pH conditions. The E_H-pH diagram simplifies the situation by showing only the predominant species for each area. The addition of ligands, like carbonate, will complicate the system shown in **Figure 2.1**.

Plutonium sorption to minerals, colloids, and other surfaces varies with oxidation state, pH, temperature, ionic strength, and surface type. Plutonium sorbs more strongly in

the (IV) oxidation state than in the higher dioxo (V) and (VI) states; the actinide tends to follow the generic trend in terms of increasing sorption affinity:

$$Pu(IV) > Pu(III) \approx Pu(VI) > Pu(V)$$

This trend follows the trend of decreasing effective charge of the ions (Choppin and Rao, 1984). Keeney-Kennicutt and Morse (1985) speculated that Pu(IV) is typically associated with sediments, while Pu(V) and (VI) are associated with the aqueous phase. Even at low pH values, Pu(IV) forms strong hydroxide complexes and precipitates as $Pu(OH)_4$ (s) in neutral pH solutions (Powell *et al.*, 2005). Due to the strong affinity of $Pu(OH)_4$ to sediments and suspended particulates, Pu(IV) sorption is the limiting factor in the plutonium transport process (Choppin, 2007). Generally, Pu(IV) has such a high affinity for the solid phase that it yields sediment distribution coefficients two to three orders of magnitude higher than Pu(V) (Powell *et al.*, 2002).

Complexation with ligands can significantly impact plutonium sorption to surfaces. The strength of complexation decreases with decreasing effective charge. This sequence of complexation strength does vary and depends on solution conditions (Choppin *et al.*, 1997). The general trend for the strength of complexed plutonium with various ligands is shown below (Silva and Nitsche, 1995).

$$OH^- \geq CO_3^{2-} > F^- > HPO_4^{2-} > SO_4^{2-} > Cl^- > NO_3^-$$

As a result, hydrolysis and carbonate complexation reactions are some of the most important reactions for plutonium in environmental systems. In noncomplexing media, the hydrolysis of Pu(III) occurs around pH 5, while hydrolysis of Pu(IV) is already significant by pH 1 (Choppin *et al.*, 1997). Plutonium(V) shows little hydrolysis below

pH 9, while Pu(VI) hydrolysis occurs in the pH range 3 to 4 (Choppin *et al.*, 1997). Plutonium(IV) hydrolyzes at very low pH values due to its high effective charge. Under these conditions, Pu(IV) tends to strongly sorb to mineral surfaces through the formation of complexes with surface hydroxyl groups (Powell *et al.*, 2013a). Extensive hydrolysis continues until the neutral species $Pu(OH)_4$ is formed between pH 6 and 8, depending on the ionic strength of the system. Therefore, hydrolysis reactions prevent significant formation of the tetravalent free ion in natural systems.

Additionally, Pu(IV) is expected to complex with carbonate species in systems containing this ligand. Studies have shown that plutonium will sorb strongly to carbonate-bearing minerals and clays (Zavarin *et al.*, 2005; Powell *et al.*, 2013a). The interaction of plutonium with carbonate-bearing minerals is likely to affect its transport behavior in the subsurface environment (Zavarin *et al.*, 2005). Zavarin *et al.* (2005) performed experiments detailing Pu(V) sorption to calcite ($CaCO_3$). Initially, plutonium sorption appeared quite similar to other pentavalent actinides. After one week, however, the fraction of plutonium sorbed to the mineral surface greatly increased. While this may be the result of the slow incorporation of Pu(V) into the calcite, it may also result from redox changes in plutonium as a function of time (Zavarin *et al.*, 2005). The slow reduction of Pu(V) to Pu(IV) in solution, followed by the sorption of Pu(IV) to the mineral surface, could explain the observed increase in sorption (Zavarin *et al.*, 2005).

Alternatively, surface-mediated reduction could explain this increased sorption to calcite. Powell *et al.* (2005) observed a steady decrease of Pu(V) and subsequent increase in Pu(IV) within hematite (Fe_2O_3) and goethite (FeOOH) systems, implying the

reduction of Pu(V) to Pu(IV). Measurement of plutonium in the aqueous phase showed only Pu(V), regardless of pH (Powel *et al.*, 2005). Additionally, no adsorption or reduction was noted in systems at pH 3. Therefore, Powell *et al.* (2005) inferred that the reduction of Pu(V) occurred on the mineral surfaces. Reduction of Pu(V) has also been observed on "non-redox" active or even oxidizing minerals such as quartz and pyrolusite, respectively (Hixon *et al.*, 2013; Powell *et al.*, 2006). In these systems, reduction was proposed to be due to a thermodynamic favorability of Pu(IV) surface species; these species can effectively lower the redox potential of the Pu(V)/Pu(IV) couple (Powell *et al.*, 2005; Powell *et al.*, 2006; Hixon *et al.*, 2013).

The surface-mediated reduction and oxidation of plutonium was observed in several other studies. Kirsch *et al.* (2011) used X-ray absorption near edge structure (XANES) and extended X-ray absorption fine structure (EXAFS) to investigate Pu(V) reactions with magnetite (Fe_3O_4), mackinawite (FeS), and chukanovite ($Fe_2CO_3(OH)_2$) under anoxic conditions. The authors observed Pu(V) reduction in the presence of all three minerals. Spectra of Pu(V) reacted with mackinawite and chukanovite were similar to those of crystalline PuO_2, suggesting the prevalence of tetravalent plutonium and precipitation of PuO_2 nanocolloids in the samples (Kirsch *et al.*, 2011). Reduction to Pu(III) was observed on magnetite. Detailed analysis of the EXAFS spectra indicated complexation of Pu(III) as a tridentate complex on the octahedrally terminated {111} face of magnetite.

Shaughnessy *et al.* (2003) noted the capacity of the pure manganese minerals manganite ($Mn^{III}OOH$) and hausmannite ($Mn^{II}Mn^{III}{}_2O_4$) to reduce plutonium from the

hexavalent to the tetravalent form using XANES. Duff *et al.* (1999) observed the oxidation of Pu(V) to Pu(VI) on the surface of Yucca Mountain Tuff, specifically on a ranceite grain. However, Powell *et al.* (2006) measured the same samples two years later and revealed that the majority of the plutonium eventually reduced to Pu(IV). Similar initial oxidation followed by reduction was observed on pyrolusite (Powell *et al.*, 2006). These studies indicate that reduction of Pu(V) to Pu(IV) will occur on almost all surfaces even though the rates may differ significantly. This is significant for the current work; the model presented in this work considered coupled sorption and redox processes, even for non-redox active minerals such as gibbsite (AlOOH) and quartz (SiO_2).

Oxidation State Analogs

Plutonium's sensitivity to oxidation state transformations makes predicting its redox speciation difficult. As a result, the study of cations of a stable oxidation state provides valuable information regarding plutonium behavior. Oxidation state analogs can be studied in macro concentrations since the oxidation state distribution is not a function of concentration, as it is for plutonium (Choppin, 2007). The primary requirements when choosing an analog include the same oxidation state and similar ionic radius (Choppin, 2007). Neptunium(V) is commonly used as a chemical oxidation state analog for Pu(V), because it meets these two conditions. However, it is noteworthy that only chemical parameters such as sorption, complexation, and solubility can be compared. Due to their differing redox potentials, no comparisons with redox reactions can be made. The negative electrochemical potential of the Np(V)/Np(IV) couple indicates Np(V) stability under many environmental conditions. Alternatively, the

positive redox potential of the Pu(V)/Pu(IV) couple implies Pu(IV) stability within the environment. Differences in sorption behavior between initially Pu(V) and Np(V) systems can be used to infer reduction of Pu(V) to Pu(IV).

Modeling Approaches

Surface complexation modeling approaches can be divided into two categories: (1) the generalized composite approach and (2) the component additivity approach (Davis *et al.*, 1998). In the generalized composite (GC) approach, the surface composition of the mineral assemblage is too complex to be quantified in terms of the contributions of individual phases to adsorption (Davis *et al.*, 1998). Instead, the reactivity of the surface can be described by surface complexation equilibria written with "generic" surface functional groups (Davis *et al.*, 1998). Stability constants and reaction stoichiometries are determined by fitting experimental data. The number of site types and chemical reactions are increased as necessary to meet modeling objectives.

In the component additivity (CA) approach, the modeler attempts to predict sorption on a complex mineral assemblage (Davis *et al.*, 1998). This is achieved using the results of a surface characterization, as well as sorption data for the pure reference minerals. No fitting of data is required to develop the model for the mixed mineral assemblage. Comparisons of model simulations and experimental sorption data are needed to build confidence in the model (Davis *et al.*, 1998). This approach assumes that the surface is composed of a mixture of one or more mineral phases whose properties are known from independent studies and predicts overall sorption by the sum sorption of each specific mineral.

This work used a component additivity model based on the mineralogical characterization results. The FITEQL-based model predicted sorption onto a complex mineral assemblage by the summation of sorption to each specific sorbent. The solid phases used in the model include goethite and smectite clay. Surface complexation constants for these phases were taken from the available literature or developed using pre-existing sorption data. The model could be developed without the use of experimental data, but comparison between model simulations and actual sorption data result in increased model confidence. As a result, variable pH batch sorption data were used to refine the component additivity model.

The Pu(V)/Pu(IV) redox couple complicated this modeling approach since more than one oxidation state must be considered and most sorption models do not include redox coupled reactions. Therefore, the model incorporated the Pu(IV)/Pu(V) redox couple shown below (Powell *et al.*, 2013a).

$$Pu^{4+} + 0.25O_2(g) + 1.5H_2O \leftrightarrow PuO_2^{+} + 3H^{+} \qquad \log K = 3.32$$

The incorporation of this redox couple provided a more technically accurate model as it can predict Pu(V) as the dominant aqueous phase oxidation state and Pu(IV) as the dominant sorbed oxidation state (Keeney-Kennicutt and Morse, 1985; Powell *et al.*, 2004; Powell *et al.*, 2005). Example reactions for uncoupled and coupled plutonium sorption to a generic surface site are shown below.

Uncoupled

$$\equiv SOH + Pu^{4+} + H_2O \leftrightarrow \equiv SOPu(OH)^{2+} + 2H^+$$

$$\equiv SOH + PuO_2^{+} \leftrightarrow \equiv SOPuO_2 + H^+$$

Coupled

$$\equiv SOH + Pu^{4+} + 0.25O_2\,(g) + 1.5H_2O \leftrightarrow \equiv SOPuO_2 + 4H^+$$

For the coupled reaction, Pu(V) surface complexes are formed via oxidation of Pu^{4+} by dissolved oxygen. This couple was used for simplicity in the model and was not intended to represent a specific mechanism. The O_2 (g) fugacity was estimated from redox potential measurements; these values were used in the modeling effort as described **Chapter 5**.

CHAPTER THREE – GOAL AND TASKS

Goal

This research sought to improve the ability to predict plutonium transport by developing a mechanistic model of speciation in subsurface environments. Batch sorption experiments and detailed sediment characterization assisted in the development of a thermodynamic surface complexation model. Laboratory experiments focused on Pu(V) and Np(V) sorption to two types of Hanford soil from pH 4 to 10. These data, along with mineralogical characterization results, were used to develop a component additivity model describing sorption to the sediments and their components.

Tasks

Task 1: Variable pH batch sorption experiments were performed with Pu(V), Np(V), and two types of Hanford sediments.

Task 1.1: The effect of sorption site concentration on sorption was noted by including two soil concentrations (100 g/L and 25 g/L).

*Task 1.*2: The effect of actinide concentration on sorption was noted by including two actinide concentrations (10^{-8} M and 10^{-9} M).

*Task 1.*3: The effect of the presence of carbonate-bearing minerals on sorption was noted by including pristine and acid-leached sediments.

Task 2: Mineralogical characterization of the two Hanford sediments was performed. Analyses included x-ray diffraction (XRD), surface area measurements, and total element analysis.

Task 3: Soil column experiments were performed to describe the pH gradient produced during the initial waste disposal.

Task 4: A component additivity model was built to effectively represent the batch sorption data and aid in the prediction of the transport observed in Task 3.

CHAPTER FOUR – MATERIALS AND METHODS

Materials

Plutonium-242 working solutions were prepared from New Brunswick Certified Reference Material 130. A small aliquot of a 4.327 µM ^{242}Pu stock solution in 1 M HNO_3 was evaporated to dryness and re-dissolved in 1 mL of 1.0 M HCl and 10 µL of 0.2000 N $KMnO_4$ in a Teflon vial. After wrapping the vial in aluminum foil, the solution was left for 28 hours to allow for the oxidation of all plutonium to Pu(VI). The resulting solution was diluted approximately 20 times with 0.1 M NaCl to the pH range 2 to 3. Any remaining permanganate was precipitated with a 10 µL aliquot of 0.01 M $MnCl_2$. To avoid coprecipitation of Pu(VI), the pH remained low (< 3) during this step. The solution was then passed through a 200 nm nylon syringe filter into a Teflon bottle, and the pH was adjusted to 3 using 1 M NaOH. The solution was left for at least five days to allow for the auto-reduction of Pu(VI) to Pu(V). The solution possessed a final concentration of $2.12 \pm 0.01 \times 10^{-5}$ M with Pu(IV) at 1 ± 2%, Pu(V) at 98 ± 3% and Pu(VI) at 1 ± 2%.

Neptunium-237 working solutions were prepared using neptunium stock solutions from the Environmental Engineering and Earth Sciences inventory (initially purchased from Isotope Products in Valencia, CA). The solution was evaporated to dryness, and the residue was added to 5 mL of 8.0 M HNO_3. Water and 1.0 M hydroxylamine hydrochloride ($NH_2OH \cdot HCl$) were added to achieve a 3 M HNO_3/0.3 M $NH_2OH \cdot HCl$ solution. This solution was purified via extraction chromatography using Eichron TEVA resin packed in a Bio-Radpoly preparatory column. The neptunium solution was loaded

on a 2 mL column and washed with three column volumes of 3 M HNO_3. The Np(IV) was eluted with 0.02 M HCl and 0.2 M HF. The effluent was evaporated and redissolved in 1.0 M HNO_3. Additional 1.0 M HNO_3 was added to maintain an approximately 10 mL solution, and then the solution was evaporated to incipient dryness and redissoled in 5.0 mL of 1.0 M HNO_3. This fuming drove the neptunium to the soluble pentavalent state. A ^{237}Np working solution was created by pipetting an aliquot of the stock solution into a 100 mL Nalgene Teflon bottle and diluting with 2% BDH Aristar Ultra HNO_3; this produced a working solution with a concentration of 3.46×10^{-6} M.

Sediments from the Environmental Restoration Disposal Facility (ERDF) within the Hanford Nuclear Reservation in Washington State were provided by Dr. Andy Felmy of the Pacific Northwest National Laboratory. The depth of the silt layer at the ERDF resembled that at the contaminated Z-9 trench. The fine- and coarse-grained soils were characterized using X-ray diffraction, inorganic and organic carbon analysis, and dithionite extractable aluminum, silica, and iron. The results are shown below (**Table 4.1**).

Table 4.1. Physical and chemical data from sediment characterization.

Measurement	Fine Sediment	Coarse Sediment
pH	8.5	8.6
Particle Size Distribution (sand/silt/clay)	74/26/0	97/1/0
Organic C (%)	0.05	0.07
Inorganic C (%)	0.25	0.29
Surface Area (m^2/g)	15.36	28.56
Dithionite Silica (wt-%)	0.0167 ± 0.00017	0.0207 ± 0.0021
Dithionite Aluminum (wt-%)	0.0186 ± 0.0019	0.0153 ± 0.0016
Dithionite Iron (wt-%)	0.324 ± 0.0324	0.198 ± 0.0198
Mineralogy	Quartz, Plagioclase, K-feltspar, Mica, Calcite, Illite, Smectite, Chlorite, and Kaolinite	

Organic and inorganic carbon values were determined using a Leco 2000 analyzer. The sediments, along with a combustion catalyst, were loaded into the furnace at 1350°C; combustion gases were collected and analyzed via infrared absorption.

A sodium citrate-bicarbonate-dithionite (CBD) extraction was performed to remove iron oxides from the soil samples. The CBD procedure removed both crystalline and non-crystalline iron oxides (except highly crystalline hematite and magnetite), as well as aluminum hydrous oxides and hydrous silica associated with iron oxides in the soils. Iron, aluminum, and silica in the extraction were determined and reported as dithionite extractables.

XRD patterns for the two sediments were obtained on a Scintag x-ray diffractometer; individual scans were obtained from 2 to 65° 2θ with 0.01° step. The pattern for the fine-grained sediment is shown below (**Figure 4.1**).

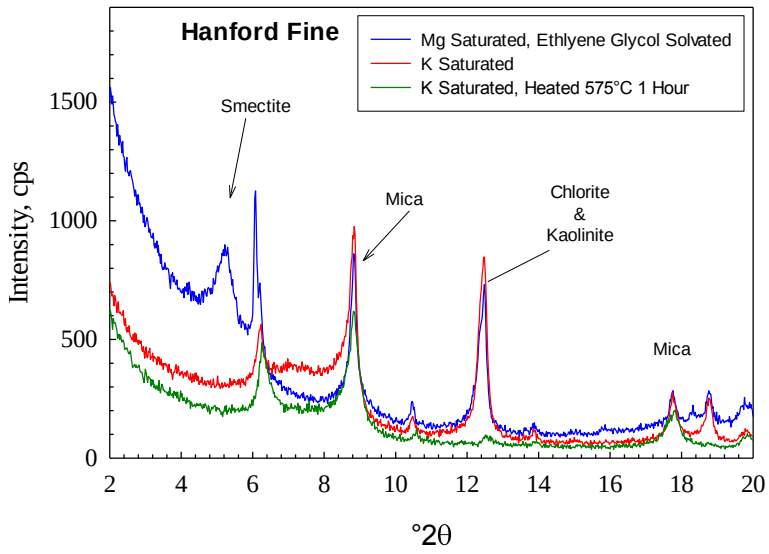

Figure 4.1. XRD spectra of the preferentially oriented < 2.0 µm fraction of the Hanford fine sediment.

The coarse-grained sediment exhibited an identical pattern.

Analyses revealed the presence of carbonate-bearing minerals in both Hanford sediments. In order to fully characterize the soils and to mimic the impacts of the acidic waste streams on the sediment reactivity, sorption experiments utilized either pristine or acid-leached soil. Leached sediment was prepared with an acid wash for the removal of these carbonate minerals. A 1.0 M HCl solution was added to the sediments until pH 4 was achieved. Approximately 0.59 g_{acid}/g_{soil} was needed to wash the fine-grained sediment, while 0.47 g_{acid}/g_{soil} was needed to wash the coarse-grained sediment. Acidification resulted in the depletion of 8.49% and 5.25% of the total mass for fine- and coarse-grained sediments, respectively. These percentages, however, were not comparable to the inorganic carbon values reported by the Savannah River National Lab. The dissolution of other soil components (salts, iron oxide coatings, etc.) during

acidification, as well as the physical loss of soil during decantation, explains this discrepancy.

All chemicals used were prepared from ACS reagent grade or higher purity. Liquid scintillation counting (LSC) was performed using Optiphase HiSafe III LSC cocktail (Perkin Elmer) and a Hidex 300SL Liquid Scintillation Counter. The distilled deionized water used in all experiments was obtained from a Millipore Super Q system with a resistivity less than 18 MΩ·cm.

Methods

Batch Sorption Experiments

Batch sorption experiments were performed using the Pu(V) and Np(V) stocks, as well as either pristine fine- or coarse-grained Hanford sediments. The experiments utilized final ^{242}Pu concentrations of either 3×10^{-9} M or 3×10^{-8} M and final ^{237}Np concentrations of either 5×10^{-9} M or 5×10^{-8} M. Also, leached sediment samples were prepared to analyze the plutonium sorption effects of carbonate-bearing minerals. Final soil concentrations were either 25 g/L or 100 g/L. For direct comparison, the full experimental matrix is shown in **Table 4.2**.

Table 4.2. Matrix of variable pH batch sorption experiments run with initially ^{242}Pu(V) and ^{237}Np(V).

Experiment	Sediment Type	Sediment Concentration	Actinide Concentration		Sediment Treatment
			^{242}Pu	^{237}Np	
A	Coarse	100 g/L	2.91×10^{-9} M	3.26×10^{-9} M	Pristine
B	Fine	100 g/L	2.90×10^{-9} M	3.24×10^{-9} M	Pristine
C	Coarse	100 g/L	2.86×10^{-8} M	3.19×10^{-8} M	Pristine
D	Fine	100 g/L	2.87×10^{-8} M	3.20×10^{-8} M	Pristine
E	Coarse	25 g/L	3.18×10^{-9} M	4.76×10^{-9} M	Pristine
F	Fine	25 g/L	3.23×10^{-9} M	4.94×10^{-9} M	Pristine
G	Coarse	25 g/L	3.02×10^{-8} M	4.68×10^{-8} M	Pristine
H	Fine	25 g/L	3.10×10^{-8} M	4.64×10^{-8} M	Pristine
I	Coarse	25 g/L	2.68×10^{-9} M	4.86×10^{-9} M	Leached
J	Fine	25 g/L	2.65×10^{-9} M	4.97×10^{-9} M	Leached
K	Coarse	25 g/L	2.56×10^{-8} M	4.72×10^{-8} M	Leached
L	Fine	25 g/L	2.56×10^{-8} M	4.71×10^{-8} M	Leached

Samples were prepared in 15 mL polypropylene centrifuge tubes. The appropriate type and amount of sediment was added to each tube, along with approximately 9 mL of deionized water and 1 mL of 0.1 M NaCl background electrolyte. The samples were spiked to the target concentrations with the Pu(V) and Np(V) working solutions. All additions were monitored gravimetrically. The sediment suspensions were adjusted to pH values ranging from 4 to 10 using incremental acid or base addition. Samples were then mixed on an end-over-end tumbler at approximately 8 rpm. During equilibration, dissolution of carbonate bearing phases and adsorption of protons caused the low and high pH samples, respectively, to drift towards pH 8.

Sampling events occurred at 7 and 30 days. The pH of each suspension was measured using a Thermo Scientific Orion ROSS glass electrode. Then, 1.25 mL of each sample was removed by pipette into a small centrifuge tube and centrifuged at 8000 RPM

for 30 minutes to remove the solid phase. These speeds and times were determined to remove particles greater than 100 nm from the supernatant using a F2402H fixed-angle rotor in an Allegra X-22R centrifuge. After centrifugation, 1 mL of the supernatant was diluted with 9 mL of 2% BDH Aristar Ultra HNO_3 for analysis on the Thermo Scientific X Series 2 inductively-coupled plasma mass spectrometer (ICP-MS). National Institute of Standards and Technology (NIST) Standard Reference Materials were used to calibrate the ICP-MS for the quantification of ^{242}Pu and ^{237}Np. Calibration using the NIST standards is described below.

ICP-MS Calibration

A NIST Standard Reference Material (NIST SRM 4334I) was used to prepare a stock ^{242}Pu solution by dilution in 2% BDH Aristar Ultra HNO_3. This working solution was then used to create a set of 0.01, 0.05, 0.5, 1.0, 5.0, and 10.0 parts per billion (ppb) standards by dilution using 2% HNO_3. All volume additions were monitored gravimetrically. These standards were used to calibrate the ICP-MS for quantification of ^{242}Pu.

Similarily, a NIST Standard Reference Material (NIST SRM 4341) was used to prepare a stock ^{237}Np solution by dilution in 2% BDH Aristar Ultra HNO_3. This solution was used to create a set of 0.01, 0.05, 1.0, 2.0, 5.0, and 10.0 ppb standards by dilution using 2% HNO_3. Again, all volume additions were monitored gravimetrically. These standards were used to calibrate the ICP-MS for quantification of ^{237}Np.

Instrument performance was monitored using ^{208}Pb and ^{238}U as internal standards. Internal standard recoveries remained within standard QA/QC protocols for the

instrument (between 95% and 120%). Calibration curves were then used to calculate the measured concentrations of plutonium and neptunium in the samples. An example calibration curve is shown in **Figure 4.2**; the curve resulted in a minimum detectable limit of 0.00012 ppb for ^{242}Pu.

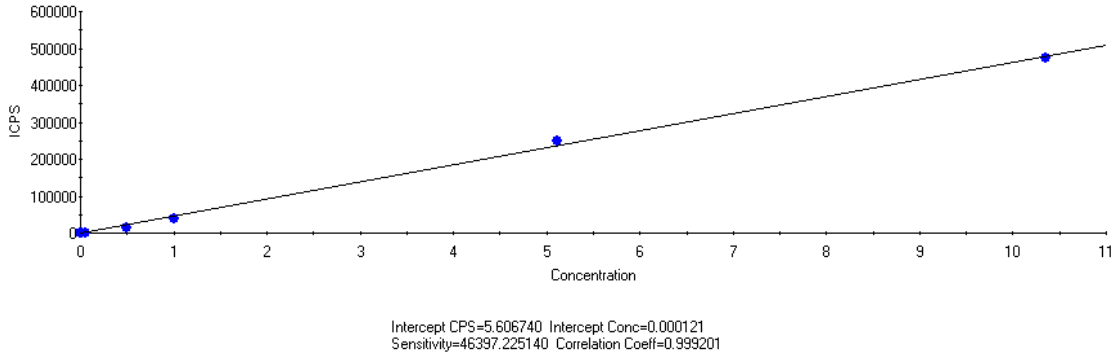

Figure 4.2. Example of a typical ^{242}Pu calibration curve using Thermo PlasmaLab software for data collection and analysis.

Oxidation State Analysis

Oxidation state analysis of plutonium within the samples was performed using lanthanum fluoride coprecipitation and solvent extraction. This technique yields the total oxidation state distribution of plutonium in contact with the sediment surface and the associated aqueous phase. The technique considers Pu(IV), Pu(V), and Pu(VI). Plutonium(III) is not considered or quantified in the separation scheme as it will be unstable under experimental conditions.

The separation of plutonium oxidation state by lanthanum fluoride was based on the method described by Kobashi *et al.* (1988). The coprecipitation reaction was performed by transferring 0.5 mL of the sample to a 1.5 mL centrifuge vial and adding

1.0 mL of $La(NO_3)_3$ stock followed by 10 µL of concentrated HF. The sample was mixed end-over-end for 2 minutes and centrifuged at 8000 RPM for 1 minute. The supernatant was then mixed with 5.0 mL of HiSafe III cocktail and analyzed for Pu(V)/Pu(VI) content by LSC on a Hidex 300SL. The Pu(IV) fraction was calculated by difference.

The separation of plutonium oxidation states by solvent extraction was performed using 0.025 M 4-benzyol-3-methyl-1-phenyl-2-pyrazolin-5-one (PMBP) in hexane and 0.50 M bis-(ethylhexyl)-phosphoric acid (HDEHP) in cyclohexane as the extractants. The PMBP extraction was performed by adding 0.8 mL of the sample to 0.5 mL of PMBP and 0.2 mL of 5.0 M HCl. The sample was mixed end-over-end for 3 minutes and centrifuged briefly to aid in separating the organic and aqueous phases. Each phase was diluted with 5.0 mL of HiSafe III cocktail and analyzed by LSC. The organic phase contained Pu(IV), while the aqueous phase contained Pu(V)/Pu(VI). The HDEHP extraction was performed with the same method and volumes as the PMBP extraction. The organic phase of this extraction contained the Pu(IV)/Pu(VI) fraction, while the aqueous phase contained the Pu(V) fraction.

Soil Column Experiments

Soil column experiments were performed using both the fine- and coarse-grained sediments. Fine-grained soil was tightly packed into 1.5 cm by 8.3 cm (outer diameter, height) polycarbonate columns. The sediment addition was monitored gravimetrically. The column was then attached to a Masterflex L/S Variable Speed Modular Drive from Cole-Parmer and an Eldex Universal Fraction Collector. A 0.1 M NaCl solution adjusted

to pH 2.5 was pumped upwards through the column at a rate of 0.04 mL per minute. A 2 mL aliquot was collected every 50 minutes, and the pH of each sample was measured using a ROSS electrode. Even though thirty pore volumes passed through the column, the pH of the aliquots remained around 8.09 ± 0.04. As a result, additional experiments were not conducted to see the effects of pumping a low pH, high ionic strength solution similar to the waste stream at the Z-Plant complex through the sediments.

Modeling

A component additivity model was built using the mineralogical characterization results and a FITEQL-based modeling program. FIT4FD, a FITEQL 4.0 program, was recompiled in Fortran 90 with additional features including b-dot activity correction, an improved minimization routine, and improved speciation database retrieval (Herbelin and Westall, 1999). The FIT4FD model used during this project predicted sorption onto a complex mineral assemblage by the summation of sorption to each specific sorbent. The target solid phases used included gibbsite, silica, and goethite. Surface complexation constants for these phases were developed or taken from available literature. Model development and results are described in **Chapter 5**.

CHAPTER FIVE – RESULTS AND DISCUSSION

Surface Site Behavior

Surface protonation refers to the transfer of protons between the bulk solution and the binding sites on a solid surface. This adsorption and desorption of protons arises from the acid/base properties of the surface-bound hydroxyl groups. Surface protonation reactions are typically expressed as follows:

$$\equiv SOH + H^+ \leftrightarrow \equiv SOH_2^+$$

$$\equiv SOH \leftrightarrow \equiv SO^- + H^+$$

The species ≡SOH exhibits basic behavior by absorbing a proton to form a positively charged surface species. Alternatively, the same species exhibits acidic behavior by releasing a proton to yield a negatively charged surface species. Goethite, gibbsite, and silica exhibit this amphoteric behavior (**Figure 5.1**).

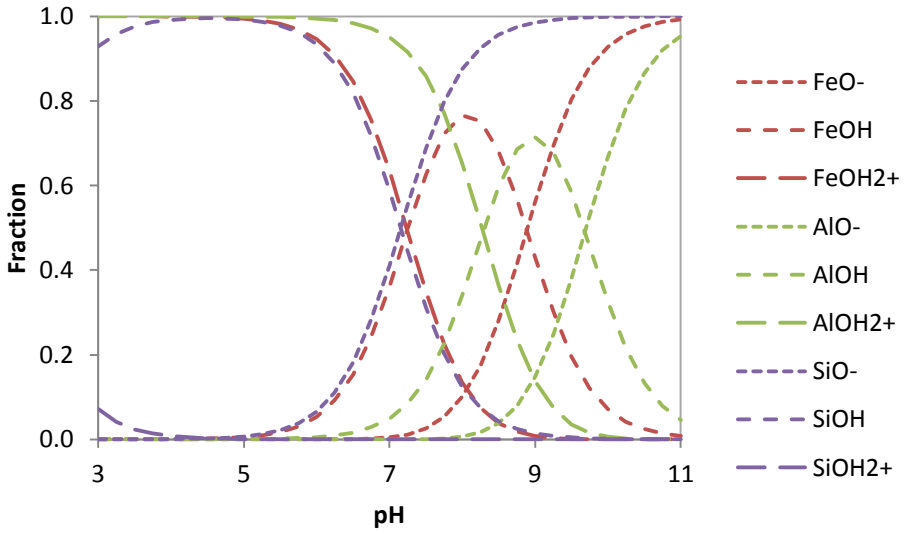

Figure 5.1. Surface protonation behavior of goethite, gibbsite, and silica. Mineral concentrations of 1 x 10^{-7} M in a 0.10 M NaCl background.

For example, iron oxide sites on the goethite surface are protonated in acidic solutions, forming $\equiv FeOH_2^+$. As the pH of the solution increases, the sites deprotonate to form $\equiv FeOH$ and $\equiv FeO^-$. Therefore, the surface transitions from having a net positive charge to having a net negative charge. The fraction of protonated versus deprotonated sites is dependent on the mineral characteristics and the solution ionic strength. The point of zero charge corresponds to the pH value at which the net surface charge is zero, i.e. where the number of doubly protonated sites is equal to the number of deprotonated sites (**Figure 5.2**).

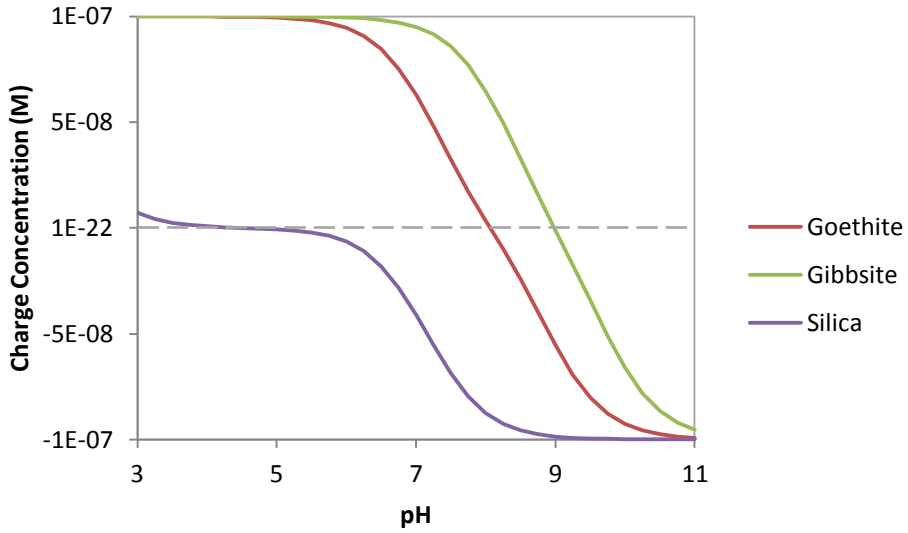

Figure 5.2. Net surface charge profiles for goethite, gibbsite, and silica. Mineral concentrations of 1 x 10^{-7} M in a 0.10 M NaCl background.

Changes in surface charge profoundly affect the sorption of charged ions like PuO_2^+. In acidic solutions, the surface sites possess a net positive charge. Cationic PuO_2^+ is repelled by the surface, resulting in negligible sorption. As the pH of the solution increases, the surface sites acquire a net negative charge, and Pu(V) sorption increases.

Stability Constants

Reactions and surface complexation constants for plutonium sorption to goethite were developed using data from Sanchez *et al.* (1985). Alternatively, relevant reactions and stability constants for plutonium sorption to silica and gibbsite were obtained from Powell *et al.* (2013b). **Tables 5.1** and **5.2** summarizes all reactions used in this modeling process. It contains reactions for Pu(IV) sorption, Pu(V) sorption, and coupled Pu(IV)/Pu(V) sorption to the minerals. The study of sorption to Hanford sediments required the use of Np(V) as a stable oxidation state analog. As a result, the Pu(V) sorption constants listed in **Table 5.1** were applied to Np(V) data.

As discussed in **Chapter 2**, the various plutonium oxidation states possess different sorption behaviors. Therefore, a more technically accurate model must predict oxidation state speciation, as well as plutonium partitioning. When considering the Pu(IV)/Pu(V) redox couple, the surface and aqueous Pu(V) species were all rewritten in terms of the following reaction:

$$Pu^{4+} + 0.25O_2(g) + 1.5H_2O \leftrightarrow PuO_2^{+} + 3H^{+} \qquad \log K = 3.32$$

The models developed in this thesis only considered this Pu(IV)/Pu(V) redox couple.

Table 5.1. Stability constants for sorbed species used during modeling.

Dataset	CO_2(g)	Reaction	Species	Uncoupled log K	Coupled log K**
Pu(IV)-gibbsite*	free	$AlOH + Pu^{4+} + H_2O \leftrightarrow AlOPu(OH)^{++} + 2H^+$	$AlOPu(OH)^{++}$	14.59	16.88
		$AlOH + Pu^{4+} + 2H_2O \leftrightarrow AlOPu(OH)_2^{+} + 3H^+$	$AlOPu(OH)_2^{+}$	5.774	--
		$AlOH + Pu^{4+} + 3H_2O \leftrightarrow AlOPu(OH)_3 + 4H^+$	$AlOPu(OH)_3$	-2.59	-0.8013
Pu(IV)-gibbsite*	equilibrated	$AlOH + Pu^{4+} + H_2O \leftrightarrow AlOPu(OH)^{++} + 2H^+$	$AlOPu(OH)^{++}$	13.87	16.19
		$AlOH + Pu^{4+} + 2H_2O \leftrightarrow AlOPu(OH)_2^{+} + 3H^+$	$AlOPu(OH)_2^{+}$	5.459	--
		$AlOH + Pu^{4+} + 3H_2O \leftrightarrow AlOPu(OH)_3 + 4H^+$	$AlOPu(OH)_3$	-2.92	-0.9479
Pu(IV)-silica*	free	$SiOH + Pu^{4+} + 2H_2O \leftrightarrow SiOPu(OH)_2^{+} + 3H^+$	$SiOPu(OH)_2^{+}$	2.166	--
		$SiOH + Pu^{4+} + 3H_2O \leftrightarrow SiOPu(OH)_3 + 4H^+$	$SiOPu(OH)_3$	-1.858	0.361
Pu(IV)-silica*	equilibrated	$SiOH + Pu^{4+} + 2H_2O \leftrightarrow SiOPu(OH)_2^{+} + 3H^+$	$SiOPu(OH)_2^{+}$	2.202	--
		$SiOH + Pu^{4+} + 3H_2O \leftrightarrow SiOPu(OH)_3 + 4H^+$	$SiOPu(OH)_3$	-2.189	8.684×10^{-2}
Pu(IV)-goethite	free	$FeOH + Pu^{4+} + H_2O \leftrightarrow FeOPu(OH)^{++} + 2H^+$	$FeOPu(OH)^{++}$	12.94	--
		$FeOH + Pu^{4+} + 2H_2O \leftrightarrow FeOPu(OH)_2^{+} + 3H^+$	$FeOPu(OH)_2^{+}$	--	7.549
		$FeOH + Pu^{4+} + 3H_2O \leftrightarrow FeOPu(OH)_3 + 4H^+$	$FeOPu(OH)_3$	-2.937	--
Pu(V)-gibbsite*	free	$AlOH + PuO_2^{+} \leftrightarrow AlOPuO_2 + H^+$	$AlOPuO_2$	-3.09	0.23
Pu(V)-silica*	free	$SiOH + PuO_2^{+} \leftrightarrow SiOHPuO_2^{+}$	$SiOHPuO_2^{+}$	4.22	7.54
Pu(V)-goethite	free	$FeOH + PuO_2^{+} \leftrightarrow FeOPuO_2 + H^+$	$FeOPuO_2$	-2.885	0.435

*From Powell *et al.* (2013b).
**Pu(IV) and Pu(V) coupled by $Pu^{4+} + 0.25O_2(g) + 1.5H_2O \leftrightarrow PuO_2^{+} + 3H^+$

Table 5.2. Stability constants for aqueous species and surface sites used during modeling.

Species	Reaction	log K	Reference
OH^-	$H_2O \leftrightarrow OH^- + H^+$	-14	Smith and Martell (1989)
CO_2 (aq)	$H^+ + HCO_3^- \leftrightarrow H_2CO_3$ (aq)	6.34	Smith and Martell (1989)
CO_3^{--}	$CO_3^{2-} + H^+ \leftrightarrow HCO_3^-$	-10.33	Smith and Martell (1989)
NaCl (aq)	$Na^+ + Cl^- \leftrightarrow$ NaCl (aq)	-0.777	Smith and Martell (1989)
$NaCO_3^-$	$Na^+ + HCO_3^- \leftrightarrow H^+ + NaCO_3^-$	-9.814	Smith and Martell (1989)
$NaHCO_3$ (aq)	$Na^+ + HCO_3^- \leftrightarrow NaCO_3^-$	0.154	Smith and Martell (1989)
NaOH (aq)	$Na^+ + H_2O \leftrightarrow$ NaOH (aq) $+ H^+$	-14.205	Smith and Martell (1989)
$PuOH^{+++}$	$Pu^{4+} + H_2O \leftrightarrow PuOH^{3+} + H^+$	0.6	Neck and Kim (2001)
$Pu(OH)_2^{++}$	$Pu^{4+} + 2H_2O \leftrightarrow Pu(OH)_2^{2+} + 2H^+$	0.6	Neck and Kim (2001)
$Pu(OH)_3^+$	$Pu^{4+} + 3H_2O \leftrightarrow Pu(OH)_3^+ + 3H^+$	-2.3	Neck and Kim (2001)
$Pu(OH)_4$ (aq)	$Pu^{4+} + 4H_2O \leftrightarrow Pu(OH)_4$ (aq) $+ 4H^+$	-8.5	Neck and Kim (2001)
$Pu(CO3)_4^{----}$	$Pu^{4+} + 4HCO_3^- \leftrightarrow Pu(CO3)_4^{4-} + 4H^+$	-4.62	Guillaumont *et al.* (2003)
$Pu(CO3)_5^{(6-)}$	$Pu^{4+} + 5HCO_3^- \leftrightarrow Pu(CO3)_5^{(6-)} + 5H^+$	-16.3	Guillaumont *et al.* (2003)
PuO_2OH (aq)	$PuO_2^+ + H_2O \leftrightarrow PuO_2OH$ (aq) + H+	-9.73	Guillaumont *et al.* (2003)
$PuO_2CO_3^-$	$PuO_2^+ + HCO_3^- \leftrightarrow PuO_2CO_3^- + H^+$	-5.21	Guillaumont *et al.* (2003)
$PuO_2(CO_3)_3^{(5-)}$	$PuO_2^+ + 3HCO_3^- \leftrightarrow PuO_2(CO3)_3^{(5-)} + 3H^+$	-25.87	Guillaumont *et al.* (2003)
NpO_2OH (aq)	$NpO_2^+ + H_2O \leftrightarrow NpO_2OH$ (aq) + H+	-9.08	Guillaumont *et al.* (2003)
PuO_2^+	$Pu^{4+} + 0.25O_2$ (g) $+ 1.5H_2O \leftrightarrow PuO_2^+ + 3H^+$	3.32	Guillaumont *et al.* (2003)
$\equiv AlO^-$	$\equiv AlOH \leftrightarrow \equiv AlO^- + H^+$	-9.73	Turner (1995)
$\equiv AlOH_2^+$	$\equiv AlOH + H^+ \leftrightarrow \equiv AlOH_2^+$	8.33	Turner (1995)
$\equiv SiO^-$	$\equiv SiOH \leftrightarrow \equiv SiO^- + H^+$	-7.2	Turner (1995)
$\equiv SiOH_2^+$	$\equiv SiOH + H^+ \leftrightarrow \equiv SiOH_2^+$	1.93	Turner (1995)
$\equiv FeO^-$	$\equiv FeOH \leftrightarrow \equiv FeO^- + H^+$	-8.93	Turner (1995)
$\equiv FeOH_2^+$	$\equiv FeOH + H^+ \leftrightarrow \equiv FeOH_2^+$	7.29	Turner (1995)

Plutonium Sorption to Goethite

In 1985, Sanchez *et al.* examined Pu(IV) and Pu(V) sorption to goethite as a function of pH. The sorption profiles for initially Pu(IV) and initially Pu(V) systems on goethite are shown in **Figures 5.3** and **5.4**. The models shown in these figures were developed for this thesis.

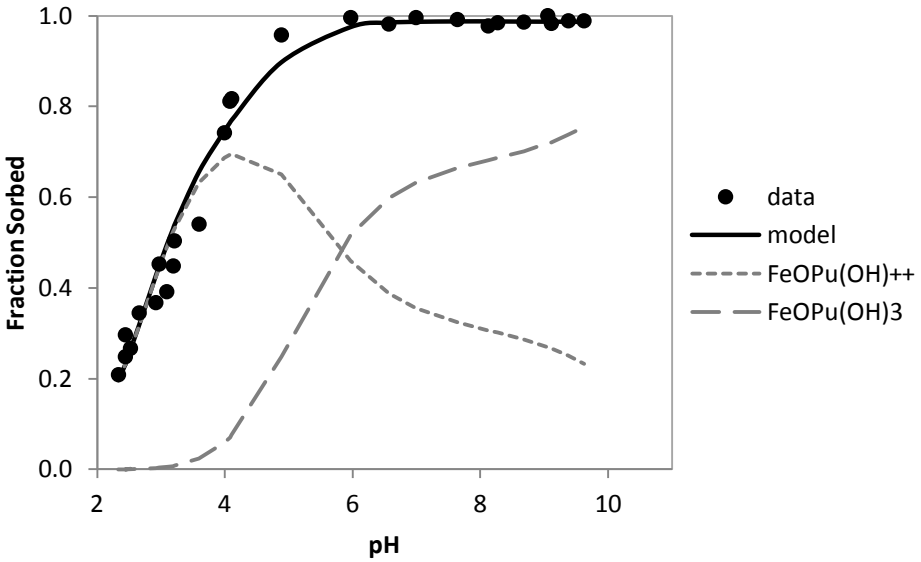

Figure 5.3. Sorption of Pu(IV) on goethite as a function of pH. Goethite surface area concentration of 28.5 m^2/L and ^{238}Pu concentration of 1 x 10^{-11} M in a 0.10 M $NaNO_3$ background. Data collected after a 96 hour equilibration period. Model produced stability constants of 12.94 for $FeOPu(OH)^{++}$ and -2.937 for $FeOPu(OH)_3$. Data from Sanchez *et al.* (1985).

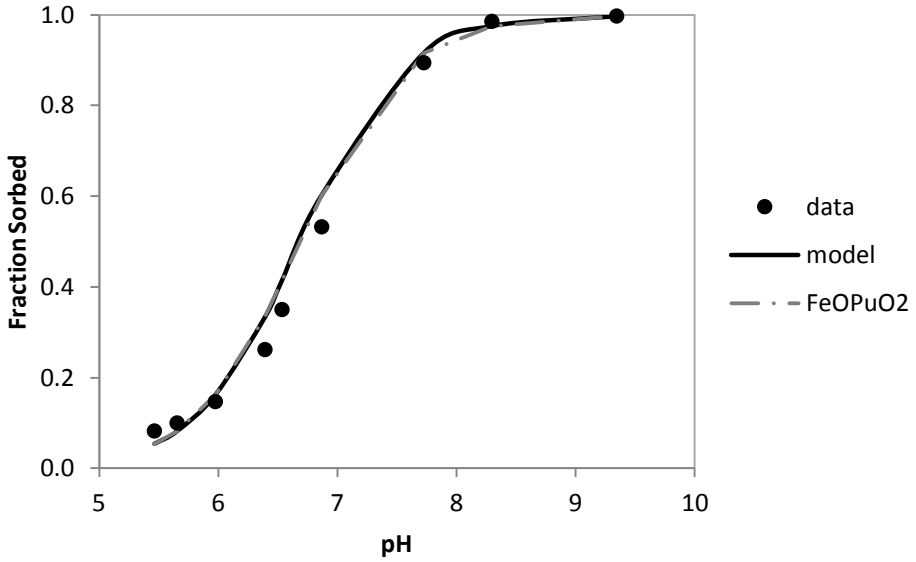

Figure 5.4. Sorption of Pu(V) on goethite as a function of pH. Goethite surface area concentration of 28.5 m^2/L and ^{238}Pu concentration of 1 x 10^{-11} M in a 0.10 M $NaNO_3$ background. Data collected after a 25 day equilibration period. Model produced stability constant of -2.885 for $FeOPuO_2$. Data from Sanchez *et al.* (1985).

The models shown were developed using FIT4FD, a modification of the program FITEQL. Two different sorption species were required to fit the Pu(IV) system; $FeOPu(OH)^{++}$ dominated at the lower pH values, while $FeOPu(OH)_3$ dominated at the higher pH values. Alternatively, the Pu(V) system required one sorption species, $FeOPuO_2$. The increasing sorption in these systems can be explained by (1) the changing plutonium sorption species and (2) the protonation and deprotonation of surface hydroxyl groups (Powell *et al.*, 2013a). Plutonium(IV) tends to sorb to mineral surfaces through the formation of complexes with surface hydroxyl groups. As a result, plutonium hydrolysis triggers the formation of various sorption species. The degree of hydrolysis varies with pH and produces sorption complexes like $FeOPu(OH)^{++}$ and $FeOPu(OH)_3$ (shown in **Figure 5.3**). Changes in surface charge affect the sorption of charged ions like PuO_2^+. As the pH of the solution increases, the surface sites transition from having a net

positive charge to having a net negative charge. Therefore, the PuO_2^+ species is repelled by the surface in acidic solutions, while the PuO_2^+ species is attracted to the surface in basic solutions (**Figure 5.4**).

Over time, Sanchez *et al.* (1985) observed a gradual increase in sorption for the initially Pu(V) system. They suggested that the shift in the adsorption edge resulted from the reduction of Pu(V) to Pu(IV). Sanchez *et al.* (1985) speculated that the Pu(V) was adsorbing to the goethite surface and subsequently reducing to Pu(IV). Therefore, more accurate models must consider oxidation state speciation. The coupled Pu(IV) and Pu(V) reaction can be seen below:

Uncoupled

$$\equiv FeOH + Pu^{4+} + H_2O \leftrightarrow \equiv FeOPu(OH)^{2+} + 2H^+$$

$$\equiv FeOH + PuO_2^+ \leftrightarrow \equiv FeOPuO_2 + H^+$$

Coupled

$$\equiv FeOH + Pu^{4+} + 0.25O_2\,(g) + 1.5H_2O \leftrightarrow \equiv FeOPuO_2 + 4H^+$$

Figure 5.5a below illustrates the sorption profile for coupled Pu(IV) and Pu(V) on goethite. **Figure 5.5b** depicts the aqueous system for this profile. This model utilized pO_2 (g) to couple Pu(IV) and Pu(V), because E_H measurements were not recorded during the sampling event. (Alternatively, the other models used E_H measurements to couple the two reactions.) The model revealed Pu(IV) as the dominant sorption species and Pu(V) as the dominant aqueous species. This coupled system provided stability constants that were used to model the Hanford experimental data.

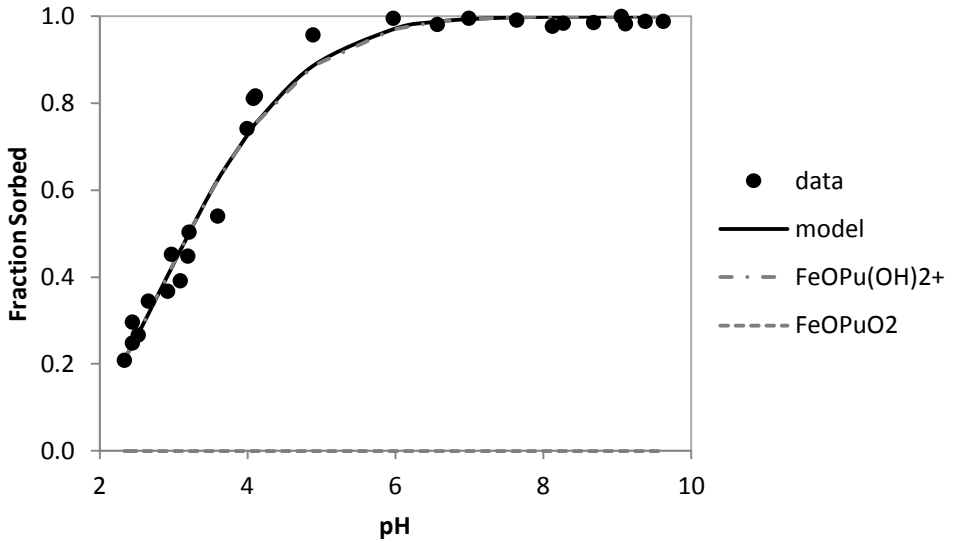

Figure 5.5a. Sorption of coupled Pu(IV) and Pu(V) on goethite as a function of pH. Goethite surface area concentration of 28.5 m^2/L and ^{238}Pu concentration of 1 x 10^{-11} M in a 0.10 M $NaNO_3$ background. Data collected after a 96 hour equilibration period. Model produced stability constants of 7.549 for $FeOPu(OH)_2^+$ and 0.435 for $FeOPuO_2$. Data from Sanchez *et al.* (1985).

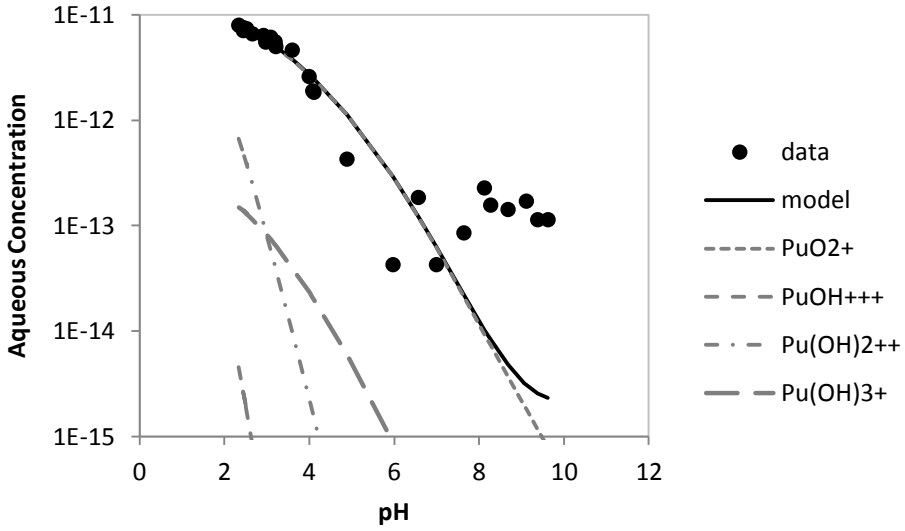

Figure 5.5b. Aqueous species present in the coupled Pu(IV) and Pu(V) on goethite system. The modeled fraction of each species is shown with dashed lines; only species with a contribution of 1 x 10^{-15} M or greater are shown. Data from Sanchez *et al.* (1985).

Plutonium Sorption to Aluminosilicates

In a 2013 paper, Powell *et al.* examined Pu(IV) and Pu(V) interactions with silica and gibbsite as a function of pH. The sorption of Pu(IV) and Pu(V) to both minerals increased with pH. As expected, the Pu(IV) system exhibited a greater degree of sorption than the Pu(V) system. The strong hydrolysis of Pu(IV) resulted in significant plutonium sorption, even at low pH values.

Effects of carbonate on the system were also examined, and several datasets were generated under CO_2 (g) free and CO_2 (g) equilibrated conditions. Powell *et al.* (2013a) observed changes in Pu(V) sorption in the presence of carbonate. While sorption of Pu(V) steadily increased in the carbonate-free system, a diversion in sorption behavior arose in the carbonate-equilibrated system. At high pH values, anionic plutonyl-carbonate species (such as $PuO_2CO_3^-$) formed and remained in the aqueous phase, resulting in decreased Pu(V) sorption (Powell *et al.*, 2013a). Similar behavior at high pH values was not observed for the Pu(IV) systems. The strength of Pu(IV) hydrolysis outweighed the strength of carbonate complexation; as a result, the formation of Pu(IV)-carbonate species required high carbonate concentrations.

Additionally, Powell *et al.* (2013a) observed an increase in Pu(V) sorption with time. The Pu(V) sorption edge drifted between sampling events; the slope of the edge decreased and more closely resembled the sorption profile for Pu(IV). Presumably, the Pu(V) sorption edge would eventually align with the Pu(IV) sorption edge (Powell *et al.*, 2013a). The observed shift in sorption indicated the reduction of Pu(V) to Pu(IV).

Stability constants for carbonate-free and carbonate-equilibrated systems were determined for both oxidation states and minerals. **Figures 5.6a** and **5.7a** show the sorption profiles for the carbonate-equilibrated Pu(IV) and Pu(V) mineral systems. **Figures 5.6b** and **5.7b** exhibit the aqueous phase concentrations for these systems.

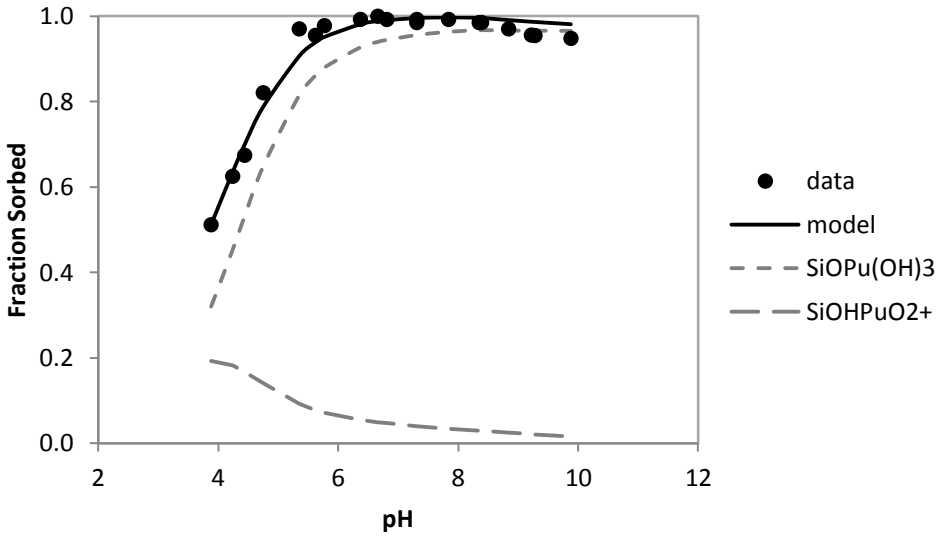

Figure 5.6a. Sorption of coupled Pu(IV) and Pu(V) on silica as a function of pH within a carbonate-equilibrated system. Silica surface area concentration of 10 m^2/L and ^{238}Pu concentration of 1.35 x 10^{-10} M in a 0.01 M NaCl background. Data collected after a 62 day equilibration period. Model produced stability constants of 8.684 x 10^{-2} for $SiOPu(OH)_3$ and 7.54 for $SiOHPuO_2^+$. Data and model from Powell *et al.* (2013b).

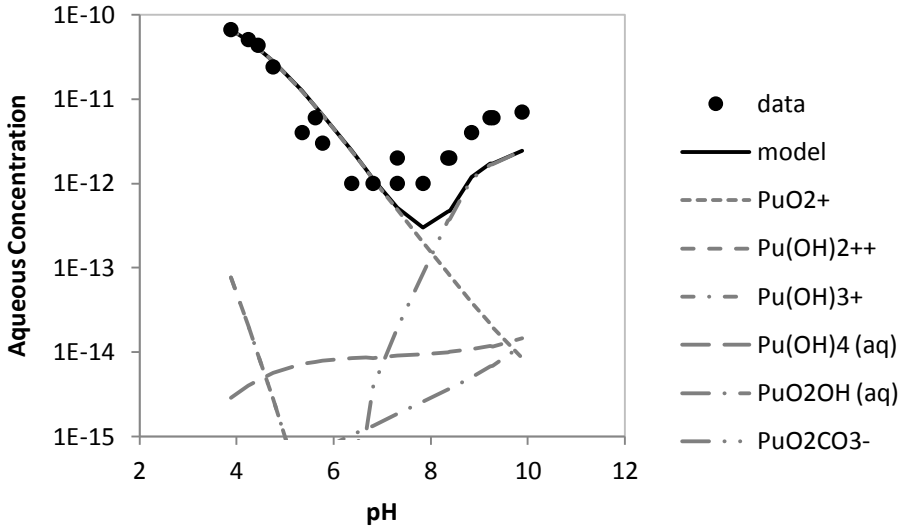

Figure 5.6b. Aqueous species present in the coupled Pu(IV) and Pu(V) on silica system. The modeled fraction of each species is shown with dashed lines; only species with a contribution of 1 x 10^{-15} M or greater are shown. Data and model from Powell *et al.* (2013b).

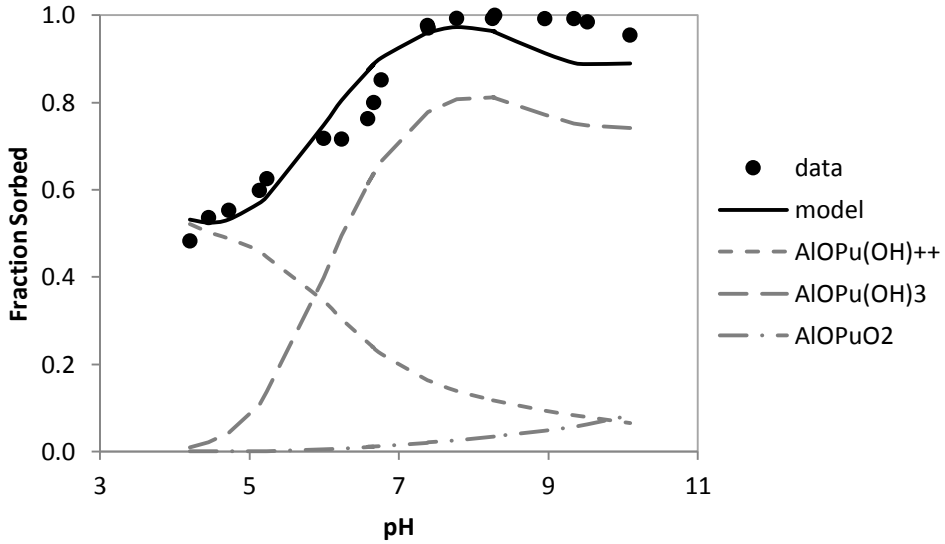

Figure 5.7a. Sorption of coupled Pu(IV) and Pu(V) on gibbsite as a function of pH within a carbonate-equilibrated system. Gibbsite surface area concentration of 10 m^2/L and ^{238}Pu concentration of 1.34 x 10^{-10} M in a 0.01 M NaCl background. Data collected after a 62 day equilibration period. Model produced stability constants of 16.19 for $AlOPu(OH)^{++}$, -0.9479 for $AlOPu(OH)_3$, and 0.23 for $AlOPuO_2$. Data and model from Powell *et al.* (2013b).

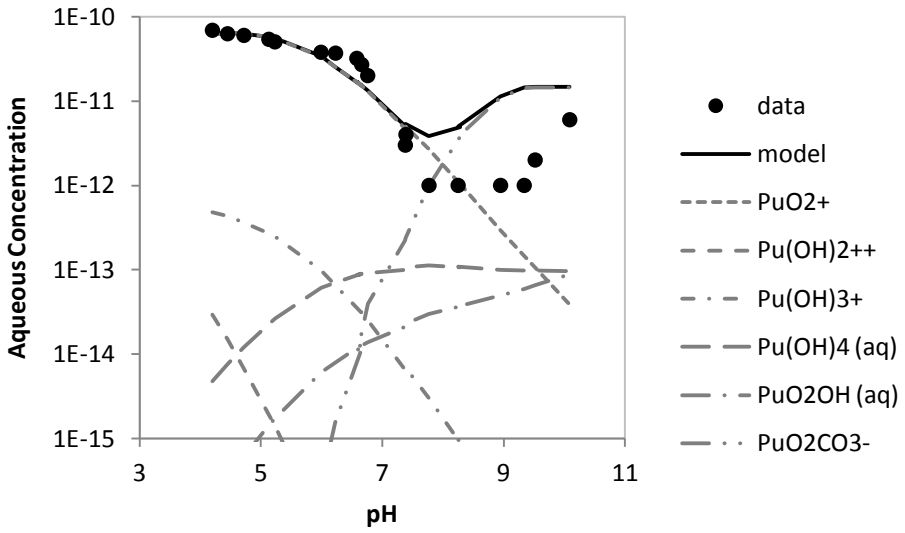

Figure 5.7b. Aqueous species present in the coupled Pu(IV) and Pu(V) on gibbsite system. The modeled fraction of each species is shown with dashed lines; only species with a contribution of 1 x 10^{-15} M or greater are shown. Data and model from Powell *et al.* (2013b).

Batch Sorption Experiments with Hanford Sediments

Batch sorption experiments were performed using ^{242}Pu and ^{237}Np with pristine coarse- and fine-grained sediments. **Figure 5.8a** shows the sorption profile for an initially Pu(V) and Np(V) system on 100 g/L of pristine, coarse-grained soil. Alternatively, **Figure 5.8b** shows the sorption profile for an initially Pu(V) and Np(V) system on 100 g/L of pristine, fine-grained soil. Significant sorption to the sediment occurred in both systems; typically, the fraction sorbed increased with pH. The stronger adsorption of plutonium at lower pH values relative to the Np(V) system indicated the reduction of Pu(V) to Pu(IV). The decrease in plutonium sorption with increasing pH was due to the influences of carbonate. This is discussed in detail below.

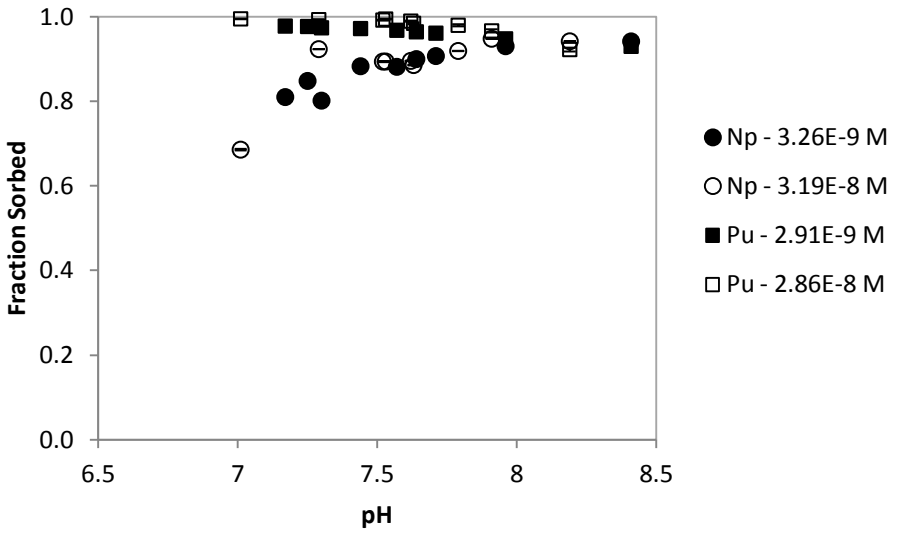

Figure 5.8a. Sorption of initially Pu(V) and Np(V) on coarse, pristine Hanford sediment as a function of pH. Sediment concentration of 100 g/L in a 0.01 M NaCl background. Data collected after a 30 day equilibration period.

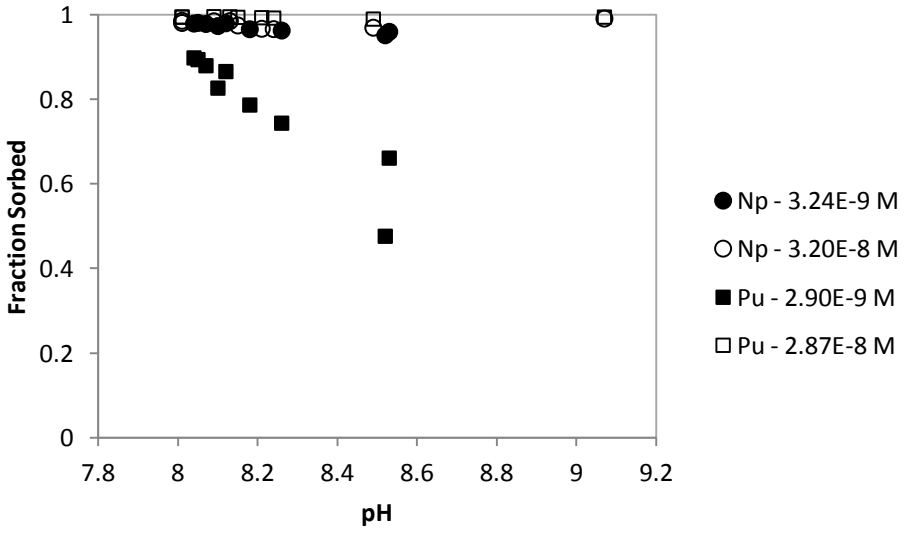

Figure 5.8b. Sorption of initially Pu(V) and Np(V) on fine, pristine Hanford sediment as a function of pH. Sediment concentration of 100 g/L in a 0.01 M NaCl background. Data collected after a 30 day equilibration period.

These samples were initially set to span a pH range from 4 to 10. After a week of mixing, however, the solutions did not remain at the desired pH values. This fluctuation was most likely due to the dissolution of carbonate-bearing minerals and the subsequent buffering of the solutions. This effect was exacerbated by the high soil concentration within this sample set. The buffering capacity of the sediment could have played a significant role in the downward migration of plutonium at the Hanford Reservation. The coarse-grained sediment may have neutralized the highly acidic, plutonium-bearing waste stream. Once the waste stream reached the fine-grained soil, the solution pH was comparable to the surrounding pore water pH. As a result, the plutonium sorbed to the fine-grained sediment after passing through the coarse-grained soil. Thus, the low influent pH could explain the enhanced actinide mobility observed at the site.

In order to produce distinct sorption profiles with minimal acid and base addition, the sediment concentrations were reduced from 100 g/L to 25 g/L, and the experiments were run again. This adjustment decreased the number of available sorption sites and thereby decreased the degree of sorption. **Figures 5.9a** and **5.9b** show the sorption profiles for an initially Pu(V) and Np(V) system on 25 g/L of pristine, coarse- and fine-grained sediment, respectively.

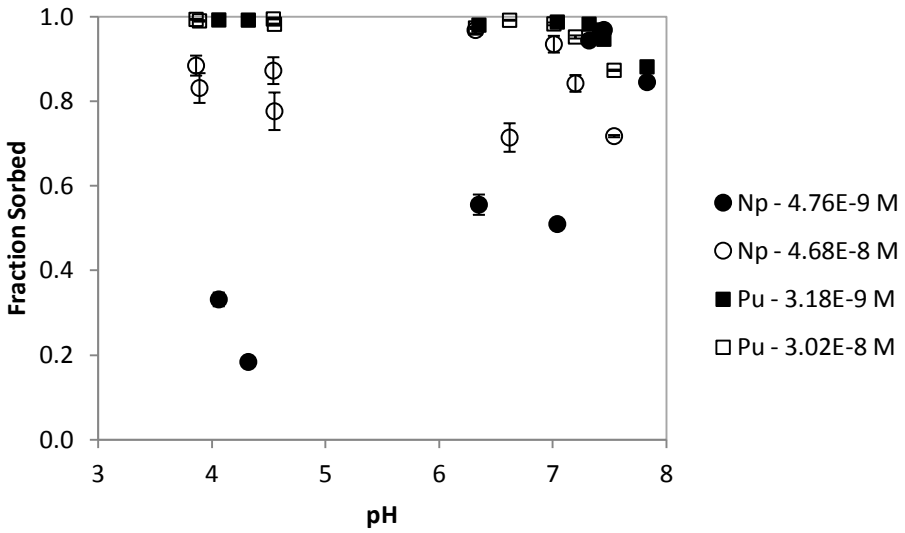

Figure 5.9a. Sorption of initially Pu(V) and Np(V) on coarse, pristine Hanford sediment as a function of pH. Sediment concentration of 25 g/L in a 0.01 M NaCl background. Data collected after a 30 day equilibration period.

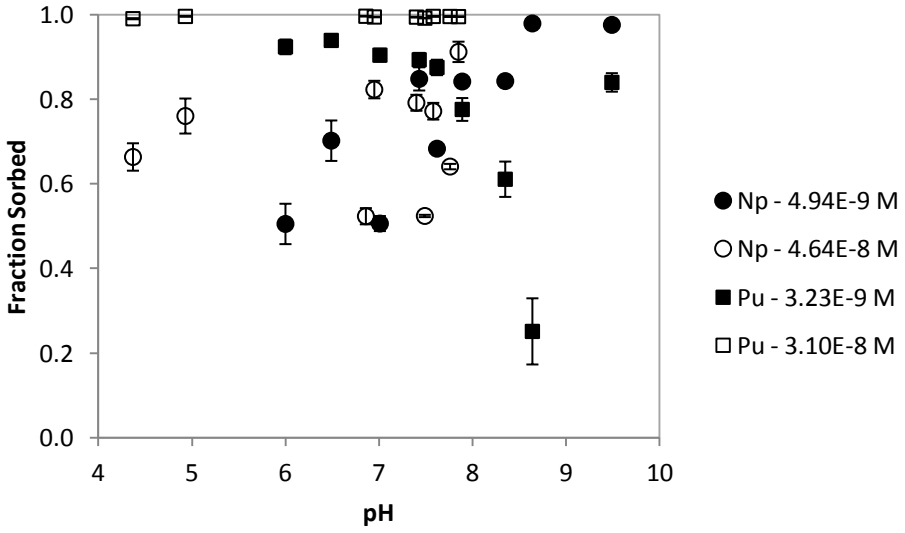

Figure 5.9b. Sorption of initially Pu(V) and Np(V) on fine, pristine Hanford sediment as a function of pH. Sediment concentration of 25 g/L in a 0.01 M NaCl background. Data collected after a 30 day equilibration period.

Again, the fraction sorbed generally increased with pH for both plutonium and neptunium. Plutonium's sorption curve, however, did not complement neptunium's sorption curve. The increased sorption of plutonium in the initially Pu(V) system suggested the surface-mediated reduction of Pu(V) to Pu(IV). The obvious scatter in the datasets may have been an experimental artifact related to the large amount of acid added to the system to achieve the low pH values. This addition likely caused mineral dissolution within the system. As a result, potentially complexing (carbonate) and competing (calcium, iron) ions would be released into solution. Additionally, the possibility could arise for the production of "new" surface sites resulting from the dissolution of the initial surface sites; these sites may be highly reactive and heterogeneously distributed. These points could help explain the scatter seen in the neptunium dataset. If similar processes were occurring within the Hanford 200 area subsurface, modification of the sediment through interaction with the low pH influent could be a potential mechanism for the observed plutonium transport.

Figures 5.10a and **5.10b** show the sorption profiles for an initially Pu(V) and Np(V) system on 25 g/L of leached, coarse- and fine-grained sediment, respectively. As previously seen, the fraction sorbed increased with pH. Again, the strong sorption of plutonium relative to neptunium indicated Pu(V) reduction to Pu(IV).

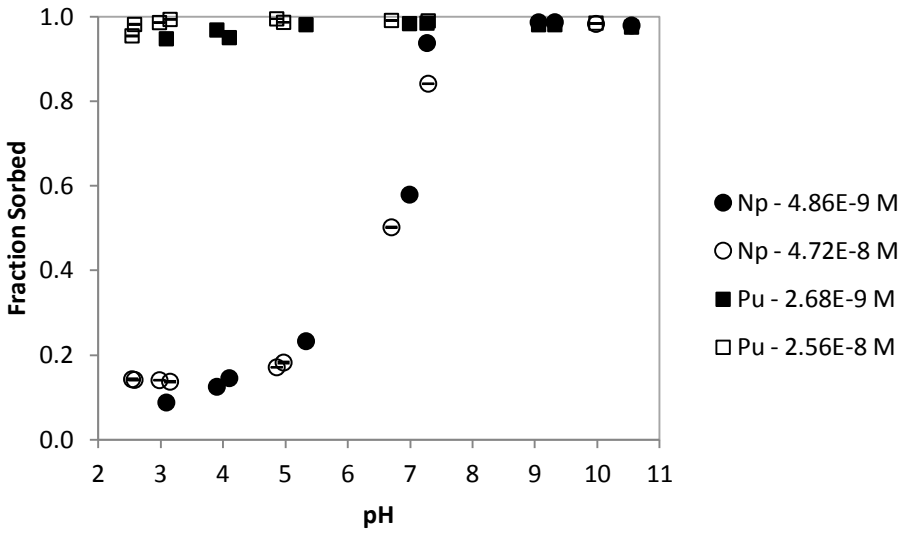

Figure 5.10a. Sorption of initially Pu(V) and Np(V) on coarse, leached Hanford sediment as a function of pH. Sediment concentration of 25 g/L in a 0.01 M NaCl background. Data collected after a 30 day equilibration period.

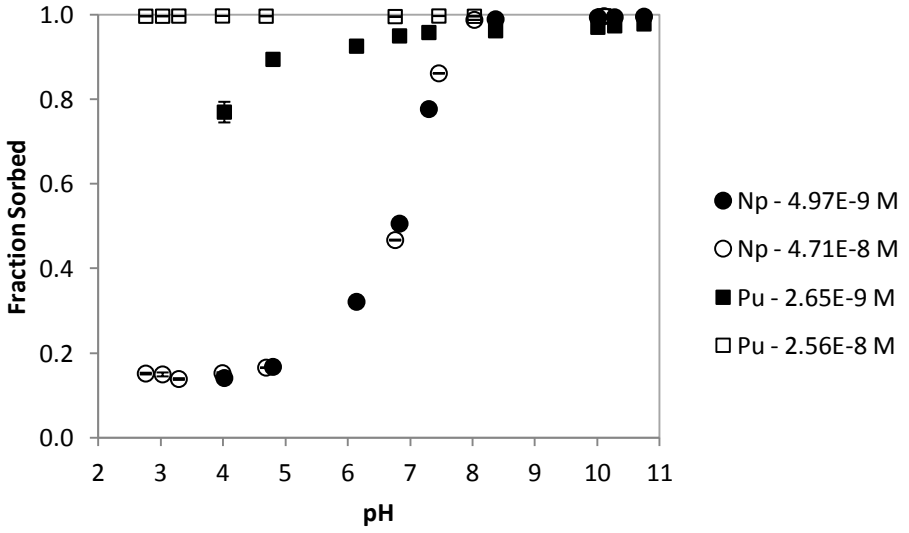

Figure 5.10b. Sorption of initially Pu(V) and Np(V) on fine, leached Hanford sediment as a function of pH. Sediment concentration of 25 g/L in a 0.01 M NaCl background. Data collected after a 30 day equilibration period.

The removal of carbonate-bearing minerals resulted in slightly reduced sorption for both actinides. Also, the trends observed in these data more closely resembled traditional sorption edges. Therefore, the proposed influence of dissolved ions generated by acidification of the pristine sample (discussed above) may explain the source of scatter in **Figures 5.10a** and **5.10b**. When acid leaching the soils, the leachate water was decanted, and the dissolved ions were removed from solution.

Oxidation State Analysis

In order to better understand the behavior of plutonium in these systems, additional samples were prepared at high pH ranges. Ten samples were produced for this analysis--five with pristine, coarse-grained sediment and five with pristine, fine-grained sediment. In order to more quickly achieve thermodynamic equilibrium, Pu(IV) rather than Pu(V) was spiked into solutions containing 25 g/L of the appropriate sediment. **Figures 5.11** and **5.12** show the sorption curves for these systems.

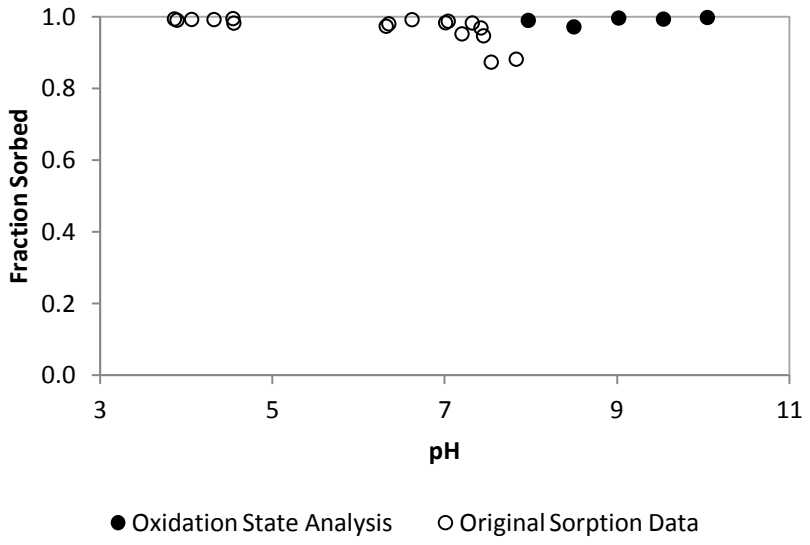

Figure 5.11. Sorption results for ^{238}Pu on pristine, coarse-grained Hanford sediment including original sorption data and additional samples for oxidation state analysis. Sediment concentration of 25 g/L and ^{238}Pu concentration of 1.31×10^{-10} M (1200 cpm/mL) in a 0.01 M NaCl background. Data collected after a 30 day equilibration period.

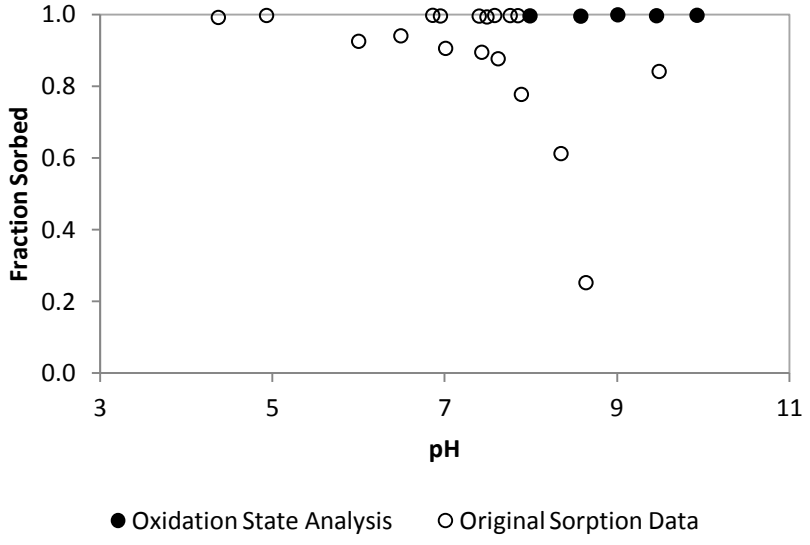

Figure 5.12. Sorption results for ^{238}Pu on pristine, fine-grained Hanford sediment including original sorption data and additional samples for oxidation state analysis. Sediment concentration of 25 g/L and ^{238}Pu concentration of 1.31×10^{-10} M (1200 cpm/mL) in a 0.01 M NaCl background. Data collected after a 30 day equilibration period.

These additional data points appeared to follow the sorption scheme from the original data set. The batch sorption experiment used ^{242}Pu, while the oxidation state analysis used ^{238}Pu. Therefore, the concentration of plutonium in both systems varied by as much as two orders of magnitude. Also, while Pu(V) was spiked into the original experiment, Pu(IV) was utilized in the oxidation state analysis. These points suggested that both experiments reached a similar thermodynamic endpoint.

Figure 5.13 shows the results from the oxidation state analysis of the aqueous phase for the additional ten samples. The results from this analysis were later compared to the model outputs. Both coarse- and fine-grained systems contained Pu(IV) and Pu(V) in the aqueous phase. The presence of Pu(IV) with relatively high aqueous phase concentration was surprising given the strong sorption affinity of Pu(IV) for mineral surfaces. Therefore, complexation with carbonate likely caused the solubilization of Pu(IV). Following the same logic of this conceptual model, the increase in sorption above pH 9 likely represented competition between carbonate and hydroxide for Pu(IV). As the pH (and hydroxide concentration) increased, the hydroxide species became more favorable, prevented formation of the Pu(IV)-carbonate complexes, and resulted in sorption of Pu(IV).

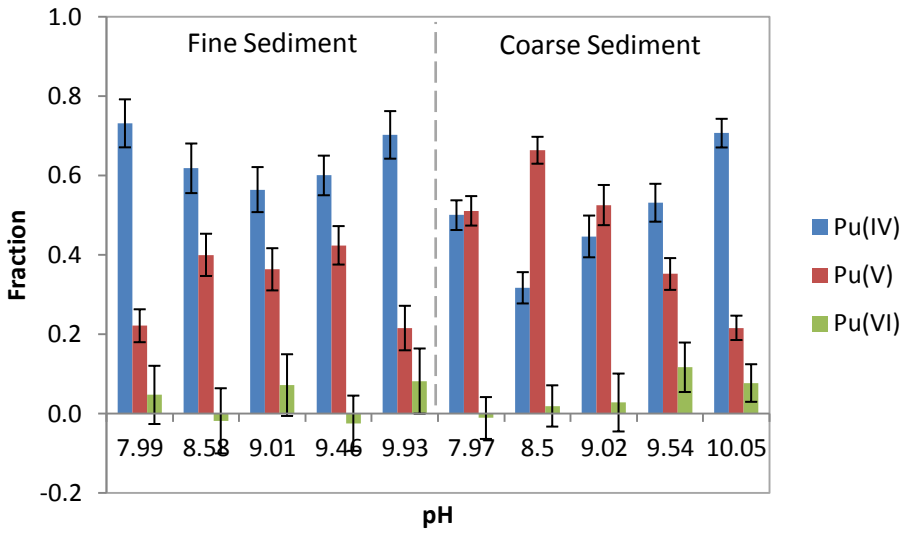

Figure 5.13. Oxidation state analysis results for ^{238}Pu on pristine, fine- and coarse-grained Hanford sediments as a function of pH. Results for the aqueous phase. Sediment concentration of 25 g/L and ^{238}Pu concentration of 1.31×10^{-10} M (1200 cpm/mL) in a 0.01 M NaCl background. Data collected after a 30 day equilibration period.

Modeling Approach

In the model, surface sites were represented by a generic ≡SOH, where S denoted either Al, Si, or Fe. These surface sites were allowed to protonate and deprotonate based on pH to become $\equiv SOH_2^+$ and $\equiv SO^-$, respectively. Surface site concentrations were varied in order to fit the batch sorption data. The estimates of the percent active area used for each surface in each of the eleven models are shown in **Table 5.3**.

Table 5.3. Mineral concentrations used for each model.

Model Number	Silica Fraction		Gibbsite Fraction		Goethite Fraction	
	Coarse	*Fine*	*Coarse*	*Fine*	*Coarse*	*Fine*
1a	0.01%	0.26%	0.01%	0.26%	0.2%	0.32%
1b	0.05%	1.3%	0.05%	1.3%	0.2%	0.32%
1c	0.1%	2.6%	0.1%	2.6%	0.2%	0.32%
2a	0.1%	2.6%	0.1%	2.6%	0.02%	0.032%
2b	0.1%	2.6%	0.1%	2.6%	2.0%	3.2%
3	0.001%	0.026%	0.001%	0.026%	0.2%	0.32%
4a	0.01%	0.26%	0.01%	0.26%	0.02%	0.032%
4b	0.01%	0.26%	0.01%	0.26%	0.002%	0.0032%
5a	0.001%	0.026%	0.001%	0.026%	0.02%	0.032%
5b	0.001%	0.026%	0.001%	0.026%	0.002%	0.0032%

These percentages were translated into molar concentrations for the modeling process. For example, the concentrations used in Model 1a for the coarse-grained sediment were determined as follows:

Silica $$\frac{25\ g}{L}\cdot\frac{28.56\ m^2}{g}\cdot\left(\frac{1E9\ nm}{m}\right)^2\cdot\frac{2.3\ sites}{nm^2}\cdot\frac{mol}{6.022E23\ sites}\cdot 0.01\%\cdot 66\% = 1.80E-7\ M$$

Gibbsite $$\frac{25\ g}{L}\cdot\frac{28.56\ m^2}{g}\cdot\left(\frac{1E9\ nm}{m}\right)^2\cdot\frac{2.3\ sites}{nm^2}\cdot\frac{mol}{6.022E23\ sites}\cdot 0.01\%\cdot 33\% = 8.99E-8\ M$$

Goethite $$\frac{25\ g}{L}\cdot\frac{28.56\ m^2}{g}\cdot\left(\frac{1E9\ nm}{m}\right)^2\cdot\frac{2.3\ sites}{nm^2}\cdot\frac{mol}{6.022E23\ sites}\cdot 0.20\% = 5.45E-6\ M$$

The clay portions of the sediments contained silica-gibbsite-silica layers. As a result, two thirds of the sorption edges incorporated silica, while one-third of the edges incorporated gibbsite. This accounted for the 66% and 33% in the silica and gibbsite calculations, respectively. All models were constructed with the appropriate stability constants and sediment concentrations.

Additionally, models containing the Pu(IV)/Pu(V) redox couple required an O_2 (g) fugacity term. It is possible to estimate fugacity from redox measurements.

Unfortunately, these measurements were not made at the time of sampling. An empirical equation, however, can be derived from pH and E_H measurements. In order to acquire these measurements, additional suspensions were prepared using the pristine, fine- and coarse-grained sediments. **Figure 5.14** shows the measured redox potentials versus the pH of the suspensions.

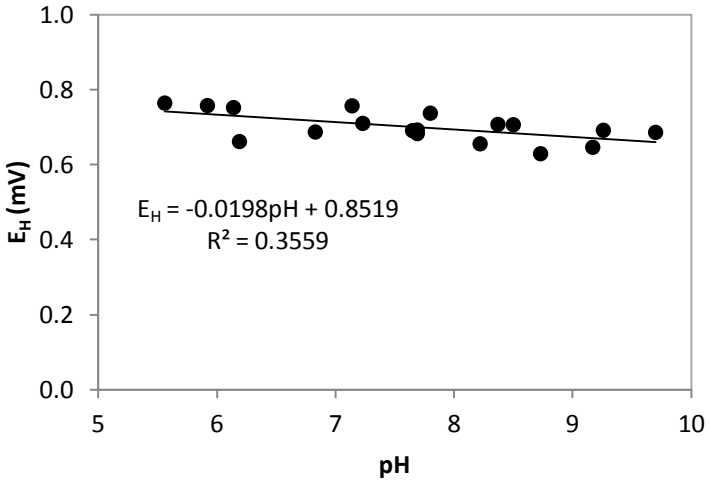

Figure 5.14. Measured redox potential versus suspension pH. Sediment concentration of 25 g/L in a 0.01 M NaCl background. Data collected after a 30 day equilibration period.

This empirical equation was combined with these two relationships:

$$¼O_2\,(g) + H^+ + e^- \leftrightarrow ½H_2O \qquad \log K = 20.75$$

$$pe = \frac{E_H F}{2.3RT}$$

Ultimately, the log O_2 (g) fugacity for each sample was calculated from the sample pH.

$$\log O_2\,(g) = 2.659pH - 28.195$$

Also, all models using pristine sediments required values for dissolved CO_2 (g). A total carbon analysis was completed on a set of suspensions containing pristine, coarse-

and fine-grained sediments. **Figure 5.15** reveals the results from this analysis in terms of total carbonate and pH.

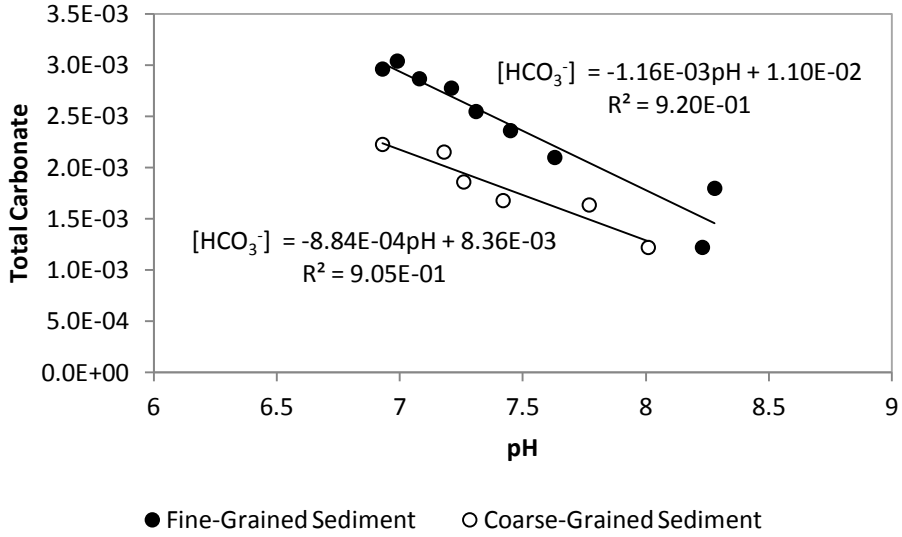

Figure 5.15. Measured total carbonate concentration versus suspension pH. Sediment concentration of 25 g/L in a 0.01 M NaCl background. Data collected after a 30 day equilibration period.

The resulting equations were used in the modeling process.

The best fit for each model, given the conditions presented in **Table 5.4**, was determined by the weighted sum of squares. **Table 5.4** outlines the most appropriate model for all nuclide-sediment combinations. Even though different models were selected for the various combinations, sediment concentrations generally remained within two orders of magnitude. For example, the best fits for the Pu(IV) on coarse sediments only varied by goethite concentration.

The following figures illustrate the best fit models for the coarse sediment combinations (see **Appendix B** for the fine sediment models). Models are shown as solid black lines, while specific sorbed species are represented by the dashed colored lines.

Figures depicting the appropriate aqueous system follow each model; these figures are invaluable when examining the models with great than 95% sorption due to the difficulties in noting model accuracy for strongly sorbed ions when plotted as “fraction sorbed”.

Table 5.4. Best fit models for each soil and actinide combination.

Radionuclide	Soil Type	Silica Fraction	Gibbsite Fraction	Goethite Fraction	Model Number
Pu(IV)	Coarse, Leached	0.1%	0.1%	2.0%	2b
	Coarse, Pristine	0.1%	0.1%	0.2%	1c
	Fine, Leached	2.6%	2.6%	3.2%	2b
	Fine, Pristine	0.26%	0.26%	0.032%	4a
Np(V)	Coarse, Leached	0.1%	0.1%	2.0%	2b
	Coarse, Pristine	0.1%	0.1%	2.0%	2b
	Fine, Leached	2.6%	2.6%	3.2%	2b
	Fine, Pristine	2.6%	2.6%	3.2%	2b
Pu(IV) - Pu(V)	Coarse, Leached	0.1%	0.1%	2.0%	2b
	Coarse, Pristine	0.1%	0.1%	0.02%	2a
	Fine, Leached	2.6%	2.6%	3.2%	2b
	Fine, Pristine	0.26%	0.26%	0.0032%	4b

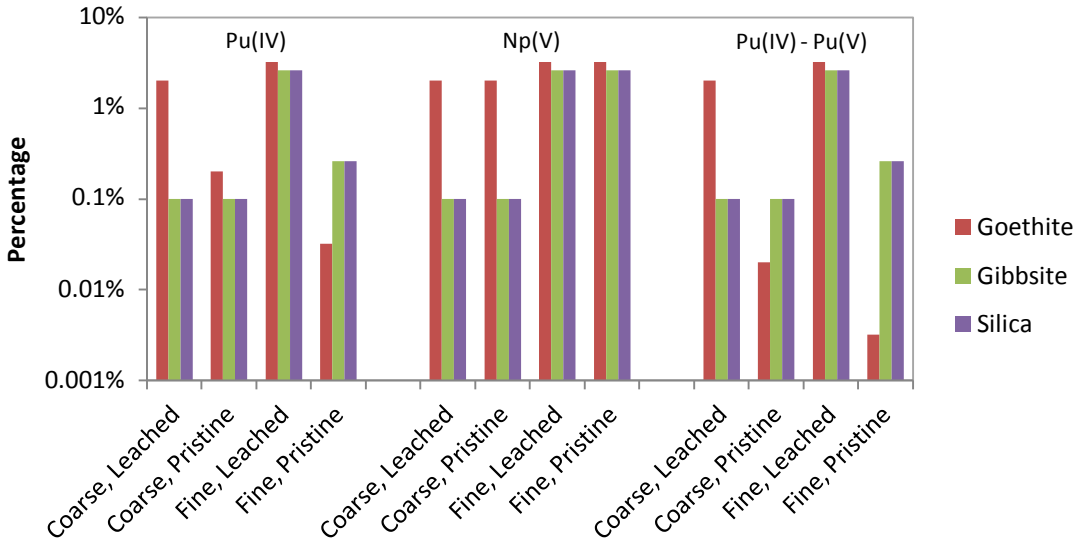

Figure 5.16. Best fit models for each soil and actinide combination.

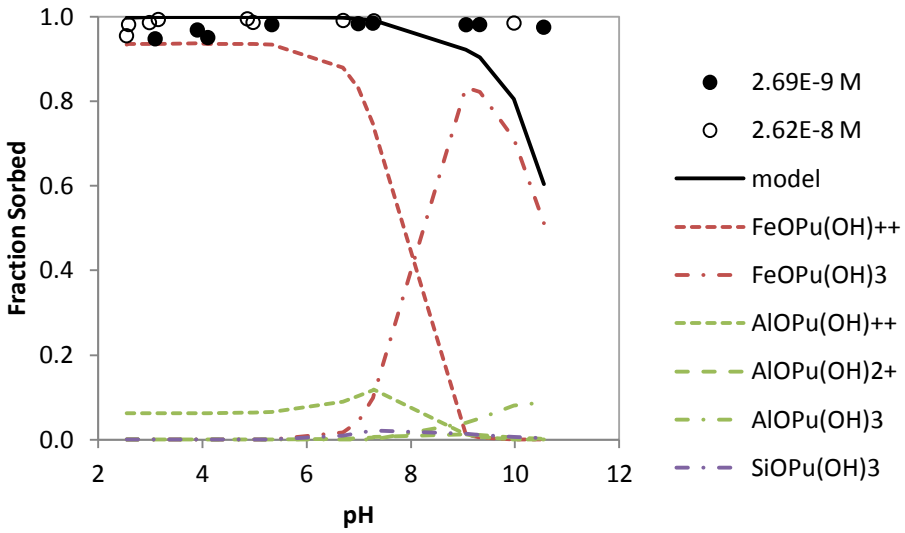

Figure 5.17a. Sorption of Pu(IV) on coarse, leached Hanford sediment with model fit (M2b). The model uses 0.1% gibbsite and silica with 2.0% goethite. The modeled fraction of each species is shown with dashed lines; only species with a contribution of 1% or greater are shown.

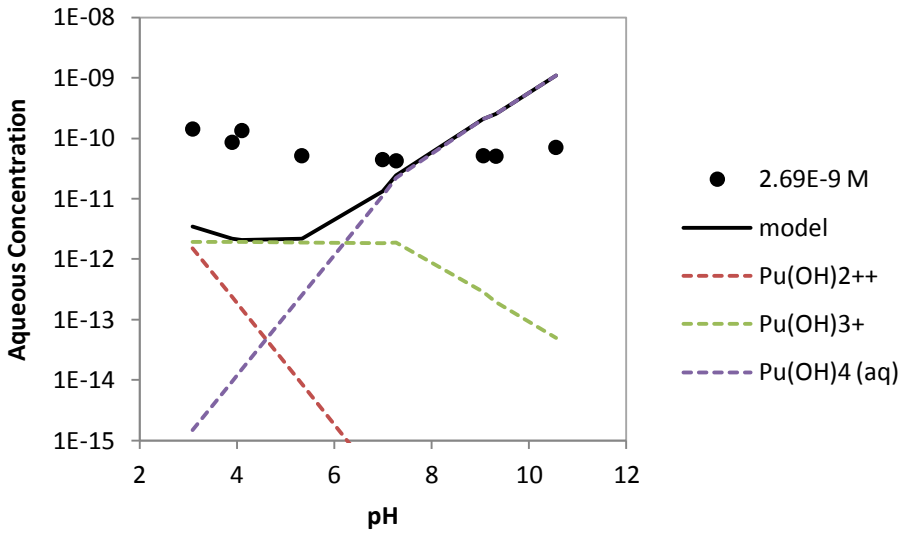

Figure 5.17b. Aqueous species present in the Pu(IV) on coarse, leached Hanford sediment experiment with model fit (M2b). The modeled fraction of each species is shown with dashed lines; only species with a contribution of 1 x 10^{-15} M or greater are shown.

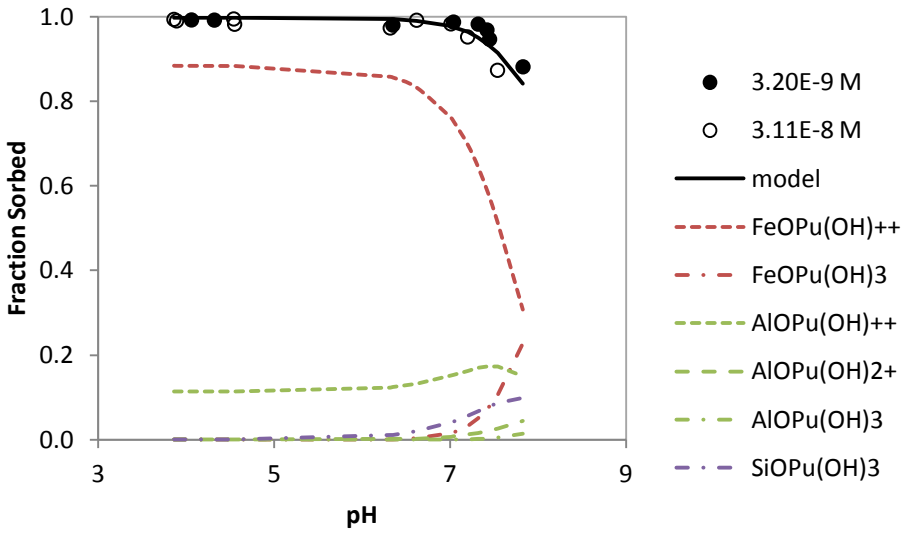

Figure 5.18a. Sorption of Pu(IV) on coarse, pristine Hanford sediment with model fit (M1c). The model uses 0.1% gibbsite and silica with 0.2% goethite. The modeled fraction of each species is shown with dashed lines; only species with a contribution of 1% or greater are shown.

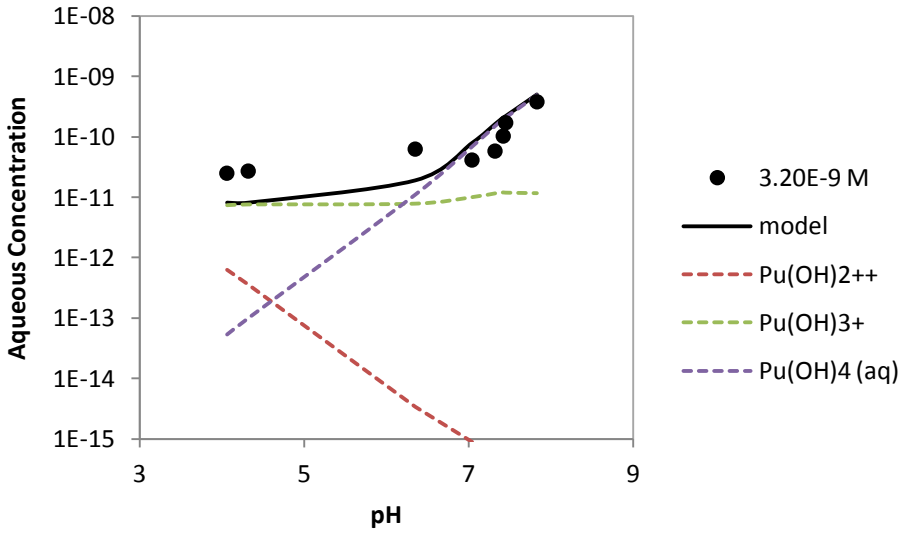

Figure 5.18b. Aqueous species present in the Pu(IV) on coarse, pristine Hanford sediment experiment with model fit (M1c). The modeled fraction of each species is shown with dashed lines; only species with a contribution of 1 x 10^{-15} M or greater are shown.

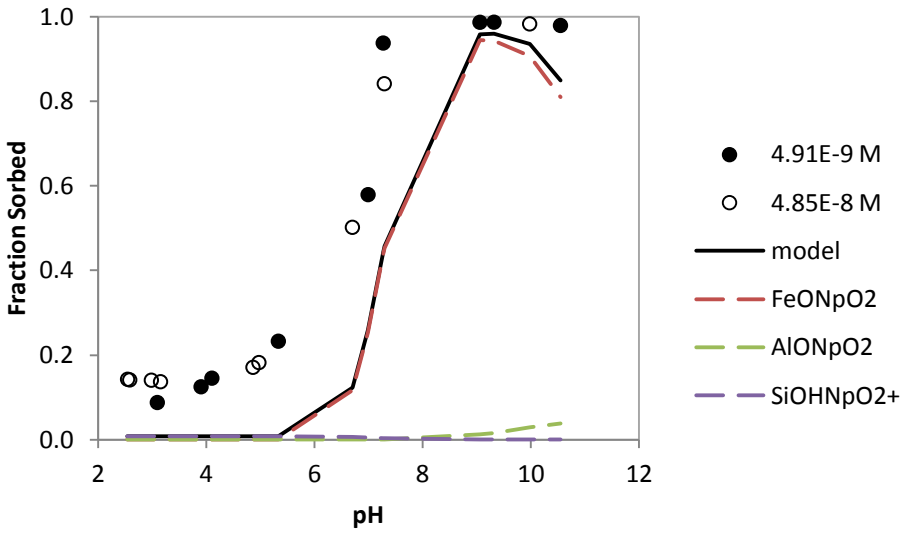

Figure 5.19a. Sorption of Np(V) on coarse, leached Hanford sediment with model fit (M2b). The model uses 0.1% gibbsite and silica with 2.0% goethite. The modeled fraction of each species is shown with dashed lines; only species with a contribution of 1% or greater are shown.

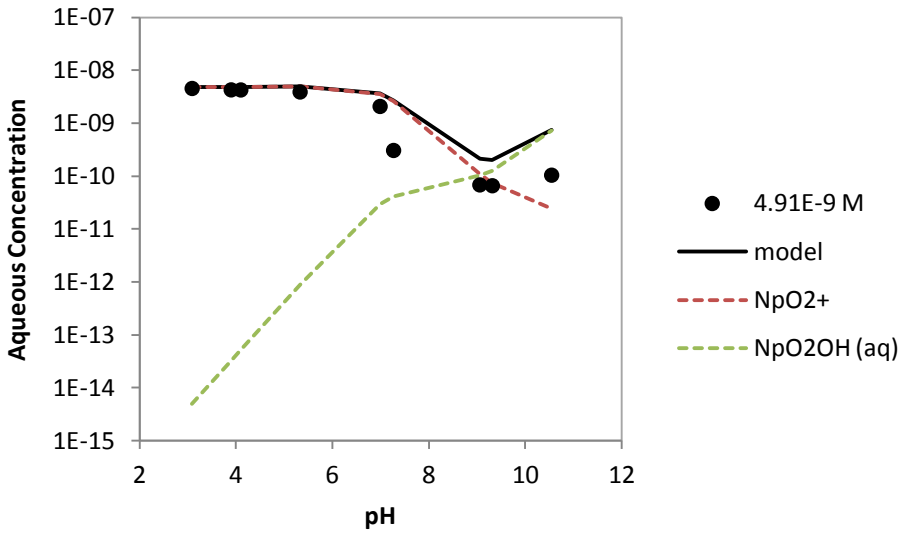

Figure 5.19b. Aqueous species present in the Np(V) on coarse, leached Hanford sediment experiment with model fit (M2b). The modeled fraction of each species is shown with dashed lines; only species with a contribution of 1 x 10^{-15} M or greater are shown.

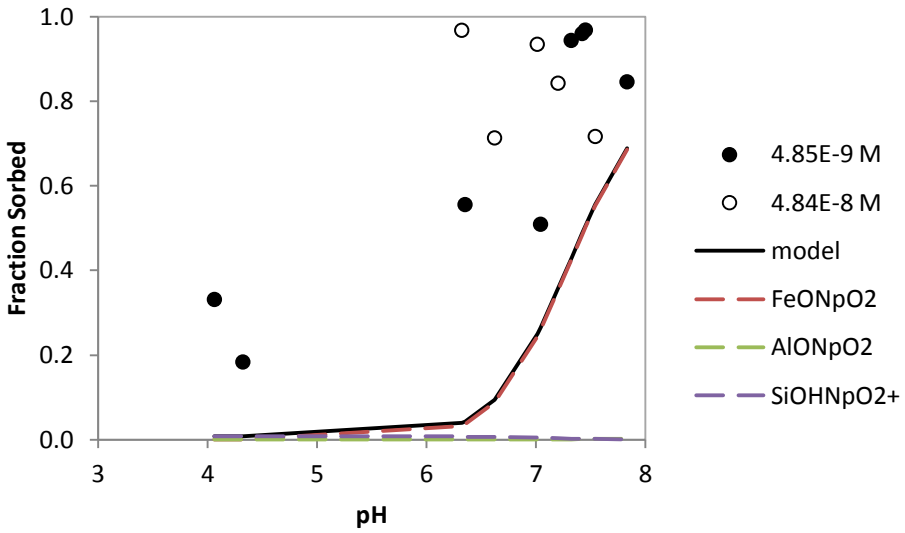

Figure 5.20a. Sorption of Np(V) on coarse, pristine Hanford sediment with model fit (M2b). The model uses 0.1% gibbsite and silica with 2.0% goethite. The modeled fraction of each species is shown with dashed lines; only species with a contribution of 1% or greater are shown.

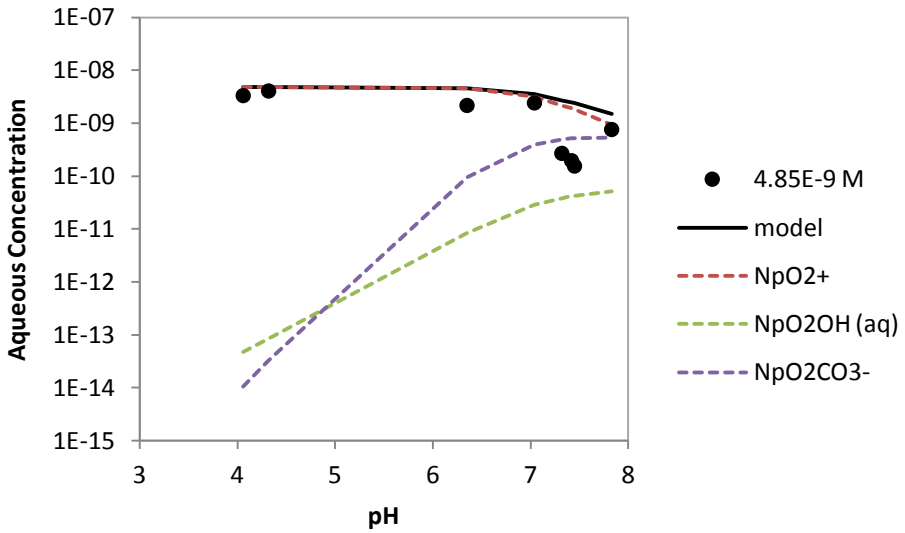

Figure 5.20b. Aqueous species present in the Np(V) on coarse, pristine Hanford sediment experiment with model fit (M2b). The modeled fraction of each species is shown with dashed lines; only species with a contribution of 1 x 10^{-15} M or greater are shown.

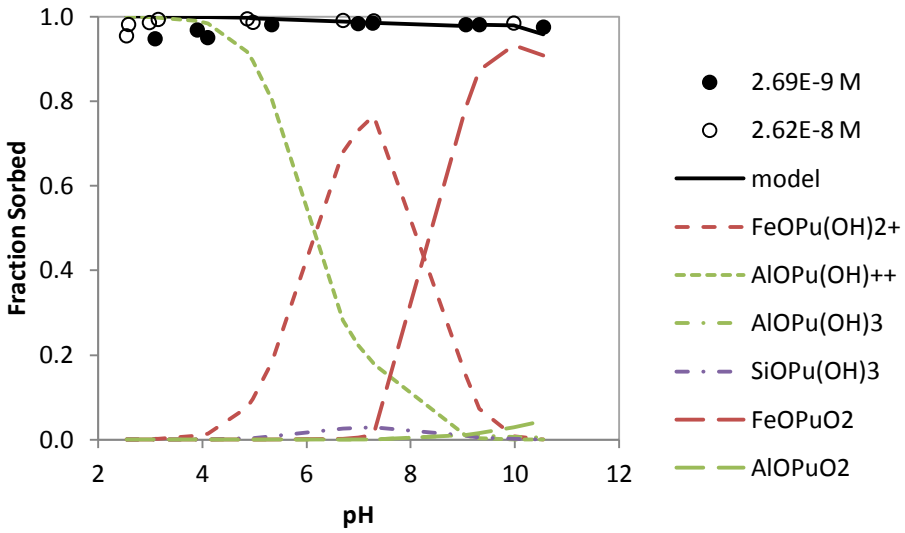

Figure 5.21a. Sorption of coupled Pu(IV) and Pu(V) on coarse, leached Hanford sediment with model fit (M2b). The model uses 0.1% gibbsite and silica with 2.0% goethite. The modeled fraction of each species is shown with dashed lines; only species with a contribution of 1% or greater are shown.

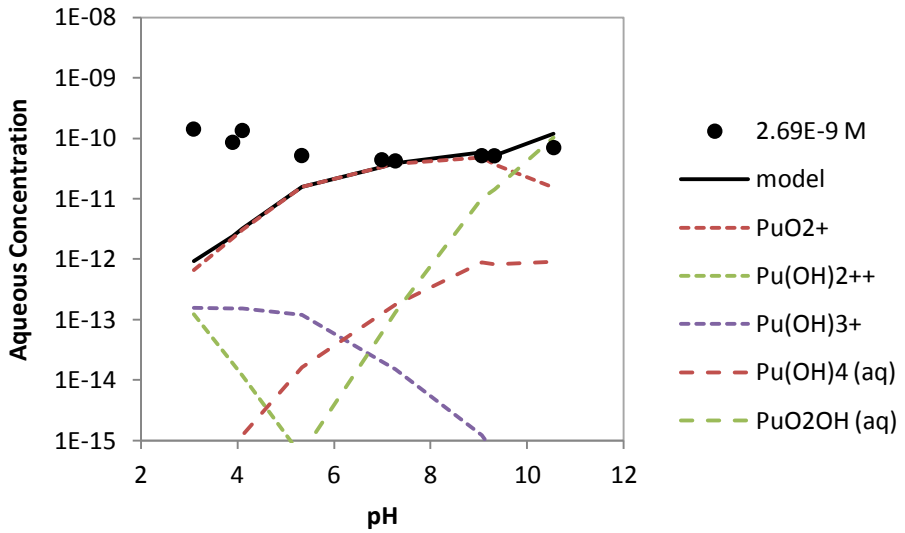

Figure 5.21b. Aqueous species present in the coupled Pu(IV) and Pu(V) on coarse, leached Hanford sediment experiment with model fit (M2b). The modeled fraction of each species is shown with dashed lines; only species with a contribution of 1 x 10^{-15} M or greater are shown.

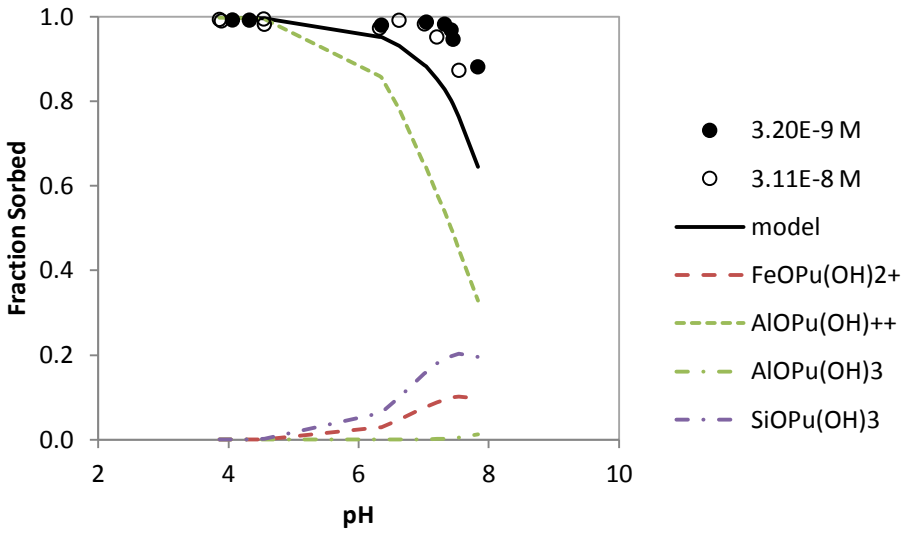

Figure 5.22a. Sorption of coupled Pu(IV) and Pu(V) on coarse, pristine Hanford sediment with model fit (M2a). The model uses 0.1% gibbsite and silica with 0.02% goethite. The modeled fraction of each species is shown with dashed lines; only species with a contribution of 1% or greater are shown.

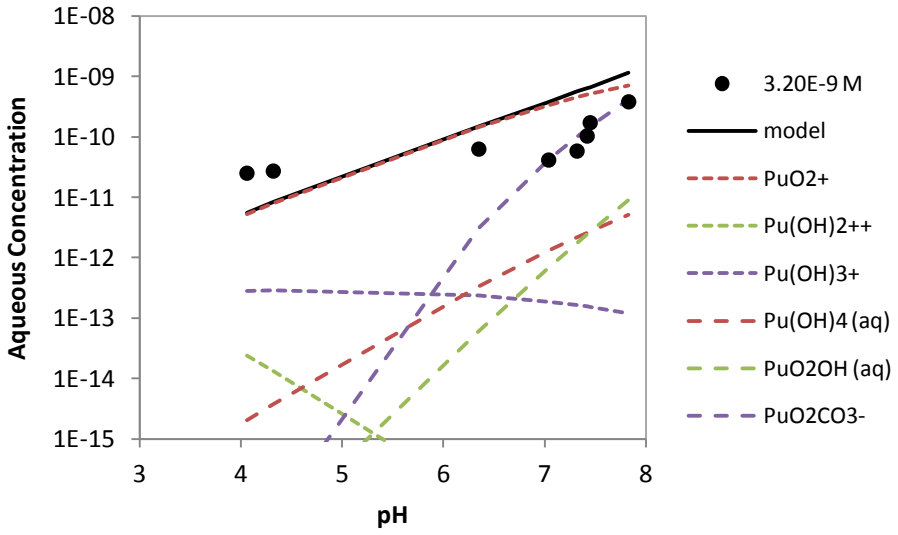

Figure 5.22b. Aqueous species present in the coupled Pu(IV) and Pu(V) on coarse, pristine Hanford sediment experiment with model fit (M2a). The modeled fraction of each species is shown with dashed lines; only species with a contribution of 1 x 10^{-15} M or greater are shown.

As previously discussed, the considerable sorption of plutonium in the initially Pu(V) system suggested the reduction of Pu(V) to Pu(IV). **Figures 5.17a** and **5.18a** support this theory by revealing greater than 85% sorption for both plutonium concentrations. In both systems, the goethite portion of the sediment controlled the simulation. The $FeOPu(OH)^{++}$ and $FeOPu(OH)_3$ complexes dominated the leached, coarse-grained system, while only the $FeOPu(OH)^{++}$ complex dominated the pristine, coarse-grained system. However, both simulations required a small fraction of gibbsite surface sites, as $AlOPu(OH)^{++}$. Unlike the leached model, the pristine simulation utilized silica surface sites at the higher pH values. This discrepancy arose from the decrease in goethite concentration (2.0% for the leached system versus 0.2% for the pristine system). As a result, the silica sites compensated for the decrease in goethite sites. It was unclear if the apparent influence of silica sites was an artifact of the model fitting results or a physical reality. Without spectroscopic data evaluating the active sorption sites, a conclusion could not be drawn.

The downturn in sorption observed in these two models could be attributed to either plutonium hydrolysis or carbonate complexation. The species $Pu(OH)_4$ (aq) dominated the aqueous system around pH 7 (**Figures 5.17b** and **5.18b**). Similarly, the downturn in sorption occurred around the same pH value. The neutral $Pu(OH)_4$ species was not attracted to the negatively charged surface site, resulting in decreased sorption. However, this analysis was based upon the aqueous stability constants used in this work. Formation of actinide-carbonate aqueous complexes which hinder or prevent sorption has been observed in many cases. Furthermore, the evaluation of Pu(IV)-carbonate

complexes discussed by Clark *et al*. (1995) indicates a high level of uncertainty in hydroxycarbonate species such as $Pu(OH)_2(CO_3)_2$ or $Pu(OH)_4(CO_3)_2$. These species were not included in the modeling effort due to this high level of uncertainty. However, it is possible their inclusion in the models could explain the observed data. Desorption was predicted with the addition of these species into the model. In order to have the hydroxycarbonate species explain the observed sorption behavior, a ternary surface-plutonium-ligand surface complex must be assumed. These species were not included in the model due to the uncertainty in the aqueous carbonate complexes and the lack of spectroscopic data verifying the existence of the ternary complex. While omitting the Pu(IV)-hydroxycarbonate species, these models included the Pu(IV)-carbonate complexes that are accepted by the Nuclear Energy Authority Thermochemical Database Project.

As expected, **Figure 5.19a** depicts increasing actinide sorption with increasing pH. Additionally, sorption was independent of actinide concentration; both Np(V) concentrations fell along the same sorption edge. Although significant scatter was present in **Figure 5.20a**, the same trend of increasing sorption with pH was observed. In both systems, the $FeONpO_2$ complex dominated the modeling process. Both models approximated the shape of the sorption curve but failed to exactly predict the data. The simulation for the leached system underestimated sorption at the low and midrange pH values; the model began to accurately predict sorption at pH values greater than 9 (**Figure 5.19a**). Similarly, the model for the pristine system greatly under predicted

sorption. However, despite the visually poor fit to the Np(V) sorption data, reasonable fits to the aqueous concentrations were observed.

The Pu(IV)/Pu(V) coupled model shown in **Figure 5.21a** used the $AlOPu(OH)^{++}$, $FeOPu(OH)_2^{+}$, and $FeOPuO_2$ complexes. This model accurately predicted sorption throughout the pH range. The corresponding aqueous phase model (**Figure 5.21b**) revealed an increase of the neutral species PuO_2OH (aq). Alternatively, the coupled model shown in **Figure 5.22a** used $AlOPu(OH)^{++}$, $SiOPu(OH)_3$, and $FeOPu(OH)_2^{+}$ to predict sorption. The model slightly underestimated sorption at the higher pH ranges. The corresponding aqueous phase model (**Figure 5.22b**) revealed an increase in the anionic plutonyl-carbonate species $PuO_2CO_3^{-}$; the formation of this complex prevented plutonium sorption at the higher pH values.

The best fits for the leached system used gibbsite and goethite complexes, and the pristine system utilized gibbsite, silica, and goethite complexes. The clay fractions for these two models were identical, while the goethite fractions varied by two orders of magnitude. The model in **Figure 5.21a** used 10^2 times more reactive goethite sites than the model in **Figure 5.22a**. This explains the inconsistency in complexes between the two models. For both systems, speciation was controlled by the strongly hydrolyzed $Pu(OH)_x^{4-x}$ species, not the weakly complexing PuO_2^{+} ion. The models accurately predicted plutonium oxidation speciation within the system; Pu(IV) dominated the solid phase, while Pu(V) dominated the aqueous phase.

Overall, these models accurately predicted the trends observed in both the sorbed and aqueous systems. Silica and gibbsite reactive fractions remained at 0.1%, and

goethite reactive fractions ranged from 0.02% to 2.0% for these coarse-grained sediment models. Alternatively, silica and gibbsite reactive fractions ranged from 0.26%% to 2.6%, and goethite reactive fractions ranged from 0.0032% to 3.2% for the fine-grained sediment models. Models for the fine-grained sediment studies can be found in **Appendix B**.

Oxidation State Analysis Results versus Model Results

Figures 5.23 and **5.24** show the oxidation state analysis (filled bars) versus the oxidation states determined by the models (shaded bars). **Figure 5.23** utilizes the best fit model for the coarse sediment (Model 2a), while **Figure 5.24** uses the best fit model for the fine sediment (Model 4b). Both models were applied to the coarse- and fine-grained sediments due to the compositional differences in the sediments. The fine-grained sediment contained a larger silt and clay fraction than the coarse-grained sediment (26:1). As a result, the fine-grained models contained larger silica and gibbsite fractions than the corresponding coarse-grained models.

These thermodynamic models did not capture the entire picture. Neither Model 2a nor Model 4b accurately predicted the oxidation state speciation in the aqueous phase. The models overestimated Pu(V) speciation for both the fine- and coarse-grained systems. These discrepancies revealed the models' sensitivity to the various inputs (pH, sediment concentration). This analysis required the models to predict speciation outside of the original pH ranges of 4 to 8 where the surface complexation constants were determined; as a result, the models were extrapolated to include the higher pH values. These models could be redesigned for an extended pH range. However, the over

prediction of Pu(V) was likely not a mistake. As discussed above, the impact of Pu(IV)-carbonate and Pu(IV)-hydroxycarbonate species may be real and the source of stabilization in some aqueous Pu(IV). Additional studies of the Pu(IV)-carbonate system are warranted based on these data and model fits.

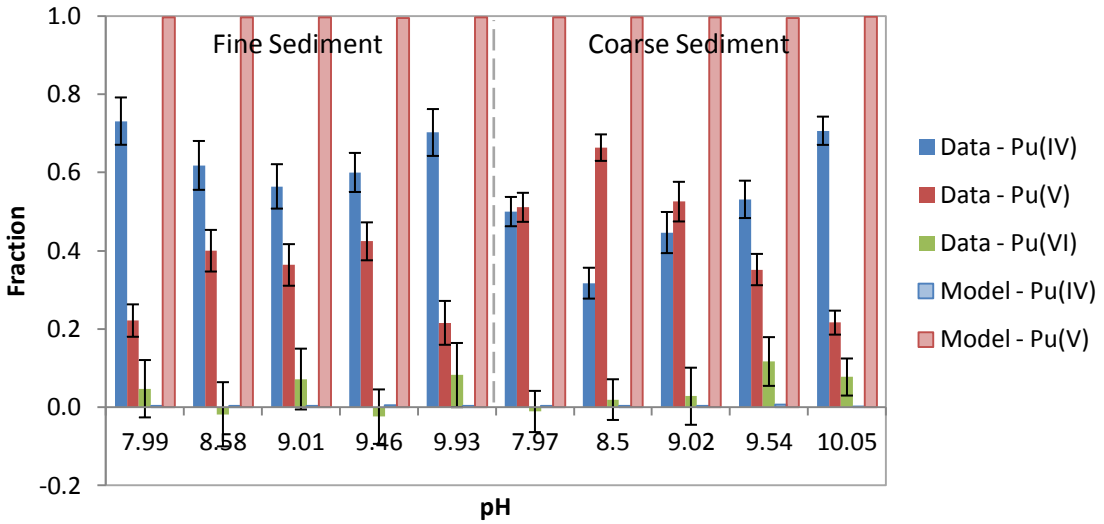

Figure 5.23. Oxidation state analysis results for the aqueous phase of ^{238}Pu with fine and coarse pristine, Hanford sediments as a function of pH. Includes oxidation states as predicted by Model 2a.

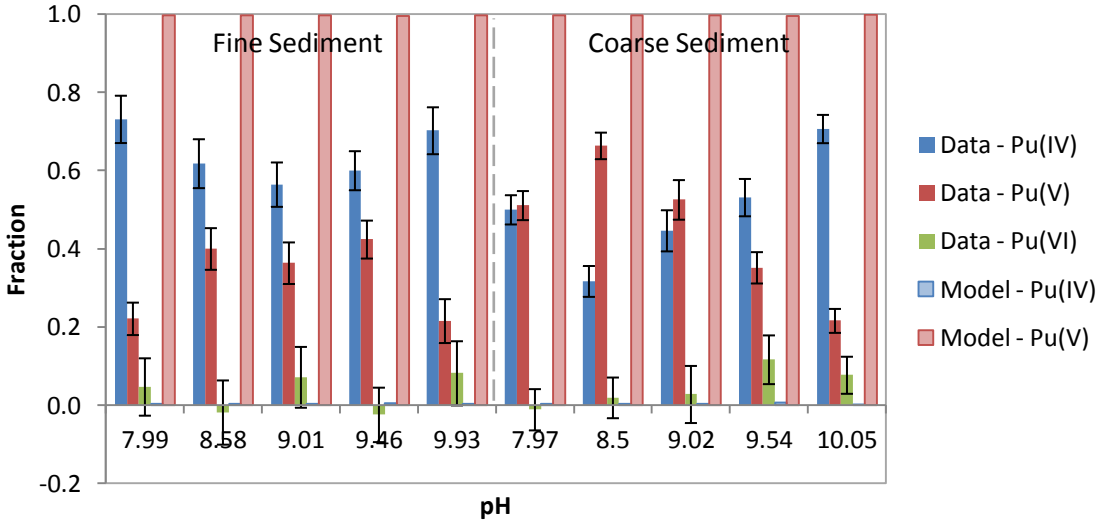

Figure 5.24. Oxidation state analysis results for the aqueous phase of ^{238}Pu with fine and coarse pristine, Hanford sediments as a function of pH. Includes oxidation states as predicted by Model 4b.

CHAPTER SIX – CONCLUSIONS AND RECOMMENDATIONS

This work successfully developed models predicting plutonium and neptunium sorption to the Hanford Nuclear Reservation subsurface sediments. Batch sorption experiments and detailed sediment characterization supported the development of this thermochemically-based surface complexation model. The FITEQL-based model predicted sorption onto a complex mineral assemblage by the summation of sorption to each specific sorbent (e.g. iron oxide and smectite clay). Surface complexation constants for these phases were taken from the available literature or developed using pre-existing sorption data. The model could be developed without the use of experimental data; however, comparison between model simulations and actual sorption data resulted in increased model confidence. As a result, the variable pH batch sorption data were used to refine the component additivity model.

Batch sorption studies revealed the reduction of Pu(V) to Pu(IV) on both the fine- and coarse-grained sediments, even though they contain non-redox active minerals like gibbsite and quartz. Consequently, this work incorporated the Pu(V)/Pu(IV) redox couple and thereby provided more technically accurate models. The strongly hydrolyzed $Pu(OH)_x^{4-x}$ species, not the weakly complexing PuO_2^+ ion, dominated speciation within the systems. The models accurately predicted plutonium oxidation state; Pu(IV) dominated the solid phases, while Pu(V) dominated the aqueous phases.

The same model, however, could not be used to describe all systems. Unlike the leached model, the pristine simulation utilized silica surface sites at the higher pH values. This discrepancy arose from the decrease in goethite surface sites; as a result, the silica

sites compensated for the decrease in available sites. This apparent influence of silica sites could be an artifact of the model fitting results or a physical reality. Spectroscopic data evaluating the active sorption sites could clarify this phenomenon.

Typically, the fraction sorbed increased with pH. The pristine, coarse-grained system, however, exhibited a downturn in sorption at the higher pH values. This downturn could be attributed to either plutonium hydrolysis or carbonate complexation. The model predicted $Pu(OH)_4$ as the dominant aqueous species at this observed decline. It was possible that the neutral $Pu(OH)_4$ species is not attracted to the negatively charge surface site, resulting in decreased sorption. However, this analysis utilized the aqueous stability constants presented in the work. Instead, the formation of actinide-carbonate aqueous complexes could hinder or prevent sorption. The high level of uncertainty in the hydroxycarbonate species prevented their use in these modeling efforts. As a result, their inclusion requires additional study of these species. The refinement of the Pu(IV)-hydroxide-carbonate system would greatly improve the current models.

Additionally, redevelopment of the stability constants could improve the current models. Ultimately, these models were not calibrated for the extended pH range seen in the acid-leached systems. This analysis required the models to predict speciation outside of the original pH ranges of 4 to 8. Therefore, these models could be redesigned for an extended pH range (4 to 10).

Finally, the batch sorption and soil column experiments could be expanded to include organic complexants (e.g. CCl_4, MBP, DBP, and TBP). Plumes of CCl_4 as a separate organic phase have migrated deep into the subsurface in the Hanford 200 areas

(Felmy *et al.*, 2010). Additional studies with CCl_4 and other organic complexants could explain the extensive plutonium transport observed at the site; transport could have occurred with the organic solvents either as a neutral complex dissolved within the solvent or as a colloid that was coated with the hydrophobic organic compound (Felmy *et al.*, 2010).

APPENDICES

APPENDIX A – LABORATORY DATA

Table A.1. Masses of each component required to prepare 10 mL samples at constant ionic strength for initially ^{242}Pu(V) and ^{237}Np(V) suspensions with 100 g/L of pristine, fine-grained sediment.

Sample ID	0.1 M NaCl (g)	Sediment (g)	DDI H_2O (g)	^{242}Pu(V) (g)	^{237}Np(V) (g)	Total Sample (g)	Target pH
HAN1-NpPu-I-28A	0.9904	0.9938	9.0939	0.0103	0.0105	11.0981	10
HAN1-NpPu-I-28B	0.9929	1.0242	9.3015	0.0101	0.0119	11.3377	9.25
HAN1-NpPu-I-28C	0.9898	1.0026	9.0416	0.0104	0.0103	11.0414	8.5
HAN1-NpPu-I-28D	0.9912	1.0016	9.2547	0.0102	0.0102	11.2718	7.75
HAN1-NpPu-I-28E	0.9885	1.0515	9.0142	0.0101	0.0105	11.068	7
HAN1-NpPu-I-28F	1.0005	1.0513	8.9668	0.0104	0.0105	11.0314	6.25
HAN1-NpPu-I-28G	0.9919	0.9859	9.2078	0.0105	0.0107	11.1938	5.5
HAN1-NpPu-I-28H	0.9869	1.0545	9.0237	0.0104	0.0103	11.0724	4.75
HAN1-NpPu-I-28I	0.9886	1.0279	9.396	0.01	0.009	11.0569	4
HAN2-NpPu-I-28A	0.9965	0.9892	9.0089	0.1011	0.1045	11.1788	10
HAN2-NpPu-I-28B	0.9937	1.0404	8.9577	0.1024	0.1039	11.1831	9.25
HAN2-NpPu-I-28C	0.9972	0.9942	9.0755	0.1031	0.1032	11.2663	8.5
HAN2-NpPu-I-28D	0.9936	0.9977	8.9917	0.1028	0.1031	11.1687	7.75
HAN2-NpPu-I-28E	0.9897	1.0278	8.9841	0.1029	0.1033	11.2009	7
HAN2-NpPu-I-28F	0.9971	1.0252	9.0549	0.103	0.1026	11.2588	6.25
HAN2-NpPu-I-28G	0.9878	0.9826	9.0344	0.1032	0.1031	11.1997	5.5
HAN2-NpPu-I-28H	0.9899	1.0965	8.9927	0.1025	0.1032	11.2786	4.75
HAN2-NpPu-I-28I	0.9899	0.9798	9.0292	0.1031	0.1031	11.1951	4

Table A.2. Masses of each component required to prepare 10 mL samples at constant ionic strength for initially ^{242}Pu(V) and ^{237}Np(V) suspensions with 100 g/L of pristine, coarse-grained sediment.

Sample ID	0.1 M NaCl (g)	Sediment (g)	DDI H_2O (g)	^{242}Pu(V) (g)	^{237}Np(V) (g)	Total Sample (g)	Target pH
HAN1-NpPu-I-29A	1.0008	1.0166	9.0504	0.0102	0.0104	11.0873	10
HAN1-NpPu-I-29B	0.9939	1.0155	9.36	0.0102	0.0102	11.3865	9.25
HAN1-NpPu-I-29C	0.9862	1.0063	9.0158	0.0104	0.0106	11.0258	8.5
HAN1-NpPu-I-29D	0.9879	1.0433	9.0576	0.0103	0.0106	11.1041	7.75
HAN1-NpPu-I-29E	0.9861	0.996	8.9667	0.0102	0.0107	10.7718	7
HAN1-NpPu-I-29F	0.9904	1.0452	8.9792	0.0102	0.0103	11.0286	6.25
HAN1-NpPu-I-29G	0.9822	1.0359	8.9147	0.0101	0.0104	10.9463	5.5
HAN1-NpPu-I-29H	0.9887	1.0259	8.9907	0.0104	0.0108	11.025	4.75
HAN1-NpPu-I-29I	0.9899	1.0411	9.0139	0.01	0.0098	11.0663	4
HAN2-NpPu-I-29A	0.9941	1.0883	9.2331	0.1031	0.1028	11.5162	10
HAN2-NpPu-I-29B	0.9943	0.9958	8.9061	0.1022	0.103	11.0975	9.25
HAN2-NpPu-I-29C	0.9897	0.9903	9.13	0.1031	0.1038	11.3134	8.5
HAN2-NpPu-I-29D	0.9884	1.0404	9.1104	0.1029	0.1034	11.3397	7.75
HAN2-NpPu-I-29E	0.9821	1.0486	8.9944	0.1032	0.1025	11.2186	7
HAN2-NpPu-I-29F	0.9811	0.9853	8.9007	0.1027	0.1031	11.0658	6.25
HAN2-NpPu-I-29G	0.9916	1.0214	8.9394	0.1032	0.1035	11.1487	5.5
HAN2-NpPu-I-29H	0.9951	1.0232	9.0201	0.1031	0.1027	11.2281	4.75
HAN2-NpPu-I-29I	0.9877	0.9739	9.0176	0.1029	0.1027	11.1714	4

Table A.3. Masses of each component required to prepare 10 mL samples at constant ionic strength for initially ^{242}Pu(V) and ^{237}Np(V) suspensions with 25 g/L of pristine, fine-grained sediment.

Sample ID	0.1 M NaCl (g)	Sediment (g)	DDI H_2O (g)	^{242}Pu(V) (g)	^{237}Np(V) (g)	Total Sample (g)	Target pH
HAN1-NpPu-I-36A	0.994	0.2649	9.0017	0.0141	0.0121	10.2844	10
HAN1-NpPu-I-36B	0.9989	0.2525	9.0722	0.0103	0.01	11.3443	9.25
HAN1-NpPu-I-36C	0.9974	0.2499	8.9803	0.0101	0.0104	10.2468	8.5
HAN1-NpPu-I-36D	0.994	0.2516	8.9188	0.0101	0.0101	10.1847	7.75
HAN1-NpPu-I-36E	0.991	0.2519	9.0282	0.0104	0.0107	10.2919	7
HAN1-NpPu-I-36F	0.9909	0.2607	9.1089	0.0103	0.0105	10.3813	6.25
HAN1-NpPu-I-36G	0.9899	0.2532	9.0297	0.0102	0.0105	10.2934	5.5
HAN1-NpPu-I-36H	0.9933	0.2593	9.0368	0.0103	0.0106	10.3098	4.75
HAN1-NpPu-I-36I	0.9915	0.2665	9.0169	0.0107	0.0104	10.2948	4
HAN2-NpPu-I-36A	0.9889	0.2562	9.1304	0.103	0.1012	10.5806	10
HAN2-NpPu-I-36B	0.9931	0.2515	8.9382	0.1025	0.1035	10.3868	9.25
HAN2-NpPu-I-36C	0.9917	0.2449	9.0239	0.1021	0.1029	10.4666	8.5
HAN2-NpPu-I-36D	0.9899	0.265	9.1062	0.1023	0.1033	10.5678	7.75
HAN2-NpPu-I-36E	0.9949	0.2583	9.1763	0.1031	0.1027	10.6355	7
HAN2-NpPu-I-36F	0.9942	0.2592	8.9687	0.1026	0.1025	10.4284	6.25
HAN2-NpPu-I-36G	0.9877	0.2466	9.359	0.1039	0.103	10.7996	5.5
HAN2-NpPu-I-36H	0.9870	0.2561	8.9956	0.1032	0.1022	10.4448	4.75
HAN2-NpPu-I-36I	0.9815	0.2505	9.1291	0.1024	0.103	10.5674	4

Table A.4. Masses of each component required to prepare 10 mL samples at constant ionic strength for initially ^{242}Pu(V) and ^{237}Np(V) suspensions with 25 g/L of pristine, coarse-grained sediment.

Sample ID	0.1 M NaCl (g)	Sediment (g)	DDI H_2O (g)	^{242}Pu(V) (g)	^{237}Np(V) (g)	Total Sample (g)	Target pH
HAN1-NpPu-I-37A	0.987	0.2528	9.0178	0.0103	0.0102	10.2783	10
HAN1-NpPu-I-37C	0.9871	0.2594	9.1802	0.0101	0.0103	10.4451	8.5
HAN1-NpPu-I-37D	0.9873	0.251	8.9384	0.0104	0.0099	10.1978	7.75
HAN1-NpPu-I-37E	0.9868	0.2589	8.9857	0.0101	0.01	10.1991	7
HAN1-NpPu-I-37F	0.9805	0.2694	8.9553	0.0101	0.0103	10.2278	6.25
HAN1-NpPu-I-37G	0.988	0.2525	8.9767	0.0102	0.0103	10.2369	5.5
HAN1-NpPu-I-37H	0.9874	0.2755	8.9464	0.0102	0.0103	10.229	4.75
HAN1-NpPu-I-37I	1.007	0.2701	8.874	0.0103	0.0105	10.1686	4
HAN2-NpPu-I-37A	0.9844	0.2555	8.9503	0.1003	0.1011	10.3918	10
HAN2-NpPu-I-37B	0.9877	0.2639	8.8997	0.1009	0.1006	10.3536	9.25
HAN2-NpPu-I-37C	0.9868	0.2573	9.1276	0.1012	0.1008	10.5754	8.5
HAN2-NpPu-I-37D	0.9903	0.2576	8.9032	0.1004	0.1014	10.353	7.75
HAN2-NpPu-I-37E	0.9865	0.2575	8.9484	0.1005	0.1011	10.3841	7
HAN2-NpPu-I-37F	0.9842	0.2585	9.0076	0.1008	0.1007	10.4517	6.25
HAN2-NpPu-I-37G	0.9817	0.251	8.9366	0.1009	0.1004	10.3708	5.5
HAN2-NpPu-I-37H	0.9868	0.2527	9.0856	0.1006	0.1009	10.5286	4.75
HAN2-NpPu-I-37I	0.9841	0.2557	9.0283	0.1003	0.1011	10.4712	4

Table A.5. Masses of each component required to prepare 10 mL samples at constant ionic strength for initially ^{242}Pu(V) and ^{237}Np(V) suspensions with 25 g/L of leached, fine-grained sediment.

Sample ID	0.1 M NaCl (g)	Sediment (g)	DDI H_2O (g)	^{242}Pu(V) (g)	^{237}Np(V) (g)	Total Sample (g)	Target pH
HAN1-NpPu-I-38A	0.9896	0.2478	9.083	0.0107	0.0121	10.3415	10
HAN1-NpPu-I-38B	0.9859	0.2496	8.8226	0.01	0.0099	10.0767	9.25
HAN1-NpPu-I-38C	0.9854	0.2458	8.9509	0.0101	0.011	10.2014	8.5
HAN1-NpPu-I-38D	0.9808	0.242	8.9233	0.0106	0.0101	10.1654	7.75
HAN1-NpPu-I-38E	0.9832	0.2535	8.9589	0.0103	0.0099	10.2139	7
HAN1-NpPu-I-38F	0.9802	0.2566	9.0281	0.0101	0.0103	10.2829	6.25
HAN1-NpPu-I-38G	0.9723	0.2504	8.9699	0.0104	0.0103	10.2114	5.5
HAN1-NpPu-I-38H	0.9835	0.2592	8.9606	0.0103	0.0102	10.2211	4.75
HAN1-NpPu-I-38I	0.9859	0.2421	8.9553	0.0103	0.0103	10.2013	4
HAN2-NpPu-I-38A	0.9839	0.2519	8.9799	0.1016	0.1013	10.4168	10
HAN2-NpPu-I-38B	0.9888	0.2403	8.9841	0.1015	0.1005	10.4093	9.25
HAN2-NpPu-I-38C	0.9799	0.2591	8.9658	0.1018	0.1008	10.405	8.5
HAN2-NpPu-I-38D	0.9866	0.2454	8.9624	0.1014	0.101	10.3941	7.75
HAN2-NpPu-I-38E	0.9839	0.245	8.9843	0.1018	0.1008	10.4107	7
HAN2-NpPu-I-38F	0.9822	0.2457	8.9426	0.1013	0.1008	10.3709	6.25
HAN2-NpPu-I-38G	0.9835	0.2578	8.9801	0.1009	0.1009	10.4231	5.5
HAN2-NpPu-I-38H	0.9866	0.2538	8.9666	0.1018	0.1009	10.4062	4.75
HAN2-NpPu-I-38I	0.9783	0.2559	8.9639	0.1017	0.1008	10.397	4

Table A.6. Masses of each component required to prepare 10 mL samples at constant ionic strength for initially $^{242}Pu(V)$ and $^{237}Np(V)$ suspensions with 25 g/L of leached, coarse-grained sediment.

Sample ID	0.1 M NaCl (g)	Sediment (g)	DDI H_2O (g)	$^{242}Pu(V)$ (g)	$^{237}Np(V)$ (g)	Total Sample (g)	Target pH
HAN1-NpPu-I-39A	0.981	0.2457	8.9455	0.0104	0.0102	10.1927	10
HAN1-NpPu-I-39B	0.9839	0.2488	8.8629	0.0104	0.01	10.1155	9.25
HAN1-NpPu-I-39C	0.9769	0.2442	8.9067	0.0104	0.0102	10.1471	8.5
HAN1-NpPu-I-39D	0.9644	0.2449	8.8824	0.0104	0.0104	10.1126	7.75
HAN1-NpPu-I-39E	0.9869	0.2478	8.8461	0.0102	0.0101	10.1005	7
HAN1-NpPu-I-39F	0.9884	0.2576	9.1819	0.0105	0.01	10.4479	6.25
HAN1-NpPu-I-39G	0.984	0.2569	8.9383	0.0103	0.0104	10.1989	5.5
HAN1-NpPu-I-39H	0.9795	0.2519	8.9009	0.0103	0.0102	10.1515	4.75
HAN1-NpPu-I-39I	0.9715	0.2559	8.9119	0.0108	0.0102	10.1592	4
HAN2-NpPu-I-39A	0.9863	0.2475	8.9399	0.1018	0.1005	10.3748	10
HAN2-NpPu-I-39B	0.9787	0.2484	8.9187	0.1014	0.101	10.3482	9.25
HAN2-NpPu-I-39C	0.9714	0.2509	8.9116	0.1013	0.1009	10.3361	8.5
HAN2-NpPu-I-39D	0.9719	0.2511	8.9079	0.1014	0.1003	10.3325	7.75
HAN2-NpPu-I-39E	0.9724	0.2589	8.9237	0.1011	0.101	10.3572	7
HAN2-NpPu-I-39F	0.9815	0.2604	8.9251	0.1017	0.1002	10.3693	6.25
HAN2-NpPu-I-39G	0.9865	0.2464	8.8949	0.1012	0.1006	10.327	5.5
HAN2-NpPu-I-39H	0.9855	0.2596	8.8285	0.1004	0.1008	10.2749	4.75
HAN2-NpPu-I-39I	0.9809	0.2469	8.9712	0.1015	0.1002	10.4008	4

Table A.7. Masses of each component required to prepare 10 mL samples for analysis on the ICP-MS for initially ^{242}Pu(V) and ^{237}Np(V) suspensions with 100 g/L of pristine, fine-grained sediment. Includes ICP-MS results and measured pH values. Data collected after a 30 day equilibration period.

Sample ID	Aliquot from Original (g)	2% HNO_3 (g)	Total Sample (g)	^{242}Pu(IV) (ppb)	^{237}Np(V) (ppb)	pH
HAN1-NpPu-I-40A	0.9938	9.0847	10.0794	0.03652	0.003684	8.52
HAN1-NpPu-I-40B	0.9915	9.0005	9.9924	0.02462	0.003189	8.53
HAN1-NpPu-I-40C	0.9881	8.9908	9.9792	0.01795	0.002841	8.26
HAN1-NpPu-I-40D	0.9884	8.9958	9.9849	0.01442	0.002513	8.18
HAN1-NpPu-I-40E	0.9893	9.2398	10.2299	0.01177	0.001967	8.1
HAN1-NpPu-I-40F	0.994	9.0618	10.0572	0.009477	0.001542	8.12
HAN1-NpPu-I-40G	0.9946	9.0396	10.0356	0.008522	0.00167	8.07
HAN1-NpPu-I-40H	0.988	9.0293	10.0185	0.007371	0.00144	8.05
HAN1-NpPu-I-40I	0.9923	9.0433	10.0367	0.00653	0.001447	8.04
HAN2-NpPu-I-40A	0.9905	9.0223	10.0144	0.006861	0.02279	8.49
HAN2-NpPu-I-40B	0.9934	9.0445	10.0392	0.00528	0.02542	8.24
HAN2-NpPu-I-40C	0.9971	9.0864	10.0851	0.004634	0.02457	8.21
HAN2-NpPu-I-40D	0.9978	9.0602	10.0599	0.00407	0.01895	8.15
HAN2-NpPu-I-40E	0.9934	9.0016	9.9956	0.003657	0.006655	9.07
HAN2-NpPu-I-40F	0.9956	8.9935	9.991	0.003271	0.01115	8.13
HAN2-NpPu-I-40G	0.9953	9.0232	10.0195	0.003009	0.01147	8.09
HAN2-NpPu-I-40H	1.0013	9.0201	10.0226	0.00356	0.01052	8.01
HAN2-NpPu-I-40I	1.0069	9.0345	10.0425	0.003691	0.01458	8.01

Table A.8. Masses of each component required to prepare 10 mL samples for analysis on the ICP-MS for initially ^{242}Pu(V) and ^{237}Np(V) suspensions with 100 g/L of pristine, coarse-grained sediment. Includes ICP-MS results and measured pH values. Data collected after a 30 day equilibration period.

Sample ID	Aliquot from Original (g)	2% HNO_3 (g)	Total Sample (g)	^{242}Pu(IV) (ppb)	^{237}Np(V) (ppb)	pH
HAN1-NpPu-I-41A	0.9941	9.0136	10.0073	0.004896	0.004465	8.41
HAN1-NpPu-I-41B	0.9829	8.9742	9.956	0.00351	0.005112	7.96
HAN1-NpPu-I-41C	0.9881	9.0111	9.9988	0.002785	0.00725	7.71
HAN1-NpPu-I-41D	0.9824	8.9888	9.9702	0.002521	0.007694	7.64
HAN1-NpPu-I-41E	0.9974	9.0125	10.011	0.002358	0.009477	7.57
HAN1-NpPu-I-41F	0.9877	9.0113	9.9987	0.001962	0.008897	7.44
HAN1-NpPu-I-41G	0.988	8.9589	9.9458	0.001862	0.01526	7.3
HAN1-NpPu-I-41H	0.9871	9.0213	10.0083	0.001673	0.01191	7.25
HAN1-NpPu-I-41I	0.9935	8.9923	9.9852	0.001509	0.01398	7.17
HAN2-NpPu-I-41A	0.9897	8.9418	9.93	0.05243	0.04297	8.19
HAN2-NpPu-I-41B	0.9974	9.0051	10.11816	0.02325	0.03941	7.91
HAN2-NpPu-I-41C	0.9952	8.9869	9.9825	0.01413	0.06116	7.79
HAN2-NpPu-I-41D	0.9951	8.9676	9.9627	0.01088	0.08597	7.63
HAN2-NpPu-I-41E	0.9954	8.9307	9.9262	0.007433	0.07949	7.62
HAN2-NpPu-I-41F	0.9935	9.1213	10.1142	0.005707	0.0802	7.52
HAN2-NpPu-I-41G	0.9919	8.989	9.9791	0.005037	0.05855	7.29
HAN2-NpPu-I-41H	0.9922	8.9906	9.9825	0.003985	0.07987	7.53
HAN2-NpPu-I-41I	0.9966	9.0062	10.0026	0.003701	0.2381	7.01

Table A.9. Masses of each component required to prepare 10 mL samples for analysis on the ICP-MS for initially ^{242}Pu(V) and ^{237}Np(V) suspensions with 25 g/L of pristine, fine-grained sediment. Includes ICP-MS results and measured pH values. Data collected after a 30 day equilibration period.

Sample ID	Aliquot from Original (g)	2% HNO_3 (g)	Total Sample (g)	^{242}Pu(IV) (ppb)	^{237}Np(V) (ppb)	pH
HAN1-NpPu-I-52A	0.9877	9.0874	10.0765	0.06894	0.002986	8.64
HAN1-NpPu-I-52B	0.994	9.0583	10.0417	0.02535	0.01635	8.35
HAN1-NpPu-I-52C	0.9968	9.0208	9.9931	0.01726	0.01766	7.89
HAN1-NpPu-I-52D	0.9925	9.0669	10.0246	0.01184	0.002679	9.49
HAN1-NpPu-I-52E	0.9935	9.0577	10.0006	0.009515	0.03725	7.62
HAN1-NpPu-I-52F	0.9939	9.0448	9.9762	0.008234	0.01689	7.43
HAN1-NpPu-I-52G	0.9962	9.0487	9.972	0.007333	0.05621	7.01
HAN1-NpPu-I-52H	0.9965	9.0299	9.9455	0.005883	0.05694	6
HAN1-NpPu-I-52I	0.9954	9.0623	9.9647	0.004869	0.03355	6.49
HAN2-NpPu-I-52A	0.9902	9.0539	9.9355	0.003071	0.09548	7.85
HAN2-NpPu-I-52B	0.9894	9.057	9.9285	0.002963	0.3996	7.76
HAN2-NpPu-I-52C	0.9915	9.0334	9.893	0.002803	0.2515	7.58
HAN2-NpPu-I-52D	0.9951	9.0328	9.638	0.006014	0.5367	7.49
HAN2-NpPu-I-52E	0.9945	9.0314	10.0292	0.003962	0.2239	7.4
HAN2-NpPu-I-52F	0.9957	9.0606	10.0533	0.00374	0.1942	6.95
HAN2-NpPu-I-52G	0.9938	9.0421	10.0252	0.002381	0.5089	6.86
HAN2-NpPu-I-52H	0.997	9.0351	10.0159	0.002731	0.2639	4.93
HAN2-NpPu-I-52I	0.9945	9.0622	10.033	0.006751	0.3656	4.37

Table A.10. Masses of each component required to prepare 10 mL samples for analysis on the ICP-MS for initially ^{242}Pu(V) and ^{237}Np(V) suspensions with 25 g/L of pristine, coarse-grained sediment. Includes ICP-MS results and measured pH values. Data collected after a 30 day equilibration period.

Sample ID	Aliquot from Original (g)	2% HNO_3 (g)	Total Sample (g)	^{242}Pu(IV) (ppb)	^{237}Np(V) (ppb)	pH
HAN1-NpPu-I-53A	0.9934	9.0092	10.0026	0.00901	0.01741	7.83
HAN1-NpPu-I-53C	0.9933	8.9903	9.9833	0.004007	0.003453	7.45
HAN1-NpPu-I-53D	0.9898	9.0175	10.0077	0.002455	0.004539	7.42
HAN1-NpPu-I-53E	0.9916	8.9988	9.9933	0.001498	0.04979	6.35
HAN1-NpPu-I-53F	0.9917	8.9893	9.9844	0.001387	0.0062	7.32
HAN1-NpPu-I-53G	0.9946	8.9799	9.976	0.000989	0.05552	7.04
HAN1-NpPu-I-53H	0.9938	9.011	10.0042	0.000597	0.07622	4.06
HAN1-NpPu-I-53I	0.9943	9.0479	10.0422	0.000649	0.09332	4.32
HAN2-NpPu-I-53A	0.99	9.01	10.0038	0.09219	0.311	7.54
HAN2-NpPu-I-53B	0.9935	8.9777	9.9734	0.03535	0.1756	7.2
HAN2-NpPu-I-53C	0.9898	8.9688	9.9584	0.01935	0.03469	6.32
HAN2-NpPu-I-53D	0.9913	8.9863	9.9794	0.01329	0.2481	4.55
HAN2-NpPu-I-53E	0.9872	8.9861	9.9749	0.01254	0.07194	7.01
HAN2-NpPu-I-53F	0.9893	8.9693	9.9578	0.007345	0.1855	3.89
HAN2-NpPu-I-53G	0.9882	8.9629	9.9489	0.006288	0.3161	6.62
HAN2-NpPu-I-53H	0.992	8.9697	9.9594	0.004792	0.1265	3.86
HAN2-NpPu-I-53I	0.9919	8.9872	9.9739	0.004057	0.1406	4.54

Table A.11. Masses of each component required to prepare 10 mL samples for analysis on the ICP-MS for initially ^{242}Pu(V) and ^{237}Np(V) suspensions with 25 g/L of leached, fine-grained sediment. Includes ICP-MS results and measured pH values. Data collected after a 30 day equilibration period.

Sample ID	Aliquot from Original (g)	2% HNO_3 (g)	Total Sample (g)	^{242}Pu(IV) (ppb)	^{237}Np(V) (ppb)	pH
HAN1-NpPu-I-54A	0.9927	8.9617	9.9543	0.01505	0.1153	4.02
HAN1-NpPu-I-54B	0.9886	8.9383	9.9266	0.006599	0.09371	4.8
HAN1-NpPu-I-54C	0.9925	8.9586	9.9505	0.004636	0.08397	6.14
HAN1-NpPu-I-54D	0.9905	8.9562	9.9467	0.003279	0.0562	6.83
HAN1-NpPu-I-54E	0.9871	8.9625	9.9496	0.002651	0.02465	7.3
HAN1-NpPu-I-54F	0.9914	8.9489	9.9406	0.002337	0.001201	8.37
HAN1-NpPu-I-54G	0.9903	8.9643	9.9549	0.001886	0.000684	10.01
HAN1-NpPu-I-54H	0.9876	8.9835	9.9708	0.00164	0.000646	10.28
HAN1-NpPu-I-54I	0.9855	8.9635	9.9479	0.001356	0.000478	10.75
HAN2-NpPu-I-54A	0.9831	8.912	9.8946	0.001985	0.943	2.76
HAN2-NpPu-I-54B	0.9828	8.9334	9.9161	0.001957	0.9361	3.03
HAN2-NpPu-I-54C	0.9862	8.9349	9.9208	0.001748	0.9542	3.29
HAN2-NpPu-I-54D	0.9869	8.9115	9.8992	0.001616	0.9444	3.99
HAN2-NpPu-I-54E	0.9816	8.9179	9.8999	0.001912	0.9215	4.69
HAN2-NpPu-I-54F	0.9874	8.8609	9.8477	0.002571	0.5972	6.76
HAN2-NpPu-I-54G	0.9814	8.9579	9.9396	0.001669	0.1521	7.46
HAN2-NpPu-I-54H	0.9867	8.9314	9.9189	0.002065	0.01318	8.03
HAN2-NpPu-I-54I	0.9756	8.9749	9.9508	0.001361	0.003494	10.11

Table A.12. Masses of each component required to prepare 10 mL samples for analysis on the ICP-MS for initially $^{242}Pu(V)$ and $^{237}Np(V)$ suspensions with 25 g/L of leached, coarse-grained sediment. Includes ICP-MS results and measured pH values. Data collected after a 30 day equilibration period.

Sample ID	Aliquot from Original (g)	2% HNO_3 (g)	Total Sample (g)	$^{242}Pu(IV)$ (ppb)	$^{237}Np(V)$ (ppb)	pH
HAN1-NpPu-I-55A	0.9884	8.9024	9.8907	0.003391	0.105	3.09
HAN1-NpPu-I-55B	0.9856	8.9107	9.8964	0.002057	0.09916	3.9
HAN1-NpPu-I-55C	0.9866	8.9193	9.9059	0.003218	0.09849	4.1
HAN1-NpPu-I-55D	0.9887	8.9447	9.9337	0.001242	0.0904	5.33
HAN1-NpPu-I-55E	0.9853	8.8999	9.8859	0.00106	0.04828	6.99
HAN1-NpPu-I-55F	0.9873	8.8783	9.8665	0.000985	0.006894	7.27
HAN1-NpPu-I-55G	0.9803	8.9248	9.9048	0.001218	0.001558	9.06
HAN1-NpPu-I-55H	0.9868	8.9041	9.8909	0.001229	0.001522	9.32
HAN1-NpPu-I-55I	0.9908	8.9521	9.9439	0.001673	0.002406	10.55
HAN2-NpPu-I-55A	0.9891	8.8948	9.883	0.02834	0.9566	2.54
HAN2-NpPu-I-55B	0.9933	8.9063	9.8995	0.01162	0.968	2.58
HAN2-NpPu-I-55C	0.9873	8.9139	9.9005	0.008772	0.963	2.98
HAN2-NpPu-I-55D	0.9841	8.8074	9.7903	0.004229	0.9693	3.15
HAN2-NpPu-I-55E	0.9917	8.8205	9.8117	0.003354	0.9405	4.86
HAN2-NpPu-I-55F	0.9846	8.7976	9.7814	0.008534	0.9156	4.97
HAN2-NpPu-I-55G	0.9884	8.8605	9.8489	0.005709	0.5605	6.7
HAN2-NpPu-I-55H	0.9852	8.7947	9.779	0.006347	0.1805	7.29
HAN2-NpPu-I-55I	0.9837	8.7798	9.7635	0.009567	0.01927	9.98

Table A.13. Measured redox potentials and pH values for pristine sediment suspensions. Sediment concentration of 25 g/L in a 0.01 M NaCl background. Data collected after a 30 day equilibration period.

Sample ID	pH	Measured E_H (mV)	Corrected E_H (mV)	Corrected E_H (V)
HAN-F-68A	9.26	269.4	691.4	0.6914
HAN-F-68B	9.7	263.9	685.9	0.6859
HAN-F-68C	8.5	284.3	706.3	0.7063
HAN-F-68D	8.37	285.1	707.1	0.7071
HAN-F-68E	7.8	315	737	0.737
HAN-F-68F	7.14	334.6	756.6	0.7566
HAN-F-68G	6.19	239.4	661.4	0.6614
HAN-F-68H	6.83	264.9	686.9	0.6869
HAN-F-68I	6.14	329.9	751.9	0.7519
HAN-C-68A	8.73	207	629	0.629
HAN-C-68B	9.17	224.1	646.1	0.6461
HAN-C-68C	8.22	233.4	655.4	0.6554
HAN-C-68D	7.69	260.6	682.6	0.6826
HAN-C-68E	7.65	268.6	690.6	0.6906
HAN-C-68F	7.69	270.1	692.1	0.6921
HAN-C-68G	7.23	287.8	709.8	0.7098
HAN-C-68H	5.56	342	764	0.764
HAN-C-68I	5.92	335.3	757.3	0.7573

Table A.14a. Masses of each component required to prepare 10 mL samples for oxidation state analysis for ^{238}Pu on pristine, fine- and coarse-grained Hanford sediments as a function of pH. ^{238}Pu concentration of 1.31 x 10^{-10} M (1200 cpm/mL).

Sample ID	0.1 M NaCl (g)	Sediment (g)	DDI H_2O (g)	$^{238}Pu(V)$ (g)	Total Sample (g)	Target pH
HAN-F-73A	1.0643	0.2665	9.0253	0.0996	10.4557	8
HAN-F-73B	1.0553	0.2559	8.991	0.0999	10.4021	8.5
HAN-F-73C	1.0697	0.2575	8.9796	0.0891	10.3959	9
HAN-F-73D	1.0775	0.2633	8.9916	0.0993	10.4317	9.5
HAN-F-73E	1.0679	0.2506	8.905	0.0983	10.3218	10
HAN-C-73A	1.0695	0.2565	8.9904	0.0997	10.4161	8
HAN-C-73B	1.0383	0.267	8.9392	0.0999	10.3444	8.5
HAN-C-73C	1.0617	0.2631	9.0142	0.0999	10.4389	9
HAN-C-73D	1.0699	0.2526	9.0275	0.0953	10.4453	9.5
HAN-C-73E	1.0666	0.2701	9.0632	0.0981	10.498	10

Table A.14b. Oxidation state analysis results for ^{238}Pu on pristine, fine- and coarse-grained Hanford sediments as a function of pH. Sediment concentration of 25 g/L and ^{238}Pu concentration of 1.31 x 10^{-10} M (1200 cpm/mL) in a 0.01 M NaCl background. Data collected after a 30 day equilibration period.

Sample ID	pH	Original (cpm)	$PMBP_{Organic}$ (cpm)	$PMBP_{Aqueous}$ (cpm)	$HDEHP_{Organic}$ (cpm)	$HDEHP_{Aqueous}$ (cpm)	$La(NO_3)_3$ (cpm)
Blank	--	2.9	--	--	--	--	--
HAN-F-73A	7.99	8.4	6.7	4.2	8	3.4	3.2
HAN-F-73B	8.58	9.4	7.7	4.5	6.8	3.3	2.9
HAN-F-73C	9.01	4.8	5.2	3.4	9.8	3.2	2.2
HAN-F-73D	9.46	8	6.2	5.9	7.4	5.9	5.8
HAN-F-73E	9.93	6.5	5	4.5	5.4	3.5	3
HAN-C-73A	7.97	15.4	10	4.4	9	4.3	3.1
HAN-C-73B	8.5	37	10.3	3.8	9.8	4	3.4
HAN-C-73C	9.02	7.6	5.8	3	7.9	3.6	2.6
HAN-C-73D	9.54	10.8	4.8	3.6	5.7	3	3.8
HAN-C-73E	10.05	5.8	6	4.9	7.8	2.8	3.6

Table A.15. FIT4FD input file for sorption of Pu(IV) on pristine, fine-grained Hanford sediment. Sediment concentration of 25 g/L in a 0.01 M NaCl background. Data collected after a 30 day equilibration period.

Sample	Use	logH+	Error	$[Pu]_{Total}$	Error	Sum0	Error	$[HCO_3^-]$	Error
1	1	-4.37	0	2.7E-08	0	2.68E-08	0	5.931E-03	0
2	1	-4.93	0	2.71E-08	0	2.7E-08	0	5.281E-03	0
3	1	-6	0	2.74E-09	0	2.53E-09	0	4.040E-03	0
4	1	-6.49	0	2.84E-09	0	2.67E-09	0	3.472E-03	0
5	1	-6.86	0	2.73E-08	0	2.72E-08	0	3.042E-03	0
6	1	-6.95	0	2.7E-08	0	2.68E-08	0	2.938E-03	0
7	1	-7.01	0	2.71E-09	0	2.45E-09	0	2.868E-03	0
8	1	-7.4	0	2.72E-08	0	2.71E-08	0	2.416E-03	0
9	1	-7.43	0	2.76E-09	0	2.47E-09	0	2.381E-03	0
10	1	-7.49	0	2.72E-08	0	2.7E-08	0	2.312E-03	0
11	1	-7.58	0	2.71E-08	0	2.7E-08	0	2.207E-03	0
12	1	-7.62	0	2.71E-09	0	2.37E-09	0	2.161E-03	0
13	1	-7.76	0	2.71E-08	0	2.7E-08	0	1.998E-03	0
14	1	-7.85	0	2.67E-08	0	2.66E-08	0	1.894E-03	0
15	1	-7.89	0	2.71E-09	0	2.1E-09	0	1.848E-03	0
16	1	-8.35	0	2.56E-09	0	1.56E-09	0	1.314E-03	0
17	1	-8.64	0	3.3E-09	0	8.32E-10	0	9.776E-04	0
18	1	-9.49	0	2.61E-09	0	2.19E-09	0	-8.400E-06	0

Table A.16. FIT4FD input file for sorption of Pu(IV) on pristine, coarse-grained Hanford sediment. Sediment concentration of 25 g/L in a 0.01 M NaCl background. Data collected after a 30 day equilibration period.

Sample	Use	logH+	Error	$[Pu]_{Total}$	Error	Sum0	Error	$[HCO_3^-]$	Error
1	1	-3.86	0	3.11E-08	0	3.090E-08	0	4.948E-03	0
2	1	-3.89	0	3.11E-08	0	3.076E-08	0	4.921E-03	0
3	1	-4.06	0	3.17E-09	0	3.141E-09	0	4.771E-03	0
4	1	-4.32	0	3.26E-09	0	3.231E-09	0	4.541E-03	0
5	1	-4.54	0	3.10E-08	0	3.078E-08	0	4.347E-03	0
6	1	-4.55	0	3.12E-08	0	3.060E-08	0	4.338E-03	0
7	1	-6.32	0	3.11E-08	0	3.030E-08	0	2.773E-03	0
8	1	-6.35	0	3.10E-09	0	3.042E-09	0	2.747E-03	0
9	1	-6.62	0	3.10E-08	0	3.078E-08	0	2.508E-03	0
10	1	-7.01	0	3.11E-08	0	3.054E-08	0	2.163E-03	0
11	1	-7.04	0	3.20E-09	0	3.155E-09	0	2.137E-03	0
12	1	-7.2	0	3.11E-08	0	2.958E-08	0	1.995E-03	0
13	1	-7.32	0	3.26E-09	0	3.200E-09	0	1.889E-03	0
14	1	-7.42	0	3.26E-09	0	3.155E-09	0	1.801E-03	0
15	1	-7.45	0	3.20E-09	0	3.026E-09	0	1.774E-03	0
16	1	-7.54	0	3.10E-08	0	2.711E-08	0	1.695E-03	0
17	1	-7.83	0	3.20E-09	0	2.817E-09	0	1.438E-03	0

Table A.17. FIT4FD input file for sorption of Pu(IV) on leached, fine-grained Hanford sediment. Sediment concentration of 25 g/L in a 0.01 M NaCl background. Data collected after a 30 day equilibration period.

Sample	Use	$logH^+$	Error	$[Pu]_{Total}$	Error	Sum0	Error
1	1	-4.02	0	2.76E-09	0	2.13E-09	0
2	1	-4.8	0	2.58E-09	0	2.31E-09	0
3	1	-6.14	0	2.61E-09	0	2.41E-09	0
4	1	-6.83	0	2.74E-09	0	2.6E-09	0
5	1	-7.3	0	2.66E-09	0	2.55E-09	0
6	1	-8.37	0	2.61E-09	0	2.51E-09	0
7	1	-10.01	0	2.69E-09	0	2.61E-09	0
8	1	-10.28	0	2.66E-09	0	2.59E-09	0
9	1	-10.75	0	2.66E-09	0	2.6E-09	0
10	1	-2.76	0	2.62E-08	0	2.61E-08	0
11	1	-3.03	0	2.62E-08	0	2.61E-08	0
12	1	-3.29	0	2.63E-08	0	2.62E-08	0
13	1	-3.99	0	2.62E-08	0	2.61E-08	0
14	1	-4.69	0	2.63E-08	0	2.62E-08	0
15	1	-6.76	0	2.62E-08	0	2.6E-08	0
16	1	-7.46	0	2.61E-08	0	2.6E-08	0
17	1	-8.03	0	2.63E-08	0	2.62E-08	0
18	1	-10.11	0	2.63E-08	0	2.62E-08	0

Table A.18. FIT4FD input file for sorption of Pu(IV) on leached, coarse-grained Hanford sediment. Sediment concentration of 25 g/L in a 0.01 M NaCl background. Data collected after a 30 day equilibration period.

Sample	Use	$logH^+$	Error	$[Pu]_{Total}$	Error	Sum0	Error
1	1	-3.09	0	2.69E-09	0	2.54E-09	0
2	1	-3.9	0	2.69E-09	0	2.6E-09	0
3	1	-4.1	0	2.69E-09	0	2.55E-09	0
4	1	-5.33	0	2.69E-09	0	2.63E-09	0
5	1	-6.99	0	2.63E-09	0	2.59E-09	0
6	1	-7.27	0	2.71E-09	0	2.67E-09	0
7	1	-9.06	0	2.66E-09	0	2.61E-09	0
8	1	-9.32	0	2.66E-09	0	2.61E-09	0
9	1	-10.55	0	2.79E-09	0	2.72E-09	0
10	1	-2.54	0	2.63E-08	0	2.51E-08	0
11	1	-2.58	0	2.62E-08	0	2.57E-08	0
12	1	-2.98	0	2.62E-08	0	2.58E-08	0
13	1	-3.15	0	2.62E-08	0	2.6E-08	0
14	1	-4.86	0	2.61E-08	0	2.6E-08	0
15	1	-4.97	0	2.63E-08	0	2.59E-08	0
16	1	-6.7	0	2.61E-08	0	2.59E-08	0
17	1	-7.29	0	2.59E-08	0	2.57E-08	0
18	1	-9.98	0	2.62E-08	0	2.58E-08	0

Table A.19. FIT4FD input file for sorption of Np(V) on pristine, fine-grained Hanford sediment. Sediment concentration of 25 g/L in a 0.01 M NaCl background. Data collected after a 30 day equilibration period.

Sample ID	Use	$logH^+$	Error	$[Np]_{Total}$	Error	Sum0	Error	$[HCO_3^-]$	Error
1	1	-4.37	0	4.86E-08	0	3.23E-08	0	5.931E-03	0
2	1	-4.93	0	4.85E-08	0	3.69E-08	0	5.281E-03	0
3	1	-6	0	4.97E-09	0	2.51E-09	0	4.040E-03	0
4	1	-6.49	0	4.87E-09	0	3.42E-09	0	3.472E-03	0
5	1	-6.86	0	4.88E-08	0	2.56E-08	0	3.042E-03	0
6	1	-6.95	0	4.85E-08	0	3.99E-08	0	2.938E-03	0
7	1	-7.01	0	4.92E-09	0	2.49E-09	0	2.868E-03	0
8	1	-7.4	0	4.84E-08	0	3.84E-08	0	2.416E-03	0
9	1	-7.43	0	4.87E-09	0	4.13E-09	0	2.381E-03	0
10	1	-7.49	0	4.84E-08	0	2.54E-08	0	2.312E-03	0
11	1	-7.58	0	4.83E-08	0	3.73E-08	0	2.207E-03	0
12	1	-7.62	0	5.11E-09	0	3.5E-09	0	2.161E-03	0
13	1	-7.76	0	4.87E-08	0	3.12E-08	0	1.998E-03	0
14	1	-7.85	0	4.86E-08	0	4.43E-08	0	1.894E-03	0
15	1	-7.89	0	4.82E-09	0	4.06E-09	0	1.848E-03	0
16	1	-8.35	0	5.02E-09	0	4.23E-09	0	1.314E-03	0
17	1	-8.64	0	6.46E-09	0	6.33E-09	0	9.776E-04	0
18	1	-9.49	0	4.87E-09	0	4.76E-09	0	-8.400E-06	0

Table A.20. FIT4FD input file for sorption of Np(V) on pristine, coarse-grained Hanford sediment. Sediment concentration of 25 g/L in a 0.01 M NaCl background. Data collected after a 30 day equilibration period.

Sample ID	Use	$logH^+$	Error	$[Np]_{Total}$	Error	Sum0	Error	$[HCO_3^-]$	Error
1	1	-3.86	0	4.84E-08	0	4.28E-08	0	4.948E-03	0
2	1	-3.89	0	4.84E-08	0	4.02E-08	0	4.921E-03	0
3	1	-4.06	0	4.92E-09	0	1.63E-09	0	4.771E-03	0
4	1	-4.32	0	4.92E-09	0	9.03E-10	0	4.541E-03	0
5	1	-4.54	0	4.86E-08	0	4.24E-08	0	4.347E-03	0
6	1	-4.55	0	4.84E-08	0	3.76E-08	0	4.338E-03	0
7	1	-6.32	0	4.86E-08	0	4.70E-08	0	2.773E-03	0
8	1	-6.35	0	4.82E-09	0	2.68E-09	0	2.747E-03	0
9	1	-6.62	0	4.84E-08	0	3.45E-08	0	2.508E-03	0
10	1	-7.01	0	4.85E-08	0	4.53E-08	0	2.163E-03	0
11	1	-7.04	0	4.87E-09	0	2.48E-09	0	2.137E-03	0
12	1	-7.2	0	4.84E-08	0	4.08E-08	0	1.995E-03	0
13	1	-7.32	0	4.73E-09	0	4.46E-09	0	1.889E-03	0
14	1	-7.42	0	4.82E-09	0	4.63E-09	0	1.801E-03	0
15	1	-7.45	0	4.82E-09	0	4.67E-09	0	1.774E-03	0
16	1	-7.54	0	4.84E-08	0	3.47E-08	0	1.695E-03	0
17	1	-7.83	0	4.87E-09	0	4.12E-09	0	1.438E-03	0

Table A.21. FIT4FD input file for sorption of Np(V) on leached, fine-grained Hanford sediment. Sediment concentration of 25 g/L in a 0.01 M NaCl background. Data collected after a 30 day equilibration period.

Sample	Use	$logH^+$	Error	$[Np]_{Total}$	Error	Sum0	Error
1	1	-4.02	0	5.84E-09	0	8.26E-10	0
2	1	-4.8	0	4.77E-09	0	8.02E-10	0
3	1	-6.14	0	5.31E-09	0	1.71E-09	0
4	1	-6.83	0	4.87E-09	0	2.47E-09	0
5	1	-7.3	0	4.77E-09	0	3.71E-09	0
6	1	-8.37	0	4.97E-09	0	4.92E-09	0
7	1	-10.01	0	4.97E-09	0	4.94E-09	0
8	1	-10.28	0	4.92E-09	0	4.89E-09	0
9	1	-10.75	0	4.97E-09	0	4.95E-09	0
10	1	-2.76	0	4.89E-08	0	7.43E-09	0
11	1	-3.03	0	4.85E-08	0	7.27E-09	0
12	1	-3.29	0	4.86E-08	0	6.76E-09	0
13	1	-3.99	0	4.87E-08	0	7.45E-09	0
14	1	-4.69	0	4.86E-08	0	8.07E-09	0
15	1	-6.76	0	4.86E-08	0	2.27E-08	0
16	1	-7.46	0	4.87E-08	0	4.19E-08	0
17	1	-8.03	0	4.87E-08	0	4.81E-08	0
18	1	-10.11	0	4.86E-08	0	4.85E-08	0

Table A.22. FIT4FD input file for sorption of Np(V) on leached, coarse-grained Hanford sediment. Sediment concentration of 25 g/L in a 0.01 M NaCl background. Data collected after a 30 day equilibration period.

Sample	Use	$logH^+$	Error	$[Np]_{Total}$	Error	Sum0	Error
1	1	-3.09	0	4.92E-09	0	4.32E-10	0
2	1	-3.9	0	4.82E-09	0	6.03E-10	0
3	1	-4.1	0	4.92E-09	0	7.15E-10	0
4	1	-5.33	0	5.02E-09	0	1.17E-09	0
5	1	-6.99	0	4.87E-09	0	2.82E-09	0
6	1	-7.27	0	4.82E-09	0	4.52E-09	0
7	1	-9.06	0	5.02E-09	0	4.95E-09	0
8	1	-9.32	0	4.92E-09	0	4.85E-09	0
9	1	-10.55	0	4.92E-09	0	4.82E-09	0
10	1	-2.54	0	4.85E-08	0	6.92E-09	0
11	1	-2.58	0	4.87E-08	0	6.88E-09	0
12	1	-2.98	0	4.87E-08	0	6.84E-09	0
13	1	-3.15	0	4.84E-08	0	6.62E-09	0
14	1	-4.86	0	4.87E-08	0	8.33E-09	0
15	1	-4.97	0	4.83E-08	0	8.8E-09	0
16	1	-6.7	0	4.85E-08	0	2.43E-08	0
17	1	-7.29	0	4.86E-08	0	4.09E-08	0
18	1	-9.98	0	4.83E-08	0	4.75E-08	0

Table A.23. FIT4FD input file for sorption of coupled Pu(IV) and Pu(V) on pristine, fine-grained Hanford sediment. Sediment concentration of 25 g/L in a 0.01 M NaCl background. Data collected after a 30 day equilibration period.

Sample	Use	$logH^+$	Error	$[Pu]_{Total}$	Error	Sum0	Error	$[HCO_3^-]$	Error	$log[O_2(aq)]$	Error
1	1	-4.37	0	2.7E-08	0	2.68E-08	0	5.931E-03	0	-16.57517	0
2	1	-4.93	0	2.71E-08	0	2.7E-08	0	5.281E-03	0	-15.08613	0
3	1	-6	0	2.74E-09	0	2.53E-09	0	4.040E-03	0	-12.241	0
4	1	-6.49	0	2.84E-09	0	2.67E-09	0	3.472E-03	0	-10.93809	0
5	1	-6.86	0	2.73E-08	0	2.72E-08	0	3.042E-03	0	-9.95426	0
6	1	-6.95	0	2.7E-08	0	2.68E-08	0	2.938E-03	0	-9.71495	0
7	1	-7.01	0	2.71E-09	0	2.45E-09	0	2.868E-03	0	-9.55541	0
8	1	-7.4	0	2.72E-08	0	2.71E-08	0	2.416E-03	0	-8.5184	0
9	1	-7.43	0	2.76E-09	0	2.47E-09	0	2.381E-03	0	-8.43863	0
10	1	-7.49	0	2.72E-08	0	2.7E-08	0	2.312E-03	0	-8.27909	0
11	1	-7.58	0	2.71E-08	0	2.7E-08	0	2.207E-03	0	-8.03978	0
12	1	-7.62	0	2.71E-09	0	2.37E-09	0	2.161E-03	0	-7.93342	0
13	1	-7.76	0	2.71E-08	0	2.7E-08	0	1.998E-03	0	-7.56116	0
14	1	-7.85	0	2.67E-08	0	2.66E-08	0	1.894E-03	0	-7.32185	0
15	1	-7.89	0	2.71E-09	0	2.1E-09	0	1.848E-03	0	-7.21549	0
16	1	-8.35	0	2.56E-09	0	1.56E-09	0	1.314E-03	0	-5.99235	0
17	1	-8.64	0	3.3E-09	0	8.32E-10	0	9.776E-04	0	-5.22124	0
18	1	-9.49	0	2.61E-09	0	2.19E-09	0	-8.400E-06	0	-2.96109	0

Table A.24. FIT4FD input file for sorption of coupled Pu(IV) and Pu(V) on pristine, coarse-grained Hanford sediment. Sediment concentration of 25 g/L in a 0.01 M NaCl background. Data collected after a 30 day equilibration period.

Sample	Use	$logH^+$	Error	$[Pu]_{Total}$	Error	Sum0	Error	$[HCO_3^-]$	Error	$log[O_2(aq)]$	Error
1	1	-3.86	0	3.11E-08	0	3.090E-08	0	4.948E-03	0	-17.93126	0
2	1	-3.89	0	3.11E-08	0	3.076E-08	0	4.921E-03	0	-17.85149	0
3	1	-4.06	0	3.17E-09	0	3.141E-09	0	4.771E-03	0	-17.39946	0
4	1	-4.32	0	3.26E-09	0	3.231E-09	0	4.541E-03	0	-16.70812	0
5	1	-4.54	0	3.10E-08	0	3.078E-08	0	4.347E-03	0	-16.12314	0
6	1	-4.55	0	3.12E-08	0	3.060E-08	0	4.338E-03	0	-16.09655	0
7	1	-6.32	0	3.11E-08	0	3.030E-08	0	2.773E-03	0	-11.39012	0
8	1	-6.35	0	3.10E-09	0	3.042E-09	0	2.747E-03	0	-11.31035	0
9	1	-6.62	0	3.10E-08	0	3.078E-08	0	2.508E-03	0	-10.59242	0
10	1	-7.01	0	3.11E-08	0	3.054E-08	0	2.163E-03	0	-9.55541	0
11	1	-7.04	0	3.20E-09	0	3.155E-09	0	2.137E-03	0	-9.47564	0
12	1	-7.2	0	3.11E-08	0	2.958E-08	0	1.995E-03	0	-9.0502	0
13	1	-7.32	0	3.26E-09	0	3.200E-09	0	1.889E-03	0	-8.73112	0
14	1	-7.42	0	3.26E-09	0	3.155E-09	0	1.801E-03	0	-8.46522	0
15	1	-7.45	0	3.20E-09	0	3.026E-09	0	1.774E-03	0	-8.38545	0
16	1	-7.54	0	3.10E-08	0	2.711E-08	0	1.695E-03	0	-8.14614	0
17	1	-7.83	0	3.20E-09	0	2.817E-09	0	1.438E-03	0	-7.37503	0

Table A.25. FIT4FD input file for sorption of coupled Pu(IV) and Pu(V) on leached, fine-grained Hanford sediment. Sediment concentration of 25 g/L in a 0.01 M NaCl background. Data collected after a 30 day equilibration period.

Sample	Use	$logH^+$	Error	$[Pu]_{Total}$	Error	Sum0	Error	$log[O_2(aq)]$	Error
1	1	-2.76	0	2.62E-08	0	2.61E-08	0	-20.85616	0
2	1	-3.03	0	2.62E-08	0	2.61E-08	0	-20.13823	0
3	1	-3.29	0	2.63E-08	0	2.62E-08	0	-19.44689	0
4	1	-3.99	0	2.62E-08	0	2.61E-08	0	-17.58559	0
5	1	-4.02	0	2.76E-09	0	2.13E-09	0	-17.50582	0
6	1	-4.69	0	2.63E-08	0	2.62E-08	0	-15.72429	0
7	1	-4.8	0	2.58E-09	0	2.31E-09	0	-15.4318	0
8	1	-6.14	0	2.61E-09	0	2.41E-09	0	-11.86874	0
9	1	-6.76	0	2.62E-08	0	2.6E-08	0	-10.22016	0
10	1	-6.83	0	2.74E-09	0	2.6E-09	0	-10.03403	0
11	1	-7.3	0	2.66E-09	0	2.55E-09	0	-8.7843	0
12	1	-7.46	0	2.61E-08	0	2.6E-08	0	-8.35886	0
13	1	-8.03	0	2.63E-08	0	2.62E-08	0	-6.84323	0
14	1	-8.37	0	2.61E-09	0	2.51E-09	0	-5.93917	0
15	1	-10.01	0	2.69E-09	0	2.61E-09	0	-1.57841	0
16	1	-10.11	0	2.63E-08	0	2.62E-08	0	-1.31251	0
17	1	-10.28	0	2.66E-09	0	2.59E-09	0	-0.86048	0
18	1	-10.75	0	2.66E-09	0	2.6E-09	0	0.38925	0

Table A.26. FIT4FD input file for sorption of coupled Pu(IV) and Pu(V) on leached, coarse-grained Hanford sediment. Sediment concentration of 25 g/L in a 0.01 M NaCl background. Data collected after a 30 day equilibration period.

Sample	Use	$logH^+$	Error	$[Pu]_{Total}$	Error	Sum0	Error	$log[O_2(aq)]$
1	1	-3.09	0	2.69E-09	0	2.54E-09	0	-19.97869
2	1	-3.9	0	2.69E-09	0	2.6E-09	0	-17.8249
3	1	-4.1	0	2.69E-09	0	2.55E-09	0	-17.2931
4	1	-5.33	0	2.69E-09	0	2.63E-09	0	-14.02253
5	1	-6.99	0	2.63E-09	0	2.59E-09	0	-9.60859
6	1	-7.27	0	2.71E-09	0	2.67E-09	0	-8.86407
7	1	-9.06	0	2.66E-09	0	2.61E-09	0	-4.10446
8	1	-9.32	0	2.66E-09	0	2.61E-09	0	-3.41312
9	1	-10.55	0	2.79E-09	0	2.72E-09	0	-0.14255
10	1	-2.54	0	2.63E-08	0	2.51E-08	0	-21.44114
11	1	-2.58	0	2.62E-08	0	2.57E-08	0	-21.33478
12	1	-2.98	0	2.62E-08	0	2.58E-08	0	-20.27118
13	1	-3.15	0	2.62E-08	0	2.6E-08	0	-19.81915
14	1	-4.86	0	2.61E-08	0	2.6E-08	0	-15.27226
15	1	-4.97	0	2.63E-08	0	2.59E-08	0	-14.97977
16	1	-6.7	0	2.61E-08	0	2.59E-08	0	-10.3797
17	1	-7.29	0	2.59E-08	0	2.57E-08	0	-8.81089
18	1	-9.98	0	2.62E-08	0	2.58E-08	0	-1.65818

APPENDIX B – SUPPLEMENTAL MODELS

Plutonium Sorption to Goethite

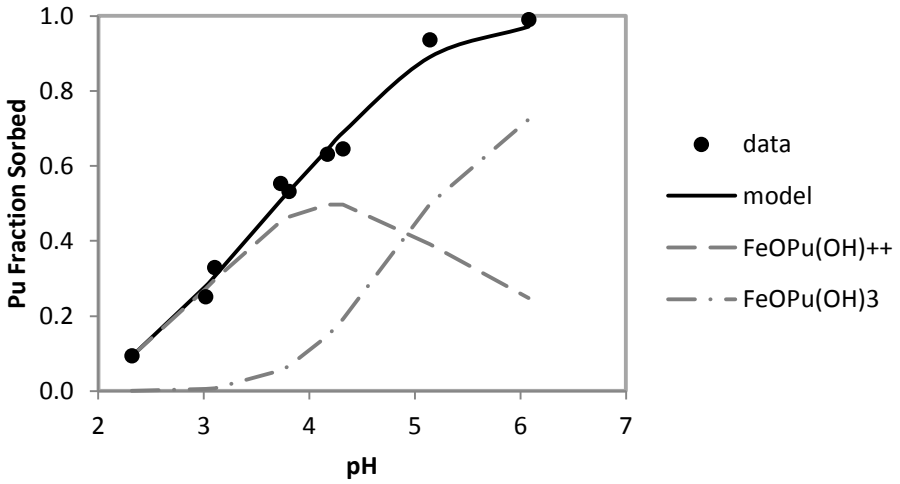

Figure B.1. Sorption of Pu(IV) on goethite as a function of pH. Goethite surface area concentration of 28.5 m^2/L and ^{238}Pu concentration of 1 x10^{-10} M in a 0.10 M $NaNO_3$ background. Data collected after a 25 day equilibration period. Model produced stability constants of 12.58 for $FeOPu(OH)^{++}$ and -2.911 for $FeOPu(OH)_3$. Data from Sanchez *et al.* (1985).

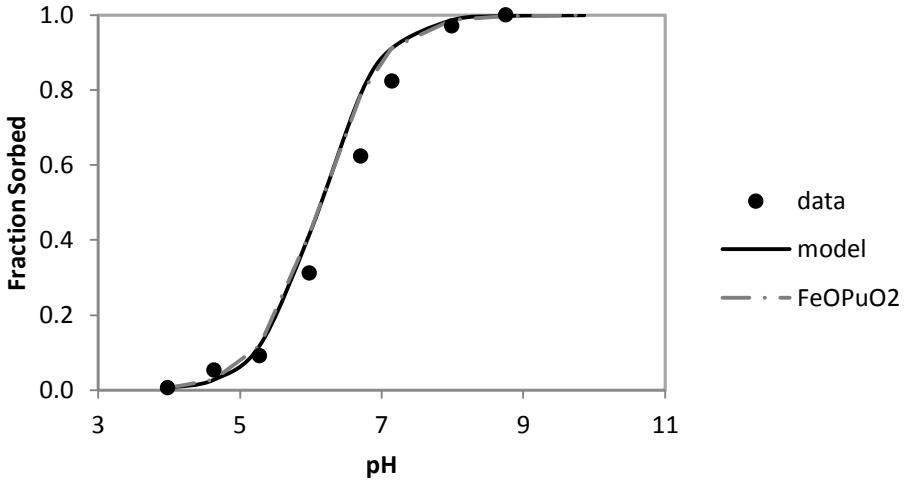

Figure B.2. Sorption of Pu(V) on goethite as a function of pH. Goethite surface area concentration of 28.5 m^2/L and ^{238}Pu concentration of 1 x 10^{-10} M in a 0.10 M $NaNO_3$ background. Data collected after a 25 day equilibration period. Model produced stability constant of -2.322 for $FeOPuO_2$. Data from Sanchez *et al.* (1985).

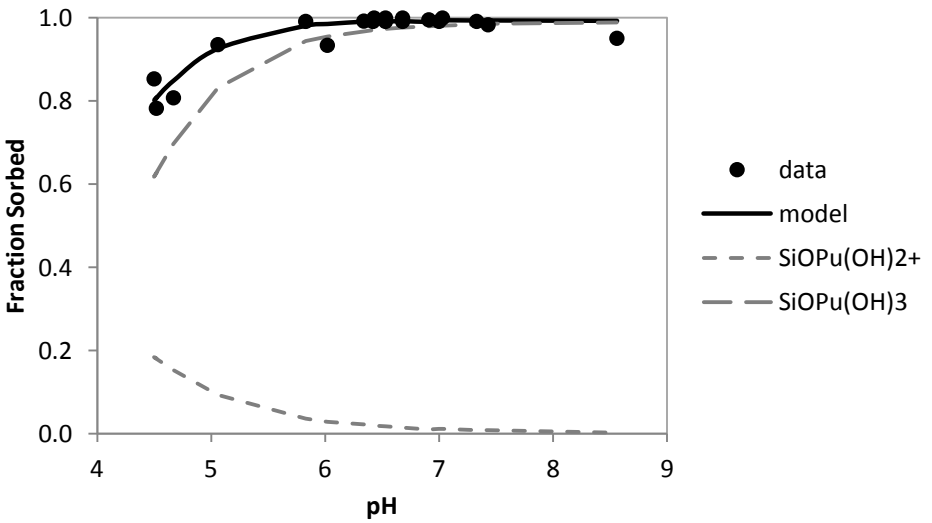

Figure B.3. Sorption of Pu(IV) on silica as a function of pH within a carbonate-free system. Silica surface area concentration of 10 m^2/L and ^{238}Pu concentration of 1.35 x 10^{-10} M in a 0.01 M NaCl background. Data collected after a 62 day equilibration period. Model produced stability constants of 2.166 for $SiOPu(OH)_2^+$ and -1.858 for $SiOPu(OH)_3$. Data and model from Powell *et al.* (2013b).

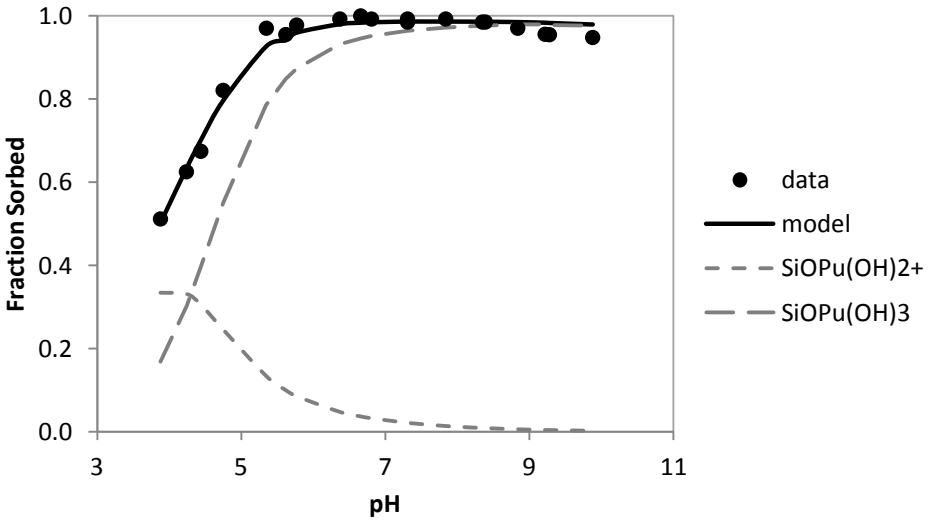

Figure B.4. Sorption of Pu(IV) on silica as a function of pH within a carbonate-equilibrated system. Silica surface area concentration of 10 m^2/L and ^{238}Pu concentration of 1.35 x 10^{-10} M in a 0.01 M NaCl background. Data collected after a 62 day equilibration period. Model produced stability constants of 2.202 for $SiOPu(OH)_2^+$ and -2.189 for $SiOPu(OH)_3$. Data and model from Powell *et al.* (2013b).

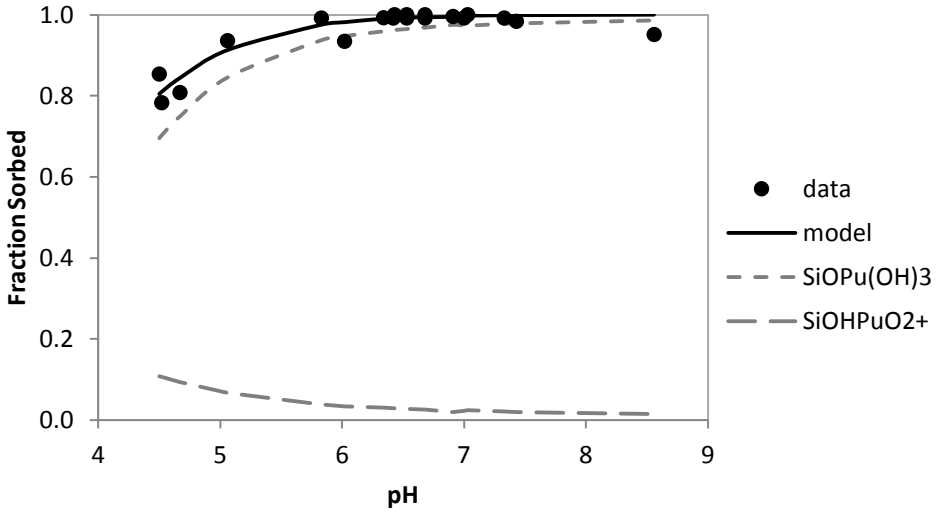

Figure B.5. Sorption of coupled Pu(IV) and Pu(V) on silica as a function of pH within a carbonate-free system. Silica surface area concentration of 10 m^2/L and ^{238}Pu concentration of 1.35 x 10^{-10} M in a 0.01 M NaCl background. Data collected after a 62 day equilibration period. Model produced stability constants of 0.361 for $SiOPu(OH)_3$ and 7.54 for $SiOHPuO_2^+$. Data and model from Powell *et al.* (2013b).

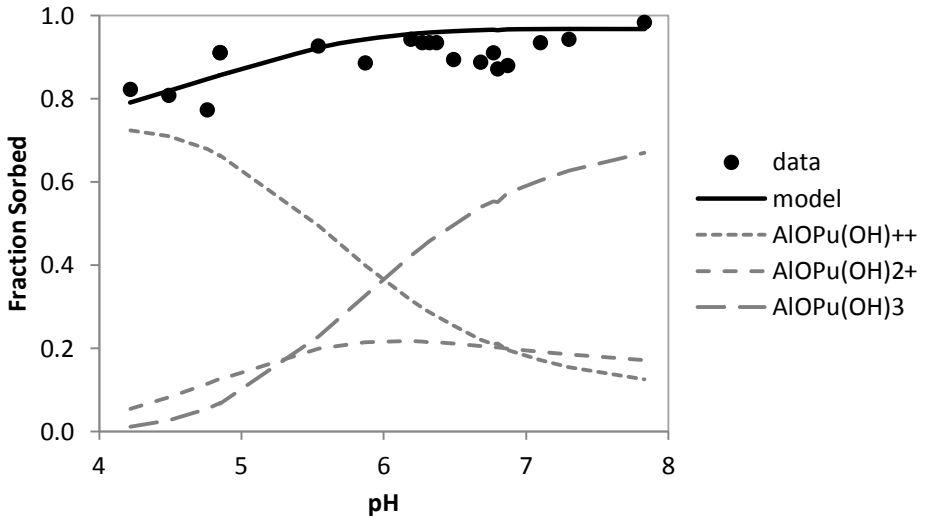

Figure B.6. Sorption of Pu(IV) on gibbsite as a function of pH within a carbonate-free system. Gibbsite surface area concentration of 10 m^2/L and ^{238}Pu concentration of 1.34 x 10^{-10} M in a 0.01 M NaCl background. Data collected after a 62 day equilibration period. Model produced stability constants of 14.59 for $AlOPu(OH)^{++}$, 5.774 for $AlOPu(OH)_2^+$ and -2.59 for $AlOPu(OH)_3$. Data and model from Powell *et al.* (2013b).

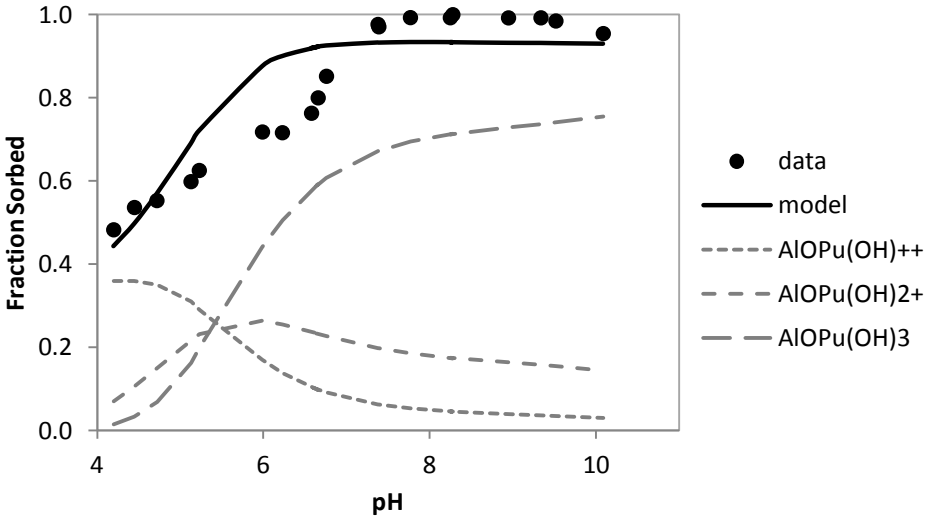

Figure B.7. Sorption of Pu(IV) on gibbsite as a function of pH within a carbonate-equilibrated system. Gibbsite surface area concentration of 10 m^2/L and ^{238}Pu concentration of 1.34 x 10^{-10} M in a 0.01 M NaCl background. Data collected after a 62 day equilibration period. Model produced stability constants of 13.87 for $AlOPu(OH)^{++}$, 5.459 for $AlOPu(OH)_2^{+}$ and -2.92 for $AlOPu(OH)_3$. Data and model from Powell *et al.* (2013b).

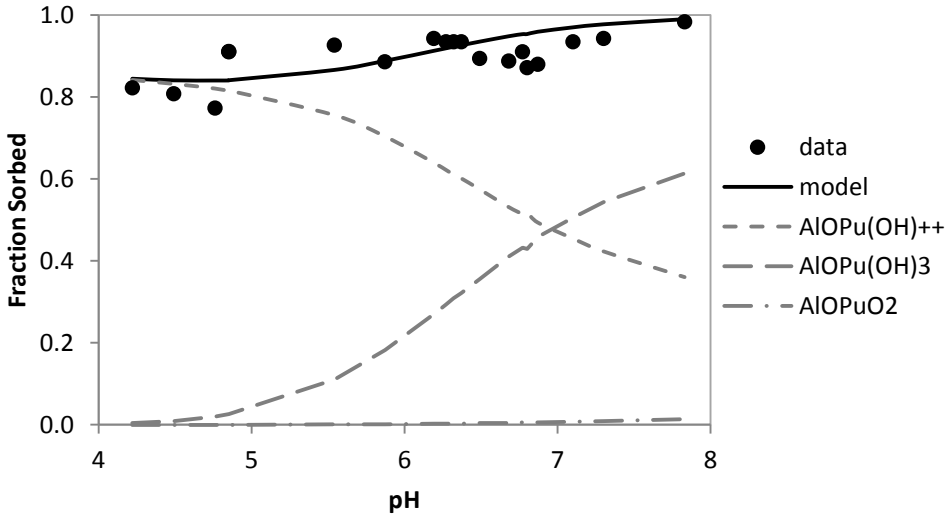

Figure B.8. Sorption of coupled Pu(IV) and Pu(V) on gibbsite as a function of pH within a carbonate-free system. Gibbsite surface area concentration of 10 m^2/L and ^{238}Pu concentration of 1.34 x 10^{-10} M in a 0.01 M NaCl background. Data collected after a 62 day equilibration period. Model produced stability constants of 16.88 for $AlOPu(OH)^{++}$, -0.8013 for $AlOPu(OH)_3$ and 0.23 for $AlOPuO_2$. Data and model from Powell *et al.* (2013b).

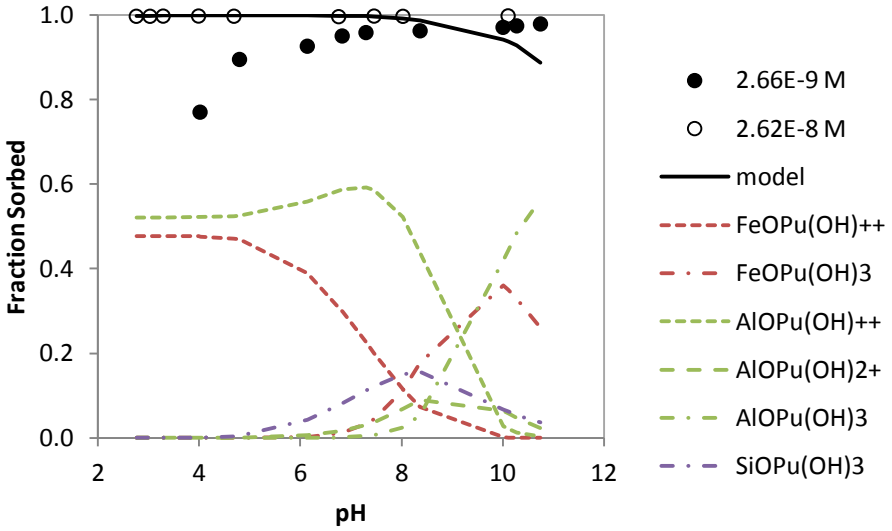

Figure B.9a. Sorption of Pu(IV) on fine, leached Hanford sediment with model fit (M2b). The model uses 2.6% gibbsite and silica with 3.2% goethite. The modeled fraction of each species is shown with dashed lines; only species with a contribution of 1% or greater are shown.

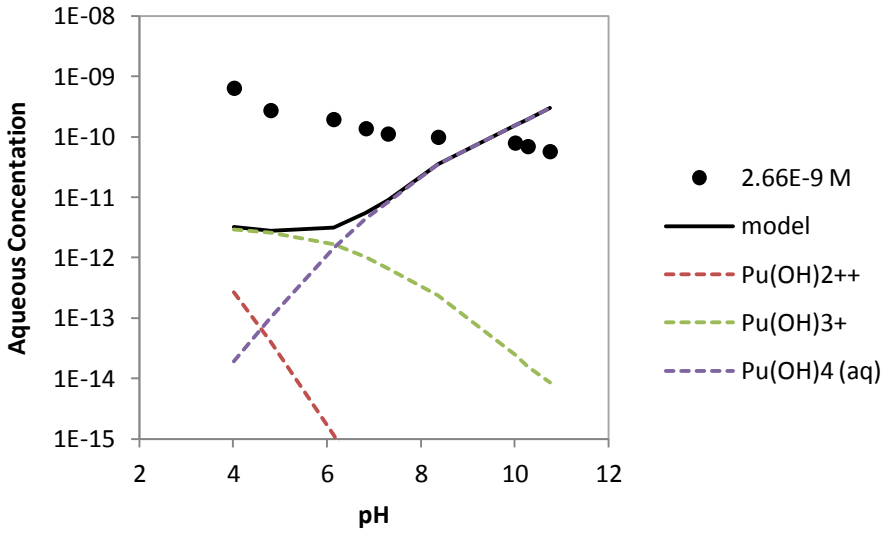

Figure B.9b. Aqueous species present in the Pu(IV) on fine, leached Hanford sediment experiment with model fit (M2b). The modeled fraction of each species is shown with dashed lines; only species with a contribution of 1 x 10^{-15} M or greater are shown.

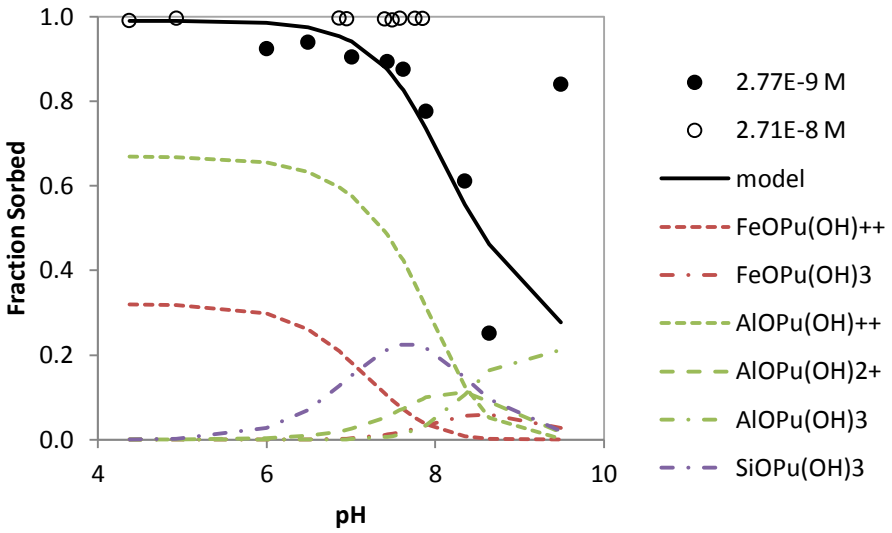

Figure B.10a. Sorption of Pu(IV) on fine, pristine Hanford sediment with model fit (M4a). The model uses 0.26% gibbsite and silica with 0.032% goethite. The modeled fraction of each species is shown with dashed lines; only species with a contribution of 1% or greater are shown.

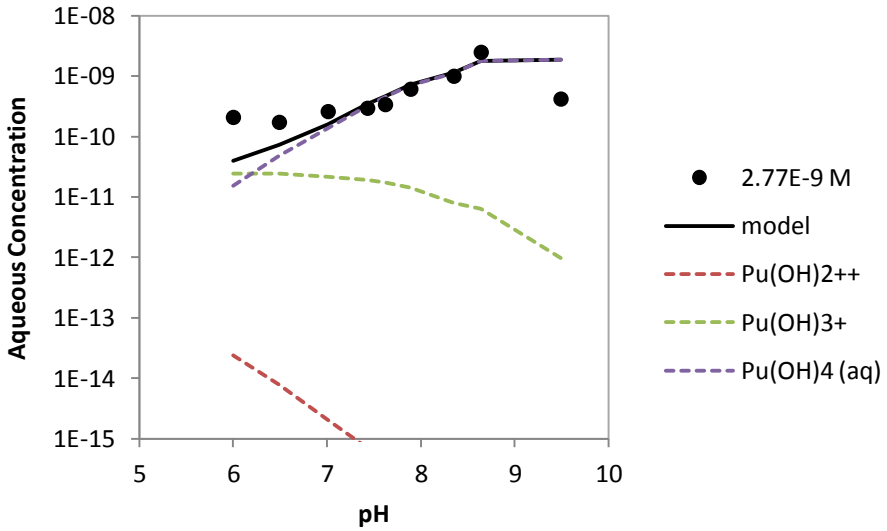

Figure B.10b. Aqueous species present in the Pu(IV) on fine, pristine Hanford sediment experiment with model fit (M4a). The modeled fraction of each species is shown with dashed lines; only species with a contribution of 1 x 10^{-15} M or greater are shown.

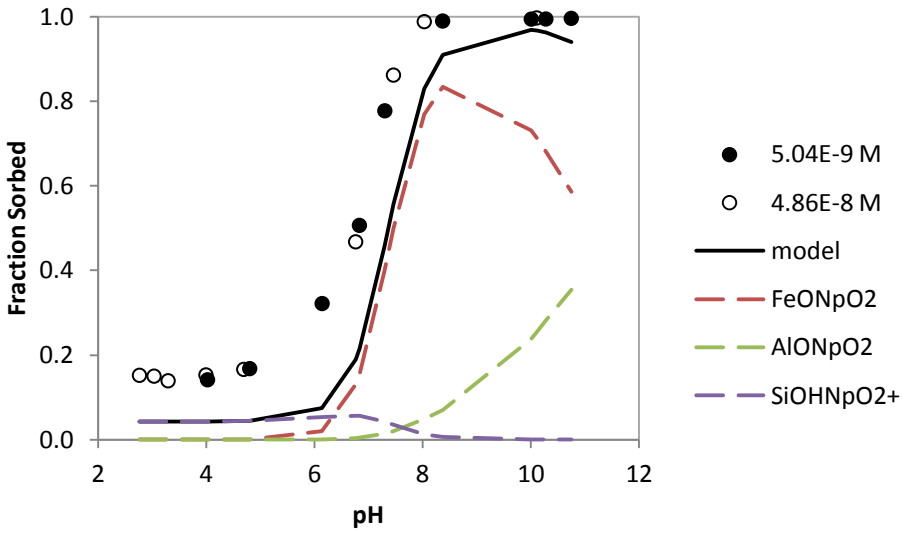

Figure B.11a. Sorption of Np(V) on fine, leached Hanford sediment with model fit (M2b). The model uses 2.6% gibbsite and silica with 3.2% goethite. The modeled fraction of each species is shown with dashed lines; only species with a contribution of 1% or greater are shown.

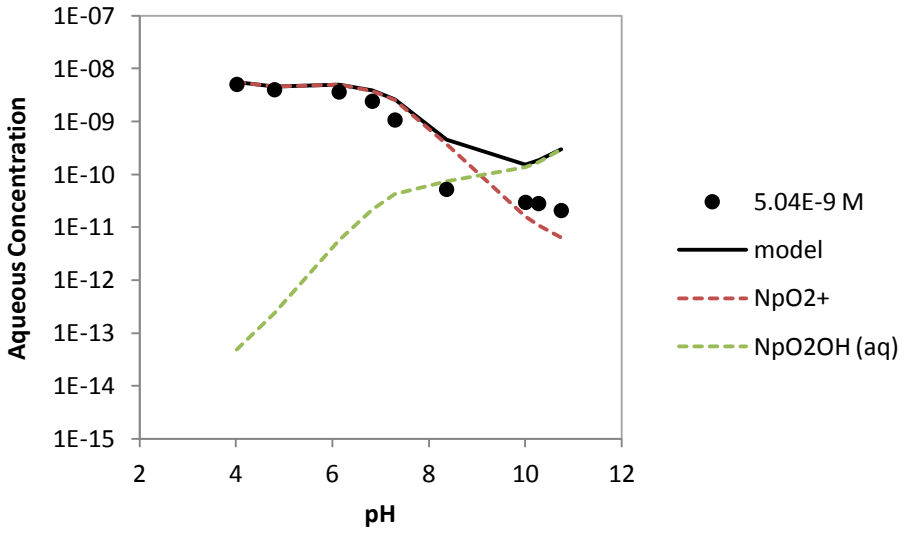

Figure B.11b. Aqueous species present in the Np(V) on fine, leached Hanford sediment experiment with model fit (M2b). The modeled fraction of each species is shown with dashed lines; only species with a contribution of 1 x 10^{-15} M or greater are shown.

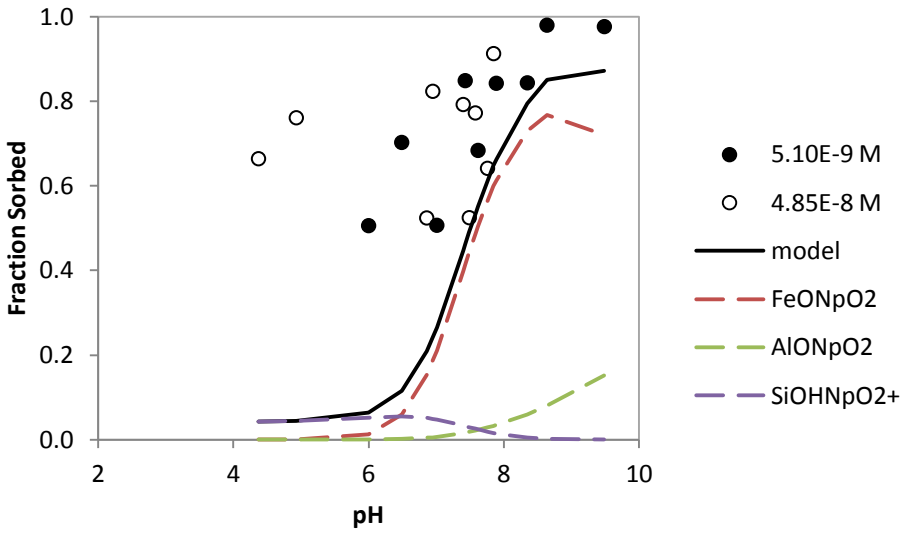

Figure B.12a. Sorption of Np(V) on fine, pristine Hanford sediment with model fit (M2b). The model uses 2.6% gibbsite and silica with 3.2% goethite. The modeled fraction of each species is shown with dashed lines; only species with a contribution of 1% or greater are shown.

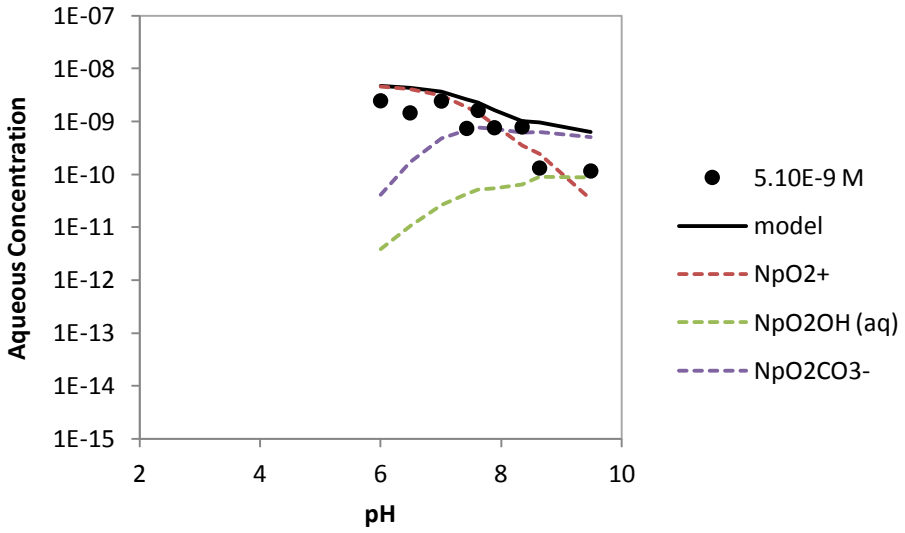

Figure B.12b. Aqueous species present in the Np(V) on fine, pristine Hanford sediment experiment with model fit (M2b). The modeled fraction of each species is shown with dashed lines; only species with a contribution of 1 x 10^{-15} M or greater are shown.

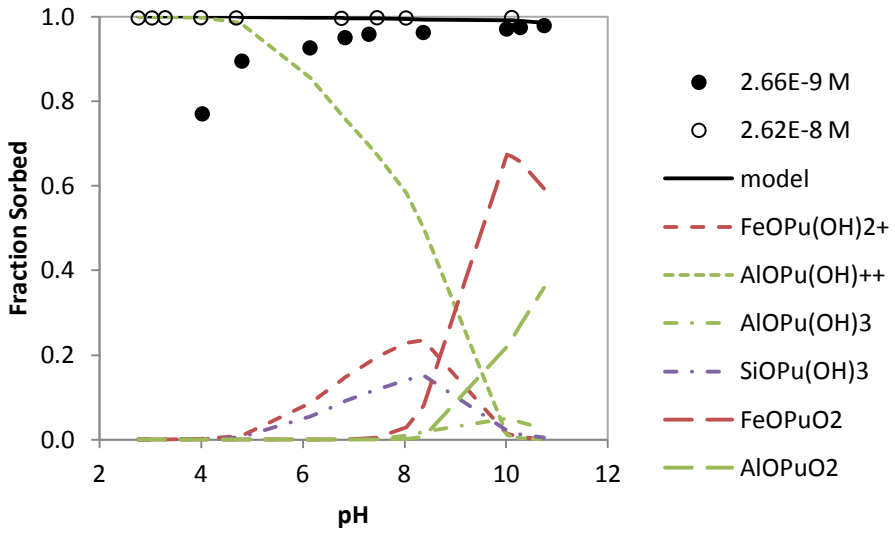

Figure B.13a. Sorption of coupled Pu(IV) and Pu(V) on fine, leached Hanford sediment with model fit (M2b). The model uses 2.6% gibbsite and silica with 3.2% goethite. The modeled fraction of each species is shown with dashed lines; only species with a contribution of 1% or greater are shown.

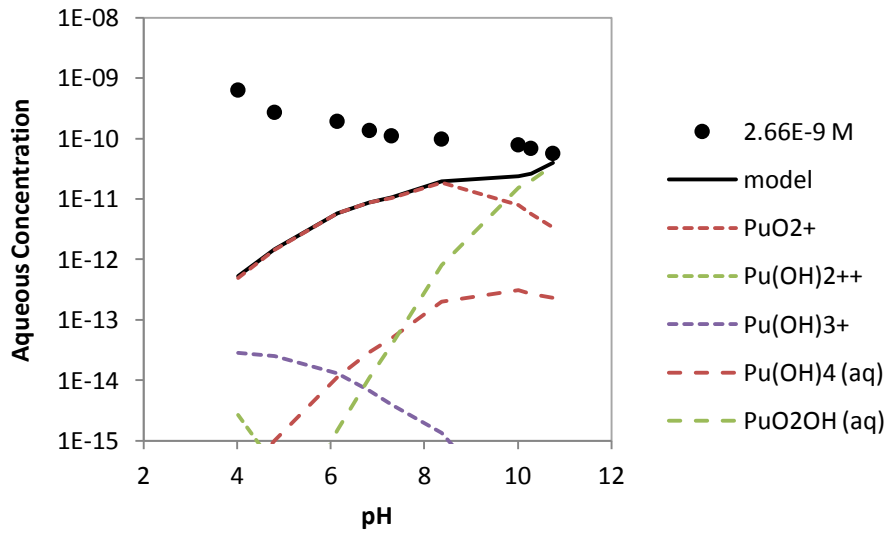

Figure B.13b. Aqueous species present in the coupled Pu(IV) and Pu(V) on fine, leached Hanford sediment experiment with model fit (M2b). The modeled fraction of each species is shown with dashed lines; only species with a contribution of 1 x 10^{-15} M or greater are shown.

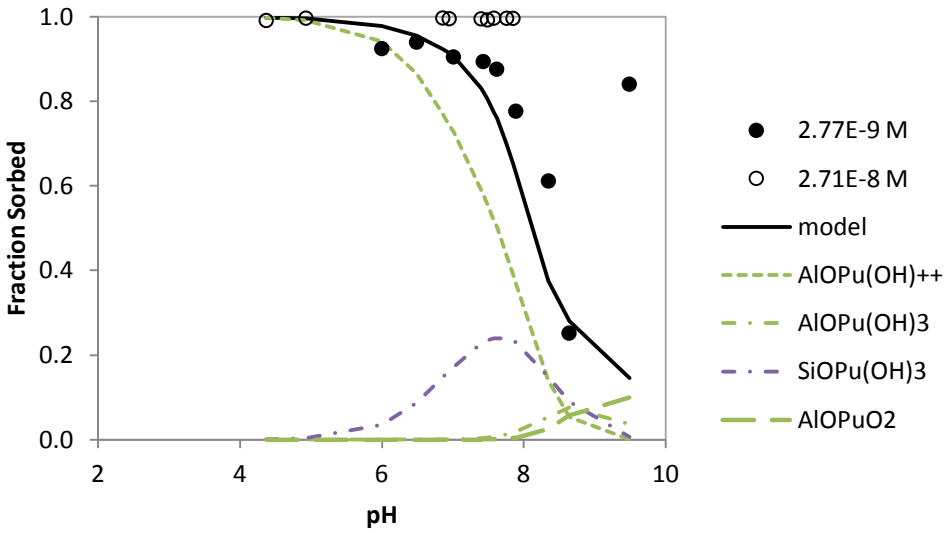

Figure B.14a. Sorption of coupled Pu(IV) and Pu(V) on fine, pristine Hanford sediment with model fit (M4b). The model uses 0.26% gibbsite and silica with 0.0032% goethite. The modeled fraction of each species is shown with dashed lines; only species with a contribution of 1% or greater are shown.

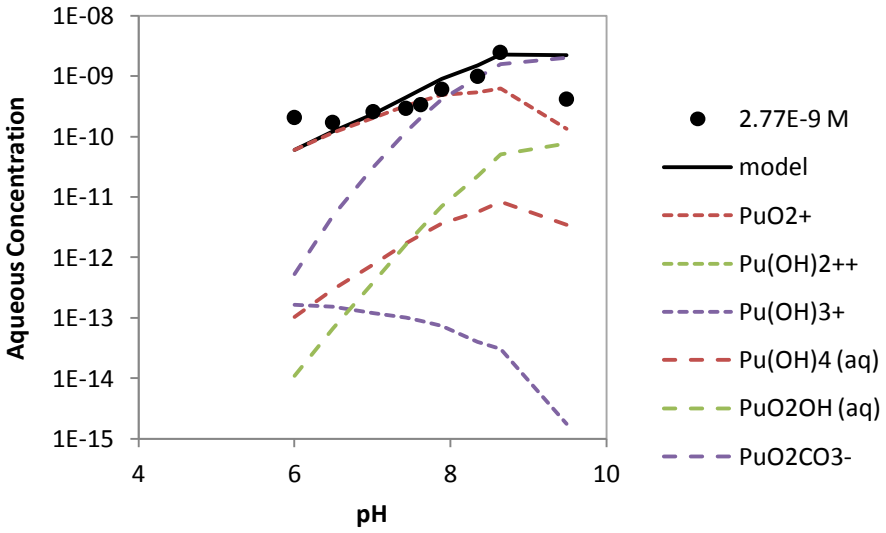

Figure B.14b. Aqueous species present in the coupled Pu(IV) and Pu(V) on fine, pristine Hanford sediment experiment with model fit (M4b). The modeled fraction of each species is shown with dashed lines; only species with a contribution of 1 x 10^{-15} M or greater are shown.

REFERENCES

Bertetti, F.P.; Pabalan, R.T.; Almendarez, M.G. Studies of Neptunium(V) sorption on quartz, clinoptilolite, montmorillonite, and α-alumina. In *Adsorption of Metals by Geomedia: Variables, Mechanisms, and Model Applications.* E.A. Jenne, Ed. Academic Press: San Diego, CA, 1998; pp 131-148.

Cantrell, K.J.; Riley, R.G. A review of subsurface behavior of plutonium and americium at 200-PW-1/3/6 operable units. Pacific Northwest National Laboratory: Richland, WA, **2008**.

Choppin, G.R. and Rao, L. Complexation of pentavalent and hexavalent actinides by fluoride. *Radiochimica Acta*, **1984**, *37*, 143-146.

Choppin, G.R.; Bond, A.H.; Hromadka, P.M. Redox speciation of plutonium. *Journal of Radioanalytical and Nuclear Chemistry*, **1997**, *219* (2), 203-210.

Choppin, G.R. Actinide speciation in the environment. *Journal of Radioanalytical and Nuclear Chemistry*, **2007**, *273* (3), 695-703.

Clark, D.L.; Janecky, D.R.; Lane, L.J. Science-based cleanup of Rocky Flats. *Physics Today*, **2006**, *59* (9), 34-40.

Davis, J.A.; Coston, J.A.; Kent, D.B.; Fuller, C.C. Application of the surface complexation concept to complex mineral assemblages. *Environmental Science and Technology*, **1998**, *32*, 2820-2828.

Dong, W.; Tokunaga, T.K.; Davis, J.A.; Wan, J. Uranium(VI) adsorption and surface complexation modeling onto background sediments from the F-Area Savannah River Site. *Environmental Science and Technology*, **2012**, *46*, 1565-1571.

Duff, M.C.; Hunter, D.B.; Triary, I.R.; Bertsch, P.M.; Reed, D.T., Sutton, S.R.; Shea-McCarthy, G.; Kitten, J.; Eng, P.; Chipera, S.J.; Vaniman, D.T. Mineral associations and average oxidation states of sorbed Pu on tuff. *Environmental Science and Technology*, **1999**, *33*, 2163-2169.

Felmy, A.R.; Cantrell, K.J.; Conradson, S.D. Plutonium contamination issues in Hanford soils and sediments: Discharges from the Z-Plant (PFP) complex. *Physics and Chemistry of the Earth*, **2010**, *35*, 292-297.

Felmy, A.R.; Moore, D.A.; Rosso, K.M.; Qafoku, O.; Rai, D.; Buck, E.C.; Ilton, E.S. Heterogeneous reduction of PuO_2 with Fe(II): Importance of the Fe(III) reaction product. *Environmental Science and Technology*, **2011**, *45* (9), 3952-3958.

Guillaumont, R.; Fanghanel, T.; Fuger, J.; Grenthe, I.; Neck, V.; Palmer, D.A.; Rand, M.H. *Update on the Chemical Thermodynamics of Uranium, Neptunium, Plutonium, Americium and Technetium.* Vol. 5. Elsevier Science: Amsterdam, 2003.

Herbelin, A.L.; Westall, J.C. FITEQL 4.0: A computer program for determination of chemical equilibrium constants from experimental data. Report 99-01, Department of Chemistry, Oregon State University, 1999.

Hixon, A.E.; Hu, Y.; Kaplan, D.I.; Kukkadapu, R.K.; Nitsche, H.; Oafoku, O.; Powell, B.A. Influence of iron redox transformations on plutonium sorption to sediments. *Radiochimica Acta*, **2010**, *98*, 685-692.

Hixon, A.E.; Aria, Y.; Powell, B.A. Examination of the effect of alpha radiolysis on plutonium(V) sorption to quartz using multiple plutonium isotopes. *Journal of Colloid Interface Science*, **2013**, *403*, 105-112.

Hu, Y.J.; Schwaiger, L.K.; Booth, C.H.; Kukkadapu, R.K.; Cristiano, E.; Kaplan, D.; Nitsche, H. Molecular interactions of plutonium(VI) with synthetic manganese-substituted goethite. *Radiochimica Acta*, **2010**, *98*, 655-663.

Kaplan, D.I.; Powell, B.A.; Demirkanli, D.I.; Fjeld, R.A.; Molz, F.J.; Serkiz, S.M.; Coates, J.T. Influence of oxidation states on plutonium mobility during long-term transport through an unsaturated subsurface environment. *Environmental Science and Technology*, **2004**, *38*, 5053-5058.

Keeney-Kennicutt, W.L.; Morse, J.W. The redox chemistry of $Pu(V)O_2^+$ interaction with common mineral surfaces in dilute solutions and seawter. *Geochimica et Cosmochimica Acta*, **1985**, *49*, 2577-2588.

Kirsch, R.; Fellauer, D.; Altmaier, M.; Neck, V.; Rossberg, A.; Fanghanel, T.; Charlet, L.; Scheinost, A.C. Oxidation state and local structure of plutonium reacted with magnetite, mackinawite, and chukanovite. *Environmental Science and Technology*, **2011**, *45*, 7267-7274.

Kobashi, A.; Choppin, G.R.; Morse, J.W. A study of techniques for separating plutonium in different oxidation states. *Radiochimica Acta*, **1988**, *43*, 211-215.

Lu, N.; Cotter, C.R.; Kitten, H.D.; Bentley, J.; Triay, I.R. Reversibility of sorption of plutonium-239 onto hematite and goethite colloids. *Radiochimica Acta*, **1998**, *83*, 167-173.

Neck, V.; Kim, J.I. Solubility and hydrolysis of tetravalent actinides. *Radiochimica Acta*, **2001**, *89*, 1-16.

Powell, B.A; Fjeld, R.A.; Coates, J.T.; Kaplan, D.I.; Serkiz, S.M. Plutonium Oxidation State Geochemistry in the SRS Subsurface Environment (U). WSRC-TR-2003-00035, Westinghouse Savannah River Company, U.S. DOE, Savannah River Site, December 2002.

Powell, B.A.; Fjeld, R.A.; Kaplan, D.I.; Coates, J.T.; Serkiz, S.M. $Pu(V)O_2^+$ adsorption and reduction by synthetic hematite and goethite. *Environmental Science and Technology*, **2005**, *39*, 2107-2114.

Powell, B.A.; Duff, M.C.; Kaplan, D.I.; Fjeld, R.A.; Newville, M.; Hunter, D.B.; Bertsch, P.M.; Coates, J.T.; Eng, P.; Rivers, M.L.; Serkiz, S.M.; Sutton, S.R.; Triay, I.R.; Vaniman, D.T. Plutonium oxidation and subsequent reduction by Mn(IV) minerals in Yucca Mountain tuff. *Environmental Science and Technology*, **2006**, *40*, 3508-3514.

Powell, B.A.; Zavarin, M.; Kersting, A.; Zhao, P. Development of a composite non-electrostatic surface complexation model describing plutonium sorption to aluminosilicates: Part I Experimental. In preparation. To be submitted to *Geochimica et Cosmochimica Acta*, **2013**.

Powell, B.A.; Herr, S.M.; Zavarin, M.; Kersting, A.; Zhao, P. Development of a composite non-electrostatic surface complexation model describing plutonium sorption to aluminosilicates: Part II Modeling. In preparation. To be submitted to *Geochimica et Cosmochimica Acta*, **2013**.

Righetto, L.; Bidoglio, G.; Marcandalii, B.; Bellobono, I.R. Surface interactions of actinides with alumina colloids. *Radiochimica Acta*, **1988**, *44/45*, 73-75.

Righetto, L.; Bidoglio, G.; Azimontl, G.; Bellobono, I.R. Competitive actinide interactions in colloidal humic acid-mineral oxide systems. *Environmental Science and Technology*, **1991**, *25* (11), 1913-1919.

Romanchuk, A.Y.; Kalmykov, S.N.; Aliev, R.A. Plutonium sorption onto hematite colloids at femto- and nanomolar concentrations. *Radiochimica Acta*, **2011**, *99*, 137-144.

Sanchez, A.L. *Chemical speciation and adsorption behavior of plutonium in natural waters.* Ph.D. dissertation, University of Washington, Seattle, WA, 1983.

Sanchez, A.L.; Murray, J.W.; Sibley, T.H. The adsorption of plutonium IV and V on goethite. *Geochimica et Cosmochimica Acta*, **1985**, *49*, 2297-2307.

Shaughnessy, D.A.; Nitsche, H.; Booth, C.H.; Shuh, D.K.; Waychunas, G.A.; Wilson, R.E.; Gill, H.; Cantrell, K.J.; Serne, R.J. Molecular interfacial reactions between Pu(VI) and manganese oxide minerals manganite and hausmannite. *Environmental Science and Technology*, **2003**, *37*, 3367-3374.

Silva, R.J.; Nitasche, H. Actinide environmental chemistry. *Radiochimica Acta*, **1995**, *70/71*, 337-396.

Smith, R.M.; Martell, A.E. *Critical Stability Constants*. Vol. 1. Plenum Press: New York, 1989.

Turner, D.R. A uniform approach to surface complexation modeling of radionuclide sorption. Center for Nuclear Waste Regulatory Analyses, CNWRA 95-001, 1995.

Turner, D.R.; Pabalan, R.T.; Bertetti, F.P. Neptunium(V) sorption on montmorillonite: an experimental and surface complexation modeling study. *Clays and Clay Minerals*, **1998**, *46* (3), 256-269.

Wang, P.; Anderko, A. Thermodynamic modeling of the adsorption of radionuclides on selected minerals. *Industrial and Engineering Chemistry Research*, **2001**, *40*, 4428-4443.

Zavarin, M.; Bruton, C.J. A non-electrostatic surface complexation approach to modeling radionuclide migration at the Nevada Test Site: Aluminosilicates. Lawrence Livermore National Laboratory, UCRL-TR-208672, 2004.

Zavarin, M.; Bruton, C.J. A non-electrostatic surface complexation approach to modeling radionuclide migration at the Nevada Test Site: Iron oxides and calcite. Lawrence Livermore National Laboratory, UCRL-TR-208673, 2004.

Zavarin, M.; Roberts, S.K.; Hakem, N.; Sawvel, A.M.; Kersting, A.B. Eu(III), Sm(III), Np(V), Pu(V) and Pu(IV) Sorption to Calcite. *Radiochimica Acta*, **2005**, *93*, 93-102.